THE ROLE OF REACTIVE OXYGEN SPECIES IN CISPLATIN- AND DOXORUBICIN-INDUCED APOPTOSIS IN KERATINOCYTES AND DERMAL PAPILLA CELLS

Miss Sudjit Luanpitpong

A Dissertation Submitted in Partial Fulfillment of the Requirements for the Degree of Doctor of Philosophy Program in Pharmaceutical Technology
Department of Pharmaceutics and Industrial Pharmacy
Faculty of Pharmaceutical Sciences
Chulalongkorn University
Academic Year 2011

Copyright of Chulalongkorn University
บทคัดย่อและแฟ้มข้อมูลฉบับเต็มของวิทยานิพนธ์ตั้งแต่ปีการศึกษา 2554 ที่ให้บริการในคลังปัญญาจุฬาฯ (CUIR)
เป็นแฟ้มข้อมูลของนิสิตเจ้าของวิทยานิพนธ์ที่ส่งผ่านทางบัณฑิตวิทยาลัย
The abstract and full text of theses from the academic year 2011 in Chulalongkorn University Intellectual Repository(CUIR)
are the thesis authors' files submitted through the Graduate School.

บทบาทของอนุพันธ์ออกซิเจนที่ว่องไวในการเกิดอะพอพโทซิส จากซิสพลาทินและด็อกโซรูบิซินในเคอราทิโนไซต์และเซลล์เดอร์มัลแฟพิลลา

นางสาวสุดจิต ล้วนพิชญ์พงศ์

วิทยานิพนธ์นี้เป็นส่วนหนึ่งของการศึกษาตามหลักสูตรปริญญาวิทยาศาสตรดุษฎีบัณฑิต
สาขาวิชาเทคโนโลยีเภสัชกรรม ภาควิชาวิทยาการเภสัชกรรมและเภสัชอุตสาหกรรม
คณะเภสัชศาสตร์ จุฬาลงกรณ์มหาวิทยาลัย
ปีการศึกษา 2554
ลิขสิทธิ์ของจุฬาลงกรณ์มหาวิทยาลัย

Thesis Title	THE ROLE OF REACTIVE OXYGEN SPECIES IN CISPLATIN- AND DOXORUBICIN-INDUCED APOPTOSIS IN KERATINOCYTES AND DERMAL PAPILLA CELLS
By	Miss Sudjit Luanpitpong
Field of Study	Pharmaceutical Technology
Thesis Advisor	Associate Professor Ubonthip Nimmannit, Ph.D
Thesis Co-Advisors	Professor Yon Rojanasakul, Ph.D
	Assistant Professor Pithi Chanvorachote, Ph.D

Accepted by the Faculty of Pharmaceuitcal Sciences, Chulalongkorn University in Partial Fulfillment of the Requirements for the Doctoral Degree

…….. Dean of the Faculty of Pharmaceutical Sciences

(Associate Professor Pintip Pongpetch, Ph.D.)

THESIS COMMITTEE

…….. Chairman

(Associate Professor Parkpoom Tengamnuay, Ph.D.)

…….. Thesis Advisor

(Associate Professor Ubonthip Nimmannit, Ph.D.)

…….. Thesis Co-Advisor

(Professor Yon Rojanasakul, Ph.D.)

…….. Thesis Co-Advisor

(Assistant Professor Pithi Chanvorachote, Ph.D.)

…….. Examiner

(Assistant Professor Nontima Vardhanabhuti, Ph.D.)

…….. Examiner

(Assistant Professor Angkana Tantituvanont, Ph.D.)

…….. External Examiner

(Professor Yindee Kitiyanant, D.V.M., M.Sc.)

สุดจิต ล้วนพิชญ์พงศ์ : บทบาทของอนุพันธ์ออกซิเจนที่ว่องไวในการเกิดอะพอพโทซิสจากซิสพลาทินและด็อกโซรูบิซินในเคอราทิโนไซต์และเซลล์เดอร์มัลแพพิลลา. (THE ROLE OF REACTIVE OXYGEN SPECIES IN CISPLATIN- AND DOXORUBICIN-INDUCED APOPTOSIS IN KERATINOCYTES AND DERMAL PAPILLA CELLS) อ. ที่ปรึกษาวิทยานิพนธ์หลัก : รศ.ภญ.ดร. อุบลทิพย์ นิมมานนิตย์, อ. ที่ปรึกษาวิทยานิพนธ์ร่วม : PROF. YON ROJANASAKUL, Ph.D., ผศ.ภก.ดร. ปิติ จันทร์วรโชติ, 131 หน้า.

การเกิดอะพอพโทซิสของเซลล์เส้นผมมีความเกี่ยวเนื่องกับการเกิดผมร่วงจากยาเคมีบำบัด แต่กลไกในระดับโมเลกุลยังไม่เป็นที่ชัดเจน งานวิจัยนี้ศึกษาผลของยาเคมีบำบัดซิสพลาทินและด็อกโซรูบิซินต่อการเกิดอะพอพโทซิสในเคอราติโนไซต์และเซลล์เดอร์มัลแพพิลลา รวมทั้งตรวจสอบการสร้างและบทบาทของอนุพันธ์ออกซิเจนที่ว่องไวสปีชีย์ต่างๆในกระบวนการดังกล่าว ผลการวิจัยพบว่าซิสพลาทินและด็อกโซรูบิซินกระตุ้นการสร้างอนุพันธ์ออกซิเจนที่ว่องไวควบคู่ไปกับการกระตุ้นเอนไซม์แคสเปสและการตายแบบอะพอพโทซิส สารต้านอนุพันธ์ออกซิเจนที่ว่องไวสามารถยับยั้งการเกิดอะพอพโทซิส แสดงให้เห็นว่าอนุพันธ์ออกซิเจนที่ว่องไวมีบทบาทสำคัญต่อกระบวนการอะพอพโทซิส การศึกษาต่อมาโดยการใช้ตัวยับยั้งที่มีความจำเพาะต่ออนุพันธ์ออกซิเจนที่ว่องไวสปีชีส์ต่างกันและอิเล็กตรอนสปินเรโซแนนซ์แสดงให้เห็นถึงบทบาทที่แตกต่างของอนุพันธ์แต่ละสปีชีส์ในการเกิดอะพอพโทซิสจากซิสพลาทินและด็อกโซรูบิซิน กล่าวคือไฮดรอกซิลเรดิคอลเป็นอนุพันธ์สำคัญในการเกิดอะพอพโทซิสจากซิสพลาทิน ในขณะที่อนุพันธ์ซุปเปอร์ออกไซด์เป็นหลักในการเกิดอะพอพโทซิสจากด็อกโซรูบิซิน อนุพันธ์ออกซิเจนที่ว่องไวเป็นสื่อควบคุมการลดระดับโปรตีนบีซีแอล-2 ผ่านกลไกการเกิดยูบิควิทิเนชันซึ่งนำไปสู่การทำลายโปรตีนด้วยโปรตีเอโซม นอกจากนี้พบว่าการเกิดยูบิควิทิเนชันและการทำลายโปรตีนบีซีแอล-2 มีความเชื่อมโยงกับการเกิดดีฟอสโฟรีเลชันของบีซีแอล-2 กลไกที่นำเสนอในงานวิจัยนี้อาจนำไปสู่การพัฒนาเพื่อป้องกันผมร่วงจากยาเคมีบำบัด

ภาควิชาวิทยาการเภสัชกรรมและเภสัชอุตสาหกรรม ลายมือชื่อนิสิต .....

สาขาวิชา เทคโนโลยีเภสัชกรรม ลายมือชื่อ อ.ที่ปรึกษาวิทยานิพนธ์หลัก .....

ปีการศึกษา 2554 ลายมือชื่อ อ.ที่ปรึกษาวิทยานิพนธ์ร่วม .....

 # # 5077109033 : MAJOR PHARMACEUTICAL TECHNOLOGY KEYWORDS : CISPLATIN / DOXORUBICIN / REACTIVE OXYGEN SPECIES / APOPTOSIS / TOXICITY

SUDJIT LUANPITPONG : THE ROLE OF REACTIVE OXYGEN SPECIES IN CISPLATIN- AND DOXORUBICIN-INDUCED APOPTOSIS IN KERATINOCYTES AND DERMAL PAPILLA CELLS. THESIS ADVISOR : ASSOC. PROF. UBONTHIP NIMMANNIT, Ph.D., THESIS CO-ADVISOR : PROF. YON ROJANASAKUL, Ph.D., ASSIST. PROF. PITHI CHANVORACHOTE, Ph.D., 131 pp.

Massive apoptosis of hair follicle cells has been implicated in the pathogenesis of chemotherapy-induced alopecia (CIA), but the underlying mechanisms of regulation are not well understood. The present study investigated the apoptotic effect of cisplatin and doxorubicin on human hair follicle dermal papilla cells and HaCaT keratinocytes, and determined the identity and role of specific reactive oxygen species (ROS) involved in the process. Treatment of the cells with cisplatin and doxorubicin induced ROS generation and a parallel increase in caspase activation and apoptotic cell death. Inhibition of ROS generation by antioxidants inhibited the apoptotic effect of cisplatin and doxorubicin, indicating the role of ROS in the process. ROS inhibition studies showed the essential role of different ROS in apoptotic effects of cisplatin and doxorubicin. Hydroxyl radical is the primary oxidative species responsible for the apoptotic effect of cisplatin, while superoxide anion is responsible for apoptosis by doxorubicin. Electron spin resonance studies confirmed the formation of hydroxyl radical and superoxide induced by cisplatin and doxorubicin, respectively. The mechanisms by which these specific ROS mediate the apoptotic effect of cisplatin and doxorubicin were shown to involve down-regulation of Bcl-2 via ubiquitin-proteasomal degradation. Ubiquitination and degradation of Bcl-2 was further shown to be mediated by dephosphorylation of Bcl-2. Together, our results indicate the essential role of ROS in cisplatin- and doxorubicin-induced cell death of hair follicle cells through Bcl-2 regulation. Since CIA is a major side effect of cisplatin, doxorubicin and many other chemotherapeutic agents with no known effective treatments, the knowledge gained from this study could be useful in the design of preventive treatment strategies for CIA through localized therapy without compromising the chemotherapy efficacy.

Department : Pharmaceutics and Industrial Pharmacy Student's Signature .....

Field of Study : Pharmaceutical Technology Advisor's Signature .....

Academic Year : 2011 Co-Advisor's Signature .....

ACKNOWLEDGEMENTS

This dissertation would have not been possible without the guidance, help and support of my advisors, committee members, colleagues, family and friends who in one way or another contributed and extended their valuable assistance and time.

First, I would like to express my greatest gratitude to Associate Professor Dr. Ubonthip Nimmannit who encouraged me to pursue the Doctoral Degree and continued her supporting role in academics as my major advisor. I would like to express warmest thanks to my abroad co-advisor Professor Dr. Yon Rojanasakul who offered me the great research experience in West Virginia University and to his wife Dr. Liying for their generous family-like hospitality. Deepest thanks go to my co-advisor Assistant Professor Dr. Pithi Chanvorachote who contributed his time practicing me the laboratory skills, conceptual thinking and inspiring my research world. It is also my pleasure to thank my thesis committee for their constructive and insightful comments that helped improve my research for the past several years.

Special thanks to classmates, colleagues, and staffs in Pharmaceutical Sciences, Chulalongkorn University and Health Sciences Center, West Virginia University for their readily cooperation and assistance. Not forgetting my best friends, Jingting Li and Vilaiphan Chantararothai, who have always been by my side.

I would also like to thank my family for their helps and understanding in any regards, not only during my degree seeking, but at all time. For my parents, they are simply the best–this thesis is dedicated to them.

Last but not least, I would like to express my deepest thanks to The Royal Golden Jubilee Ph. D. Program for grant support (5.Q.CU/49/A.1).

CONTENTS

Page

Page

LIST OF TABLES

Table **Page**

LIST OF FIGURES

Figure **Page**

Figure **Page**

Figure **Page**

Figure **Page**

LIST OF ABBREVIATIONS

~	approximately
°C	degree Celcius (centrigrade)
<	less than
%	percentage
μ	micro (10^{-6})
C3	caspase-3
C8	caspase-8
C9	caspase-9
CAT	catalase
CDDP	*cis*-diamminedichloroplatinum, cisplatin
CIA	chemotherapy-induced alopecia
CMA	concanamycin A
DCF	dichlorofluorescein
DHE	dihydroethidium
DMTU	dimethylthiourea
DMPO	5,5-dimethyl-1-pyrroline-N-oxide
DOX	doxorubicin
Emb	emblica extract
ERK1/2	p44/p42 extracellular signal-related kinases
ESR	electron spin resonance
et al.	et alii, and other
Fig.	figure
g	gram (s)

GSH	reduced glutathione
h	hour (s)
H_2DCF-DA	dihydrodichlorofluorescein diacetate
HFDPC	human hair follicle dermal papilla cells
HPF	hydroxyphenyl fluorescein
hROS	highly reactive oxygen species
IB	immunoblot
IP	immunoprecipitation
JNK	c-Jun-NH2-terminal protein kinase
k	kilo (10^3)
l	litre (s)
LAC	lactacystin
m	milli (10^{-3})
M	molar (s), micromole (s) per litre
MAP kinases	mitogen-activated protein kinases
min	minute (s)
MnSOD	manganese superoxide dismutase
MnTBAP	Mn(III)tetrakis(4-benzoic acid)porphyrin chloride
MTT	3-(4,5-dimethylthiazol-2-yl)-2,5-diphenyltetrazolium bromide
NAC	*N*-acetyl cysteine
NaFM	sodium formate
Pro-C3	pro-caspase-3, full length caspase-3
ROS	reactive oxygen species
S.D.	standard deviation
SDS-PAGE	sodium dodecyl sulfate-polyacrylamide gel electrophoresis

Ub	ubiquitin
zVAD-fmk	benzyloxycarbonyl-Val-Ala-Asp-(OMe) fluoromethyl ketone

CHAPTER I

INTRODUCTION

Chemotherapy-induced alopecia (CIA) is a frequent toxicity and arguably the most feared side effect of cancer chemotherapy (Carelle et al., 2002). The incidence of CIA is approximately 65% of all patients (Wang et al., 2006). CIA could be easily noticeable by self and others in a relative short time, thus it is linked with having cancer and chemotherapy. CIA compromises patient quality of life, especially for female and children, leading to poor therapeutic outcome.

In the last decade, important information about the CIA comes mostly from animal models; neonatal rats and adult mice (Botchkarev, 2003; Wang et al., 2006; Bodo et al., 2008). Despite significant progresses and substantial efforts in CIA research and development, no reliable and effective preventive treatment has become available. This limitation has been attributed to the lack of basic understanding of CIA pathogenesis and appropriate experimental models. The animal physiological and pathological conditions do not necessarily mimic human conditions. Altogether with the fact that molecular techniques normally have poor sensitivity in animal models, *in vitro* model using human cells might better benefit the investigation of damage response pathways, and consequently facilitate the development of effective treatment for CIA. Hair follicles are composed of two key functional populations; follicular keratinocytes and dermal papilla fibroblasts (Inui et al., 2000; Krause and Foitzik, 2006), hence, human keratinocyte HaCaT cells and human hair follicle dermal papilla cells were used as *in vitro* models with the best potential to study the effects and molecular mechanisms of chemotherapy on hair follicles.

Many chemotherapeutic agents have been shown to induce alopecia, including cisplatin and doxorubicin (Botchkarev, 2001; Apisarnthanarax and Duvic, 2003). Cisplatin and doxorubicin are widely prescribed against various malignancies and solid tumors, such as, lung, ovarian, breast, and prostate cancers (Torri et al., 2000; Arriagada et al., 2004; Minotti et al., 2004). Mechanisms of action for both cisplatin and doxorubicin are accepted to involve DNA-adduct formation as well as intracellular reactive oxygen species (ROS) induction (Baek et al., 2003; Wang et al., 2004; Wang et al., 2008). ROS namely superoxide anion, hydroxyl radical and hydrogen peroxide are continuously generated at a low level as by products of aerobic mitochondrial metabolism and in response to several exogenous stimuli, e.g. UV and ionizing radiation, chemotherapy, chemical irritants, and mitochondrial toxin. These ROS were originally shown to play a pivotal role in regulation of cellular functions involving in inflammatory process and self-defense reaction. Recently, ROS have been identified as intracellular signaling molecules in various pathways regulating cell proliferation and cell death under both physiological and pathological processes (Hancock et al., 2001; Fruehauf and Meyskens, 2007). The vast production of ROS was shown to implicate in aging and senescence as well as in the pathogenesis of cancer, diabetes mellitus, atherosclerosis, and neurodegenerative diseases (Droge, 2002).

Indeed, doxorubicin and cisplatin side effects are previously found to be tightly associated with intracellular ROS generation in various types of normal cells (Spallarossa et al., 2004; Jiang et al., 2007). Substantial evidence indicated that CIA resulted from massive induction of cell apoptosis in the hair follicle (Schilli et al., 1998; Bodo et al., 2008). During cancer apoptosis induced by cisplatin and doxorubicin, the alterations of apoptotic key proteins such as tumor suppressor p53

and Bcl-2 family proteins were previously reported (Wang et al., 2004; Wang et al., 2008). However, effects of cisplatin and doxorubicin in the regulation of these proteins on follicular cells of hair follicle are not yet elucidated. This research determined the identity and role of ROS induced by cisplatin and doxorubicin in keratinocytes and hair follicle dermal papilla cells, focusing on apoptotic signaling mechanisms.

The findings would emphasize the pathogenesis of CIA, which facilitate the development of novel preventive strategies to minimize this hair disorder. In addition, it might provide additional molecular information of other types of hair disease that associate with ROS regulations or that share the same signaling pathway.

CHAPTER II

LITERATURE REVIEW

Hair Follicle Biology

Chemotherapy causes structural damage of human scalp hairs. The effects may vary from altered hair appearance, decreased rate of hair growth, partial or complete hair loss (alopecia). To discuss the advances in the pathogenesis of CIA, an overview of hair follicle biology is first covered.

1. Hair follicle structure

Hair follicle structure changes during the various stages of hair growth cycle (see *Section 2* for review). In the anagen phase, hair structure is composed of two distinct components, hair follicle and hair shaft (Fig. 1A). The hair follicle is embedded in the connective tissue and subcutaneous fat. Contained within the hair follicle bulb is the pluripotent keratinocytes of hair matrix. Matrix cells in the lower part of hair bulb constantly divide at a high mitotic rate, whereas the matrix cells in the upper part of hair bulb have a low mitotic rate and could differentiate to form the inner root sheath (IRS) and hair shaft (HS), which are the middle and innermost layer of hair follicle, respectively. Outer root sheath (ORS), is the outermost layer of hair follicle that separates the whole organ from dermis and is believed to contain epithelial stem cells at its bulge region (Hardy, 1992; Krause and Foitzik, 2006; Alonso and Fuchs, 2006). Pigmentation of hair shaft depends on melanocytes, which reside in the hair matrix of hair follicle. Melanocytes transfer the melanin granule to keratinocytes of the growing hair shaft (Ohnemus et al., 2006). Besides the epithelial

cells, hair follicle also contains the mass of mesenchymal dermal papilla (DP) cells at its base (Fig. 1B). The DP cells are connected to capillaries to derive nutrients from the blood and also function as a regulator of hair cycle (Sakita et al., 1995). Moreover, substantial evidence supports the correlation between DP cell number and the size of hair follicle and shaft (Elliot et al., 1999; Ishino et al., 1997).

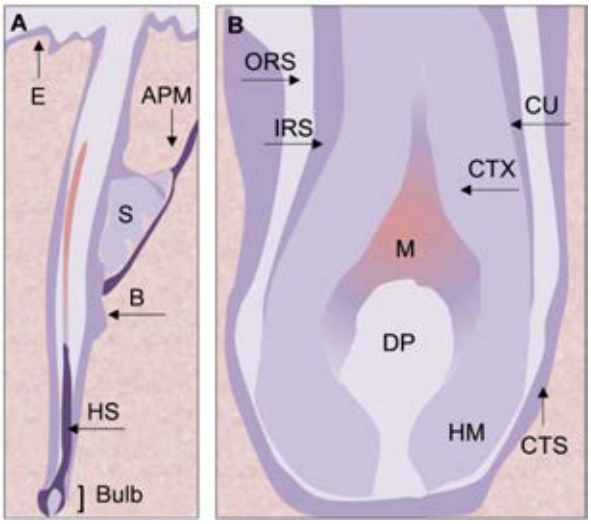

Figure 1. Diagrammatic representation of hair follicle structure in its mature anagen phase. **A** a full-length longitudinal view of hair follicle. **B** hair follicle bulb. Abbreviations: APM, arector pili muscle; B, bulge; CTS, connective tissue sheath; CTX, cortex of hair shaft; CU, cuticle of hair shaft; DP, dermal papilla; E, epidermis; HM, hair matrix; HS, hair shaft; IRS, inner root sheath; M, melanocytes; ORS, outer root sheath; S, sebaceous gland.

2. Hair growth cycle

Each hair follicle undergoes rhythmic changes through the three phases of hair cycle, which are anagen, catagen and telogen (Fig. 2). Anagen is an active growth phase of hair follicle. During anagen, daughter cells of pluripotent keratinocytes move upwards and adapt into one of the six epithelial lineages, namely Henley, Huxley and cuticle of the IRS and cuticle, cortex and medulla of the HS. As the HS cells become fully differentiated, they extrude their organelles and are tightly packed to form cysteine-rich hair keratins. The IRS and HS interlock via their cuticle structures, however, the IRS degenerates in the upper follicle, thereby releasing the HS that continues to move towards the skin surface. Subsequently, the hair follicle enters the catagen or regression phase. During catagen, there are extensive apoptosis of epithelial cells in the hair follicle bulb and ORS, leading to the formation of epithelial strands. The HS hence stops differentiation and forms the club hair, which moves up until it reaches the bulge region. Dermal papilla cells are condensed and move upwards to the bulge region. After that, the hair enters the telogen or resting phase. In this phase, the HS exhibits no significant proliferation, apoptosis or differentiation. The transition from telogen to anagen occurs when the bulge stem cells are activated (Cotsaleris and Millar, 2001; Krause and Foitzik, 2006; Alonso and Fuchs, 2006; Ohnemus et al., 2006).

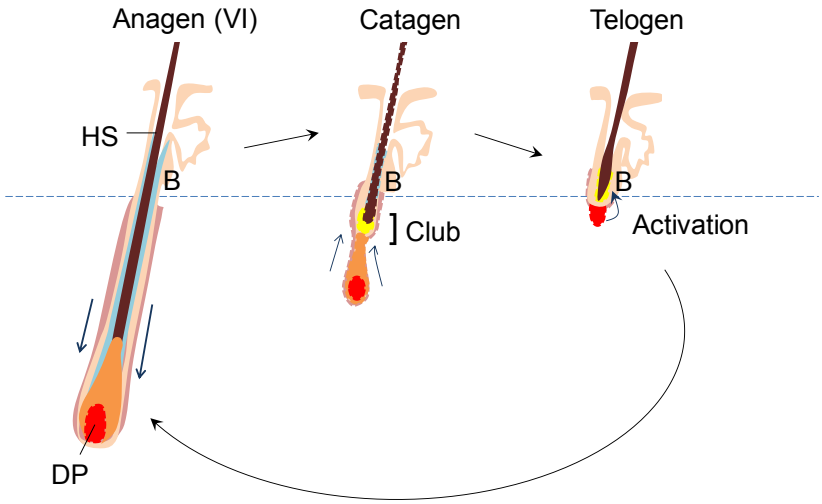

Figure 2. Hair growth cycle. A new hair shaft is produced during anagen, and the old hair is released from the follicle as the new shaft develops. Anagen VI (mature anagen) is the stage where new HS reaches the skin surface and continues to grow through the rest of anagen. During catagen, the lower two thirds of the epithelial follicle are regressed. The hair develops a club structure, which retains the hair in the follicle. Then, the follicle enters a telogen phase until a new growth cycle is activated. Abbreviations: B, bulge; DP, dermal papilla; HS, hair shaft.

Chemotherapy-Induced Alopecia

CIA or hair loss caused by chemotherapy is the most common cutaneous side effect of chemotherapy. CIA ranks among patients as a severe side effect that affects their quality of life.

1. Impact on cancer therapy

CIA has an enormous psychological and social impact on patients, which can be summarized as: (i) symbol of cancer for self (constant reminder of their treatment) and others (outwardly visible); (ii) personal confrontation of being ill or mortality; (iii)

vulnerability; (iv) powerlessness; (v) shame; (vi) loss of privacy; (vii) punishment, and (viii) change in self and other perception (Freedman, 1994; Pozo-Kaderman et al., 1999). Female and children have more difficulties coping with the CIA. Indeed, up to 8% of women are reported to reject chemotherapy for fear of CIA (Mundstedt et al., 1997; McGarvey et al., 2001). CIA also results in reduced social activities since hair partly plays a role in social and sexual communications (Batchelor, 2001). Additionally, these negative impacts of CIA may contribute to poor therapeutic outcome, as stress and depression lowers the body's immune function and is highly associated with cancer progression (Spiegel and Giese-Davis, 2003; O'Leary, 1990).

2. Pathophysiology

The basic principle of chemotherapy is to impair the mitotic and metabolic process of cancer cells. Unfortunately, certain normal cells and tissues with rapid metabolic and mitotic rates such as the hair follicles are also affected by the chemotherapy. Up to 90% of hair follicles undergo anagen, an active growth phase, at a given time. The rapid hair growth as well as the high blood flow rate around the hair bulb leading to the accumulation of drugs is a key predisposing factor for rapid and extensive alopecia (Batchelor, 2001). In humans, CIA usually begins approximately 2 to 4 weeks and is complete at 1 to 2 months after the initiation of chemotherapy (Batchelor, 2001). Hair might be easily depilated as early as 1 to 2 weeks after the treatment due to the weakening and breakage of hair shaft. The hair would fall out upon combing and in the bedding area. CIA becomes obviously noticeable after the loss of more than 50% of existing hair (Fig. 3).

Figure 3. Chemotherapy-induced alopecia (Trueb, 2009)

The degree of CIA depends on the type of chemotherapy, dosage regimen and route of administration. Almost all chemotherapies cause alopecia but with varying degrees of severity and frequency (Apisanthanarax and Duvic, 2003) as summarized in Table 1.

Table 1 Chemotherapeutic agents associated with alopecia

More common or severe		**Less common or severe**	
Bleomycin	Cyclophosphamide	Amscarine	Busulfan
Cytarabine	Cisplatin	Carmusine	Chlorambucil
Dacarbazine	Dactinomycin	Carboplatin	Epirubicin
Docetaxel	Doxorubicin	Gemcitabine	Hydroxyurea
Etoposide	Fluorouracil	Interleukin-2	Melphalan
Idarubicin	Ifosfamide	Mercaptopurine	Methotrexate
Interferon-α	Irinotecan	Mitomycin	Mitoxantrone
Mechlorethamine	Nitroureas	Procarbazine	Teniposide
Paclitaxel	Thiotepa	Vinorelbine	
Topotecan	Vinblastine		
Vincristine	Vindesine		

A high-dose intravenous chemotherapy is commonly associated with more rapid and extensive alopecia. By contrast, oral therapy at lower doses on a weekly schedule tends to cause less alopecia even though the total dose may be large (Wilkes, 1996). Combination therapy consisting of two or more chemotherapeutic agents normally causes a higher incidence and more severe CIA compared to single agent therapy. Long-term chemotherapy may also result in the loss of pubic, axillary and facial hair.

CIA is usually reversible with the hair regrowth generally occurring 3 to 6 months after the end of treatment. However, in most cases the new hair is grey or differs in color, representing the distortion of pigmentation process. Moreover, the new hair typically exhibits some changes in hair structure and texture, e.g. coarser, slow growth, and reduced density (Wang et al., 2006; Trueb, 2009). Permanent alopecia has been reported but rarely occurs (Batchelor, 2001).

3. Approaches to prevent CIA

Several approaches have been investigated to overcome CIA. These approaches can be broadly classified as physical and pharmacological, as described below.

3.1. Physical prevention

Scalp cooling or hypothermic is the commonly used approach to minimize CIA by application of cold to the scalp using a device (cap) that is pre-cooled in a freezer or exchanges coolant with reservoir. A period of cooling lasts from 5 minutes prior to chemotherapy until an hour or more after the drug administration. Many studies have shown that the efficacy of scalp cooling can range from 0-90% (for review, *see* Grevelman and Breed, 2005). The current hypotheses of the protective

effect are: (i) cooling reduces blood flow to hair follicles by vasoconstriction, resulting in a decrease in the amount of drugs available for uptake; and (ii) cooling decreases cellular metabolism and drug uptake. However, scalp cooling is practically ineffective if the chemotherapeutic agent is administered as a continuous infusion over a prolonged period. Additionally, scalp cooling increases the risk of scalp metastasis, and is therefore contraindicated in patients with hematological malignancies and cutaneous T-cell lymphoma (Dean et al., 1979; Apisanthanarax and Duvic, 2003).

Recent study suggested that heat treatment might be an effective strategy against CIA through the localized activation of stress response protein in hair follicles (Jimenez et al., 2008). Local heat treatment at 48-48.5°C for 20 minutes increases Hsp70 and subsequently protects against CIA in response to etoposide, cyclphosphamide, and taxol in neonatal rats.

3.2. Pharmacological prevention

Currently, there are no FDA-approved drug treatments for CIA but several pharmacological strategies have been proposed. Many of these strategies have shown promising results in animals but their clinical use will require further investigations.

3.2.1. Tumor targeting delivery

Tumor-specific ligands and antibodies have been used to provide targeting ability to drug carriers such as liposomes. Accordingly, these liposomes can protect patients from the side effects of chemotherapy, including hair loss. Examples of the targeting moieties are folate receptor (FR) for ovarian, colorectal, and breast cancer; transferrin for pancreatic cancer; anti-HER2 antibody for breast cancer; anti-CD19 for malignant B cells; anti-GD2 for neuroblastoma and melonoma; and prostate-specific

membrane antigen (PMSA) aptamer for prostate cancer and tumor vascular endothelium (Huges et al., 2001; Yu et al., 2009).

3.2.2. Drug-specific antibodies

MAD11 monoclonal antibody (MAb) is an anti-anthracycline antibody that reacts with doxorubicin and other anthracycline chemotherapeutics. Topical administration of liposomes containing MAD11 MAb was shown to prevent CIA in doxorubicin-treated neonatal rats at the frequency of 31 in 45 rats (Balsari et al., 1994). MAD11 MAb was encapsulated into liposomes to facilitate absorption through the stratum corneum and to delay systemic distribution of the antibody. Topical MAD11 MAb was found to be nontoxic and does not induce systemic activation of cytokines. Thus, topical MAD11-loaded liposomes might be an effective strategy in preventing anthracycline-induced alopecia in cancer patients. However, the advantage of this strategy is limited in combination therapy since the antibody could not react with the other drugs in combination.

3.2.3. Hair growth cycle modifiers

3.2.3.1. Cyclosporin A

Cyclosporine A is an immunosuppressive immunophilin ligand used in the treatment of autoimmune diseases and in post-organ transplantation to reduce patients' graft rejection. The use of cyclosporine A in alopecia originates from its common side effect of excessive hair growth called hypertrichosis. Cyclosporin A induces anagen and inhibits catagen of the hair cycle, leading to the promotion of hair growth under normal and pathologic conditions such as alopecia areata and androgenetic alopecia (Paus et al., 1989; Taylor et al., 1993; Lutz et al., 1994). In

neonatal rats, topical administration of cyclosporine A prevents CIA induced by cyclophosphamide, cytosine arabinoside and etoposide (Hussein et al., 1995). In adult mice given cyclophosphamide, topical or systemic administration of cyclosporine A retards CIA, prevents the progression of damaged hair into telogen, and thus induces faster hair regrowth.

3.2.3.2. AS101

AS101, ammonium trichloro (dioxoethylene-o,o') tellurate, is a synthetic immunomodulator that has been shown to protect mice from hemopoietic damage caused by chemotherapeutic agents such as cyclophosphamide, 5-fluorouracil, doxorubicin and etoposide. In phase II clinical trials, AS101 was shown to reduce severity of CIA in patients with non-small cell lung cancer (NSCLC) receiving a combination therapy of carboplatin and etoposide (Sredni et al., 1996).

3.2.3.3. Minoxidil

Minoxidil is one of the FDA approved drug for the treatment of androgenetic alopecia. Topical minoxidil shortens the telogen phase by inducing the entry of resting hair follicles into the anagen phase, thereby stimulating hair growth (Messenger and Rundegren, 2004). Minoxidil also prolongs the duration of anagen phase and enlarges hair follicles, probably by its proliferative and anti-apoptotic effects on dermal papilla cells (Han et al., 2004). Several studies have also investigated the effect of minoxidil on CIA. In neonatal rats, local injection of minoxidil protects against CIA induced by cytosine arabinoside but not by cyclophosphamide. However, topical minoxidil (2%) does not protect against CIA. In one randomized clinical trial, topical minoxidil (2%) was shown to shorten the duration of CIA in breast cancer patients receiving 5-fluorouracil, doxorubicin, and cyclophosphamide (Duvic et al., 1996).

3.2.4. Cytokines and growth factors

Hair follicle cells express receptors for multiple cytokines and growth factors that regulate hair growth cycle (Trueb, 2002). These regulators include fibroblast growth factors (FGF), transforming growth factors (TGF), insulin-like growth factors (IGF), epidermal growth factors (EGF), interferon and interleukins (Stenn and Paus, 2001). Moreover, hair cycle is regulated by androgens and parathyroid hormone (PTH) (Sawaya, 2001).

IL-1 and ImuVert, a biological response modifier derived from *S. Marcescens*, were reported to protect against CIA induced by cytosine arabinoside and doxorubicin in neonatal rats (Hussesin, 1993). Both agents can induce the release of multiple cytokines and growth factors. It was suggested that the protection of CIA by ImuVert is mediated through IL-1. Similarly, EGF and FGF-1 have been shown to protect against CIA induced by cytosine arabinoside but not by cyclophosphamide in neonatal rats (Jimenez and Yunis, 1992). In contrast, FGF-7 and KGF partially protect against CIA by cytosine arabinoside by retarding hair loss (Danilenko et al., 2000). In organ-culture human scalp hair follicles and HaCaT keratinocytes, KGF protects against the cytotoxicity of mafosfamide, the cell culture active derivative of cyclophosphamide (Braun et al., 2006). The mechanism of action of KGF has been proposed to involve specific signaling pathways including PI3K and ERK1/2.

PTH antagonists reduce cell apoptosis in the hair bulb matrix and delay the onset of CIA in adult mice, whereas PTH agonists enhance the apoptosis and accelerate hair regrowth after CIA. However, neither PTH agonists nor antagonists prevent CIA (Peters et al., 2001).

3.2.5. Antioxidants

Broad spectrum antioxidant *N*-acetyl cysteine (NAC), an analog and precursor of glutathione, when administered topically or parenterally, protects against CIA induced by cyclophosphamide in neonatal rats. In contrast, NAC could not protect adult mice from CIA induced by doxorubicin (Wang et al., 2006).

α-Tocopherol or vitamin E is an important lipid-soluble antioxidant. Several studies have reported the protective effect of high-dose vitamin E in patients receiving doxorubicin; however, conflicting results have also been reported. For example, a clinical study reported that 69% of the patients did not experience CIA when co-treated with vitamin E, while others reported no protective effect of vitamin E (Batchelor, 2001).

3.2.6. Cell cycle or proliferation modifiers

Rapid proliferation of keratinocytes during the anagen phase of hair follicle is one the main predisposing factors of CIA. Thus, one approach to protect against CIA is to arrest the cell cycle and inhibit cell proliferation.

3.2.6.1. Calcitriol

Multiple effects of calcitriol (1,25-dihydroxyvitamin D3) on keratinocytes, i.e., inhibition of DNA synthesis, G0/G1 cell cycle arrest, and induction of cell differentiation, have been reported (Kobayashi et al., 1998; Wang et al., 2006). Thus, it is likely that calcitriol induces changes in keratinocyte proliferation and/or terminal differentiation, subsequently altering cellular susceptibility to apoptosis. In neonatal rats, topical administration of calcitriol reduces CIA induced by cyclophosphamide, etoposide, and a combination treatment of cyclophosphamide and doxorubicin (Jimenez and Yunis., 1992). In adult mice receiving cyclophosphamide, topical

calcitriol however fails to prevent or retard CIA, but somehow reduces massive apoptosis of hair matrix keratinocytes, a key feature of CIA, and enhances the regrowth of normal hair shaft. (Paus et al., 1996; Schilli et al., 1998). In humans, calcitriol has a protective effect against CIA induced by paclitaxel (Jimenez and Yunis, 1996), but not by a combination of 5-fluorouracil, doxorubicin and cyclophosphamide (Hidalgo et al., 1999).

3.2.6.2. CDK2 inhibitor

Cyclin-dependent kinase 2 (CDK2) is a member of the serine/threonine protein kinase family that plays a key role from late G1 to late G2 of the cell cycle. Potent small inhibitors of CDK2 have been synthesized and tested for their effect on CIA. One of these synthetic inhibitors was shown to inhibit the progression from late G1 into S phase in human diploid fibroblasts and also inhibit apoptosis induced by etoposide, 5-fluorouracil, taxol, cisplatin and doxorubicin. In neonatal rats, topical application of the inhibitor reduces hair loss at the site of application in 50% of the rats having etoposide-induced CIA and in 33% of the rats with CIA induced by cyclophosphamide and doxorubicin (Davis et al., 2001). Histological examinations of the skin from etoposide-treated rats show that the inhibitor increases the number of viable hair follicles and dermal papilla, reduces the level of inflammation and amount of damage to epithelium, reduces the thickening of epidermis and decreases the number of apoptotic cells in the hair follicle matrix. However, in subsequent studies the authors reported that they were unable to reproduce the results in the neonatal rat model (Davis et al., 2002), thus the use of this inhibitor in CIA becomes questionable, although the idea of using CDK2 inhibitors is still ongoing.

3.2.7. Inhibitor of apoptosis

3.2.7.1. Caspase-3 inhibitor

Various chemotherapeutic agents induce apoptosis of hair follicle cells and cause CIA, although the underlying mechanisms are unclear. Caspase-3 is a key executor of apoptosis and its activation is normally used as an indicator of caspase-dependent apoptosis (Porter and Janicke, 1999). M50054, 2,2'-methylenebis, is an inhibitor of caspase-3 activation that was shown to inhibit etoposide-induced apoptosis in human monocytes. In neonatal rats, topical administration of M50054 reduces CIA induced by etoposide (Tsuda et al., 2001).

3.2.7.2. Anti-death FNK protein

FNK protein constructed from rat Bcl-xL by site-directed mutagenesis (Y22F/Q26N/R165K) localizes to mitochondria and functions to maintain mitochondrial membrane potential (Aosh et al., 2000). Mitochondrial membrane potential regulates the release of cytochrome C, which once binds to caspase-activating proteins such as Apaf-1 initiates the intrinsic caspase cascade and apoptosis (Li et al., 1997). Recently, FNK protein has been fused to protein transduction domain (PTD) to improve its cellular entry. Subcutaneous injection of PTD-FNK protects against CIA induced by etoposide in the neonatal rat model. The fusion protein helps retain hair follicle structures, prevent hair follicle regression and maintain the anagen duration upon etoposide treatment (Nakashima-Kamimura et al., 2008). Indeed, its protective effect on CIA suggests that it could penetrate the epidermis and reach the dermal hair follicles. Localized administration of FNK fusion protein has been suggested as a potential protein therapy for CIA without affecting the chemotherapy efficacy.

4. Current understanding in mechanisms of CIA

Molecular mechanisms of CIA are not well understood, in part due to the lack of appropriate experimental models that mimic human CIA. Much of our understanding on CIA is based on adult mouse model given cyclophosphamide.

4.1. DNA damage

Most chemotherapeutic agents including cyclophosphamide, doxorubicin and cisplatin induce DNA damage and kill both normal and cancer cells by apoptosis (Muller et al., 1998). p53 is a transcription factor and tumor suppressor protein that plays a critical role in cell cycle progression and apoptosis. Activation of p53 in response to DNA damage is associated with the degradation of Mdm2/p53 complex, leading to increased availability of p53 to bind DNA and consequently transcriptional activation of p53 target genes. Many p53 target genes, including Fas, Bax, Bcl-2, insulin-growth factor receptor type I (IGFR1), and insulin-like growth factor binding protein 3 (IGF-BP3), are expressed in the hair follicles (Lindner et al., 1997). In the adult mice, p53 was shown to be essential in the hair follicle response to DNA damage induced by cyclophosphamide. Specifically, hair loss was not observed and hair follicle cells remained active in p53-deficient mice, as shown by a large volume of hair bulb and dermal papilla, and active keratinocyte proliferation in the hair matrix (Botchkarev et al., 2000).

4.2. Apoptosis

Chemotherapy-induced apoptosis of hair follicle cells is one of the major findings from CIA animal studies. In adult mice, cyclophosphamide-treated hair follicles show a strong up-regulation of p53 in the hair matrix, particularly in TUNEL-positive apoptotic keratinocytes (Botchkarev et al., 2000). By contrast, in

p53-deficient mice, apoptosis in the matrix keratinocytes was not detected after cyclophosphamide treatment, indicating the involvement of p53 in the apoptotic process. The precise mechanism of p53-dependent apoptosis in the hair follicles remains unclear, but likely involves several p53 target genes. Cyclophosphamide-treated p53-deficient mice show strongly down-regulated Fas in the hair follicle keratinocytes and highly up-regulated Bcl-2 in the dermal papilla as compared to wild-type mice. The role of Fas in the control of cyclophosphamide-induced apoptosis in keratinocytes was also investigated using Fas-deficient mice (Sharov et al., 2004). These mice show significantly reduced CIA and a parallel decrease in apoptotic keratinocytes and FADD and caspase-8 expression. Similarly, anti-Fas ligand neutralizing antibody inhibits cyclophosphamide-induced keratinocyte apoptosis. These studies indicate that Fas signaling is an important pathway in mediating the apoptosis induced by cyclophosphamide and suggest the cross-talk between p53 and Fas death signaling. However, the eventual hair loss observed in Fas-deficient mice points to the lower resistance of hair follicles to cyclophosphamide as compared to p53-deficient mice. Thus, it is likely that Fas signaling represents only a component of the p53-dependent apoptosis machinery in the hair follicles and that other p53 targets are also involved. Cyclophosphamide treatment also alters the expression of melanogenic proteins and causes apoptosis of hair follicle melanocytes (Sharov et al., 2003). In contrast to matrix keratinocytes, the melanocytes undergo apoptosis primarily through Fas signaling but not p53 signaling. These findings suggested the cell-type dependent mechanisms of apoptosis. Furthermore, depending on treatments, p53- and Fas-independent mechanisms may also be involved in mediating hair follicle responses, as in the case of cisplatin- and doxorubicin-induced tumor cell apoptosis (Zamble et al, 1998; Tsang et al, 2003). Notably, chemotherapy-induced apoptosis is

not restricted only on the rapidly proliferating hair matrix keratinocytes, but also affects the hair follicle mesenchyme including dermal papilla fibroblasts (Bodo et al., 2007).

4.3. Reactive oxygen species

The observation that antioxidants such as NAC protect against CIA in animals suggest the involvement of reactive oxygen species (ROS) in CIA. Various chemotherapeutic agents induce oxidative stress through multiple mechanisms, i.e., activation of NADPH oxidase system and mitochondrial respiration chain. Agents that induce a high level of ROS include anthracyclines (e.g., doxorubicin, epirubicin, and daunorubicin), alkylating agents (e.g., cyclophosphamide), platinum coordination complexes (e.g., cisplatin, carboplatin, and oxaliplatin), and epipodophyllotoxins (e.g., etoposide) (Conklin, 2004). Interestingly, anthracyclines, alkylating agents, platinum complexes, and epipodophyllotoxins also induce CIA more frequently and more severely than most other agents, suggesting a relationship between ROS generation and CIA. The exact mechanism of how ROS induces or promotes CIA is unclear, but likely involves apoptosis regulation since apoptosis of hair follicles is a hallmark of CIA and since ROS generation is generally required for the induction of apoptosis by chemotherapeutic agents (Simon et al., 2000).

Reactive Oxygen Species

ROS have been identified as signaling molecules in various pathways regulating cell proliferation and cell death (Hancock et al., 2001; Droge, 2002; Valko et al., 2006). The level of intracellular ROS is determined by the balance of ROS-

generating system and antioxidant defense system. Thus, the changes in either system could lead to the alteration in cellular responses.

1. Source of ROS

Mitochondria are the major endogenous source of ROS production in living organisms. In order to minimize the oxidative stress in organelle, mitochondrial membranes are highly enriched with antioxidants including glutathione (GSH), superoxide dismutase (SOD), and glutathione peroxidase (GPx). Besides mitochondria, ROS might produce from endogenous cytochrome P450 metabolism, xanthine oxidase, and peroxisomes. In addition, exogenous substances, e.g. UV and ionizing radiation, chemotherapy, chemical irritants and mitochondrial toxins, can directly generate or indirectly induce ROS generation inside the cells.

2. Biochemical of ROS and antioxidants

ROS is primarily generated either by metabolic process or following oxygen activation by physical irradiation as superoxide anion ($O_2^{\bullet-}$). The reaction is catalyzed by NADPH oxidase with electron supplied by NADPH as in the equation below:

$$O_2 + e^- \longrightarrow O_2^{\bullet-}$$

$$2O_2 + NADPH \longrightarrow 2O_2^{\bullet-} + NADP^+ + H^+$$

Superoxide then undergoes a dismutation, a reaction of which accelerates by SOD enzyme, generating less-reactive species hydrogen peroxide (H_2O_2):

$$2O_2^{\bullet-} + 2H^+ \xrightarrow{SOD} H_2O_2 + O_2$$

The H_2O_2-removing enzymes include catalase and glutathione peroxidase:

$$H_2O_2 \xrightarrow{catalase} 2H_2O + O_2$$

$$2GSH + H_2O_2 \xrightarrow{GPx} GSSG + 2H_2O$$

Superoxide may react with H_2O_2 and form the highly reactive hydroxyl radical ($^{\bullet}OH$) by Haber-Weiss reaction:

$$O_2^{\bullet-} + H_2O_2 \longrightarrow O_2 + {}^{\bullet}OH + OH^-$$

Since the Haber-Weiss reaction is kinetically slow, transition metals such as iron and copper often serve as its catalysts. The iron-catalyzed Haber-Weiss reaction is called Fenton reaction:

$$Fe(II) + H_2O_2 \longrightarrow Fe(III) + {}^{\bullet}OH + OH^-$$

Under stress conditions, $O_2^{\bullet-}$ facilitates the release of free iron from iron-containing molecules, for example, [4Fe-4S]-containing enzymes, leading to the generation of $^{\bullet}OH$ from Fenton reaction. Moreover, $O_2^{\bullet-}$ can facilitate the $^{\bullet}OH$ production in the reaction by generating Fe(II) from the reduction of Fe(III):

$$Fe(III) + O_2^{\bullet-} \longrightarrow Fe(II) + O_2$$

Cisplatin

Cisplatin (*cis*-diamminedichloroplatinum II), a platinum coordination complex, is a widely prescribed anticancer agent against various cancers including lung, ovarian, and breast cancers (Torri et al., 2000; Arriagada et al., 2004). Mechanisms of action of cisplatin-induced cell death are accepted to involve DNA-adduct formation as well as reactive oxygen species (ROS) induction. Cisplatin are among those of chemotherapies that generate high level of ROS (Conklin, 2004). The intracellular ROS generation-induced by cisplatin has been demonstrated to implicate in its serious side effects, such as ototoxicity and nephrotoxicity (Jiang et al., 2007; Rybak et al., 2007; Pabla and Dong, 2008).

Cisplatin-induced ROS generation might result from: (i) direct binding of cisplatin to sulfhydryl group, which is an essential moiety within the enzymes including glutathione, a well-known cellular antioxidant; (ii) the induction of mitochondrial dysfunction and ROS production via disrupted respiratory chain; and (iii) the induction of cytochrome P450 system, which is a major source of catalytic iron for ROS generation in microsomes (Rybak et al., 2007; Pabla and Dong, 2008).

Doxorubicin

Doxorubicin, an anthracycline antibiotic, is a potent broad spectrum chemotherapeutic agent that is highly effective for treatment of several malignancies and solid tumors, for example, lung cancer, breast cancer, ovarian cancer and prostate cancer (Minotti et al., 2004). The cytotoxic modes of action of doxorubicin are still unclear. However, there are good evidence suggested that it may act as a topoisomerase II poison which perturbs the re-ligation step of topoisomerase II as well as the action through formation of DNA adduct (Cutts et al., 2005). In addition, doxorubicin was reported to induce ROS generation in various tumor cells indicating that ROS might play an important role in doxorubicin-induced tumor cell death (Wang et al., 2004).

Oxidative stress-induced by doxorubicin was previously found to be associated with its injuries to non-targeted tissues, such as heart, kidney and brain (Tsang et al., 2003; Chen et al., 2007). The redox cycling of doxorubicin is a possible mechanism of ROS generation. In the presence of NADPH, the quinone moiety of doxorubicin is transformed into a semiquinone via one electron reduction. Then semiquinone regenerates its parent quinone by reacting with oxygen, and

consequently produces free radical superoxide anion ($O_2^{\cdot-}$). Superoxide anion could be further changed to hydrogen peroxide (H_2O_2), hydroxyl radical ($^{\cdot}OH$) or reactive nitrogen species (RNS) (Fig. 4).

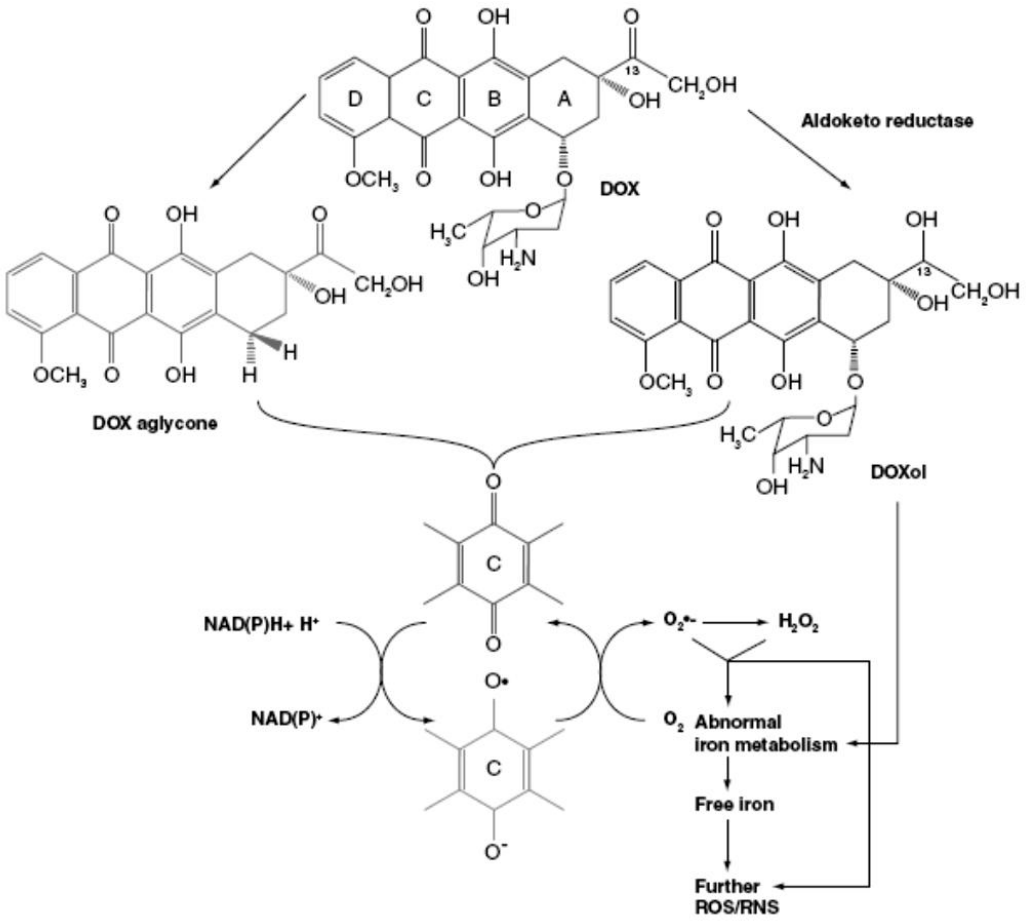

Figure 4. Doxorubicin-induced ROS generation pathway (Chen et al., 2007).

Apoptosis

Apoptosis or programmed cell death plays an important role in various physiological processes including hair follicle morphogenesis and hair cycling as well as chemical-induced cell death. Inappropriate apoptosis, either too little or too much, could contribute to human disorders, such as degenerative diseases and cancer.

Apoptotic cell is morphologically characterized by cell shrinkage, membrane blebbing, nuclear condensation and cellular fragmentation. There are two major signaling pathways of apoptosis, which are mitochondrial (intrinsic) and death receptor (extrinsic) pathways (Fig. 5).

The extrinsic apoptotic pathway is activated when specific death ligands, such as Fas ligand or TNF-α, bind to their membrane receptors. All death receptors contain an extracellular cysteine-rich domain that is required for ligand binding and intracellular death domain (DD) that is essential for initiating the apoptotic signal. Signaling via death receptors result in the recruitment of several adaptor molecules, which contain the death effector domains requiring for the interaction with similar domains of procaspase-8 and procaspase-10 to form complex called death-inducting signaling complex (DISC). DISC activates initiatior caspases (caspase-8 and caspase-10) resulting in the activation of effector caspases (caspase-3, -6 and -7). Caspase-8 may also activate the cytoplasmic protein Bid, which after its translocation to the mitochondrial induces release of cytochrome C, thus linking the extrinsic and intrinsic apoptotic pathway (Ashkenazi and Dixit, 1998; Gupta, 2003; Botchkareva et al., 2006).

The intrinsic apoptotic pathway is activated in response to a variety of apoptotic signals, including oxidative stress and DNA damage leading to mitochondria depolarization and the release of cytochrome C. The intrinsic pathway is controlled by balance of Bcl-2 protein family, which is divided into anti-apoptotic protein, e.g. Bcl-2, Bcl-X_L and Mcl-1, and pro-apoptotic protein, e.g. Bax, Bak, Bok, Bim, Bik, Bad and Bid. In addition, Bim, Bad and Bid may serve as sensors for cellular integrity and the growth factor supply. Cytochrome C binds to caspase adaptor molecule Apaf-1 and recruits procaspase-9 to form a complex called

apoptosome. Apoptosomes then promote the formation of effector caspases to induce apoptosis (Gupta, 2003; Botchkareva et al., 2006; Ruwanpura et al., 2010).

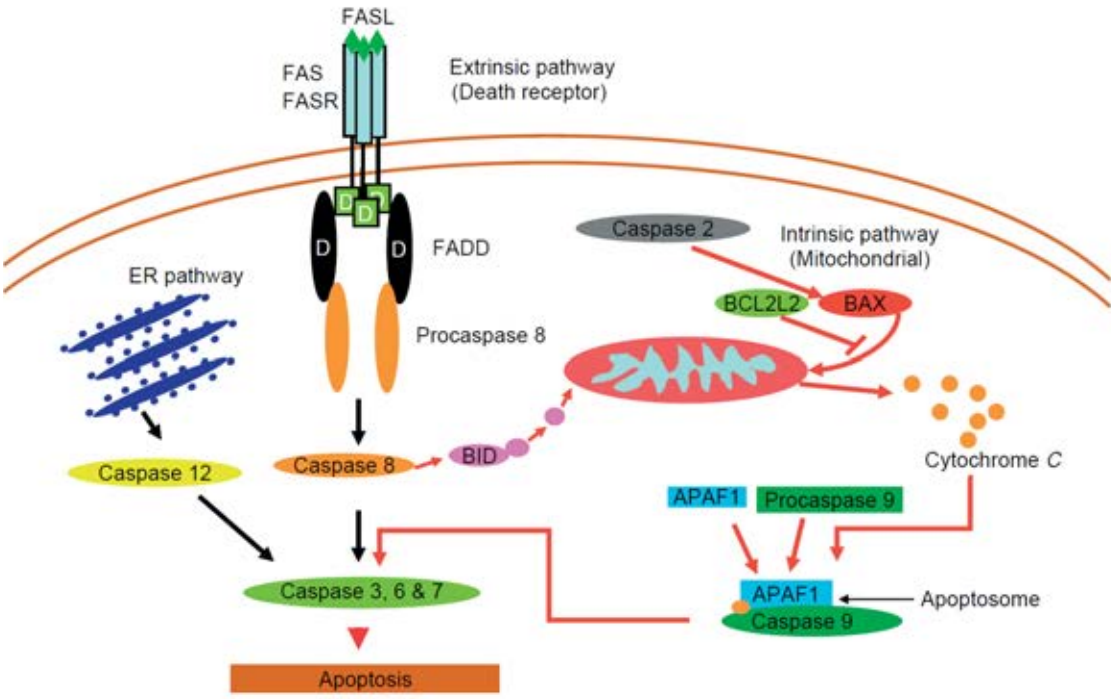

Figure 5. Molecular mechanisms of apoptotic process. Scheme demonstrates integration of the molecules involved in the control of various phases of apoptosis, which are initiation stage, intracellular response, cell fragmentation and phagocytosis (Ruwanpura et al., 2010).

It is worthy of note that tumor suppressor protein p53 plays a pivotal role in cell apoptosis. Pro-apoptotic activity of p53 was previously found to correlate with its ability to function as a transcription factor. p53 can induce the transcription of some BH3-only pro-apoptotic protein in Bcl-2 family, such as Bax, Bid, Noxa or PUMA, which regulate the mitochondrial membrane integrity. In addition, p53 may directly impact Bcl-2 activity in a transcription-independent manner. Cytoplasmic p53 may act like BH3-only protein of Bcl-2 family and antagonize Bcl-2 function, leading to

permeabilization of mitochondria and apoptosis (Hemann and Lowe, 2006; Vousden and Lane, 2007).

Protein Degradation

Protein degradation plays an important part in various cellular processes including DNA repair, cell cycle control, stress response, and apoptosis. Two mechanisms for intracellular protein degradation have been proposed; lysosomal and ubiquitin-proteasome protein degradation.

1. Lysosomal protein degradation

Lysosome, a vascuolar structure that contains various hydrolytic enzymes, is generally produced in Golgi apparatus for degradation of ingested product. Lysosome is responsible for the digestion of exogenous proteins and particles, as well as the digestion of endogenous proteins and cellular organelles (Fig. 6). The process for endogenous protein and cellular organelle degradations are called microautophagy and macroautophagy, respectively. Microautophagy refers to the engulfment of endogenous protein into lysosomes by direct invagination of the lysosomal membrane. Whereas steps for macroautophagy are briefly described as: (i) a surrounding of targeted organelle by particular membrane, and (ii) the fusion of this membrane and lysosome, forming an autophagic vacuole. The lysosome then safely releases its enzyme contents into this vacuole, thereby destroying its target. The lysosomal enzymes, e.g. cystein proteases (cathepsins), aspartate proteases and zinc protease, are specifically synthesized by endoplasmic reticulum and are activated in lysosome at an acidic pH (Ciechanover, 2005; Hideshima et al., 2005).

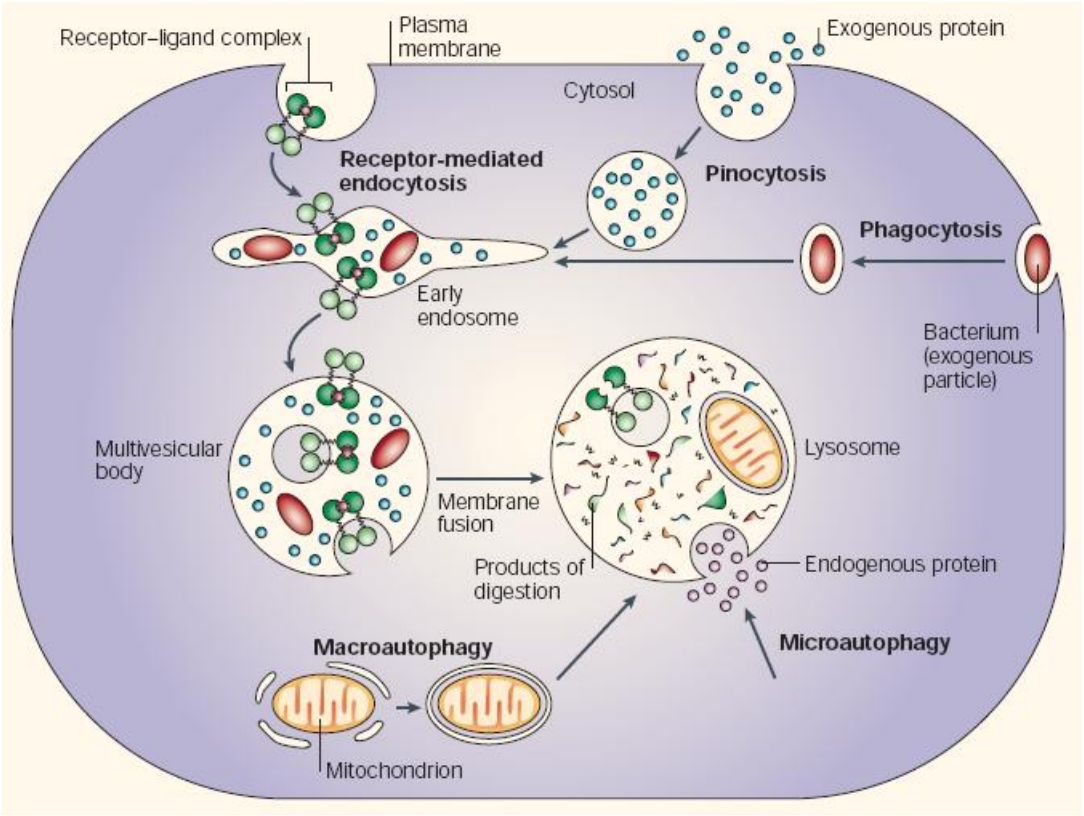

Figure 6. The many functions of lysosome (Ciechanover, 2005).

2. Ubiquitin-mediated protein degradation

Ubiquitin (Ub) is a highly conserved small protein composed of 76 amino acids. The polyubiquitin chain, attachment of multiple copies of Ub, functions as a recognition signal for degradation of protein by the 26S proteasome. Degradation of Ub-proteasomal pathway, the major nonlysosomal proteolytic system in the cytosol and nucleus of eukaryotic cells, is a multiple step process. In brief, free Ub is initially activated in an ATP-dependent manner to a high-energy thiol ester intermediate by a Ub-activating enzyme (E1). Then E1 transfers Ub to Ub-conjugating enzymes (E2), which directly ubiquitinate substrate proteins. Finally, Ub-ligases E3 enzymes function in cooperation with E2 enzymes to attach the small Ub moiety to lysine residue of acceptor proteins. E2 and/or E3 enzymes also catalyze the formation of polyubiquitinated conjugates. The polyubiquitinated protein is then subjected to the

Ub receptor subunit within the 19S complex of the 26S proteasome, resulting in the degradation of substrates to short peptides by the 20S complex (Ciechanover, 2005; Hideshima et al., 2005; Lecker et al., 2006) (Fig. 7).

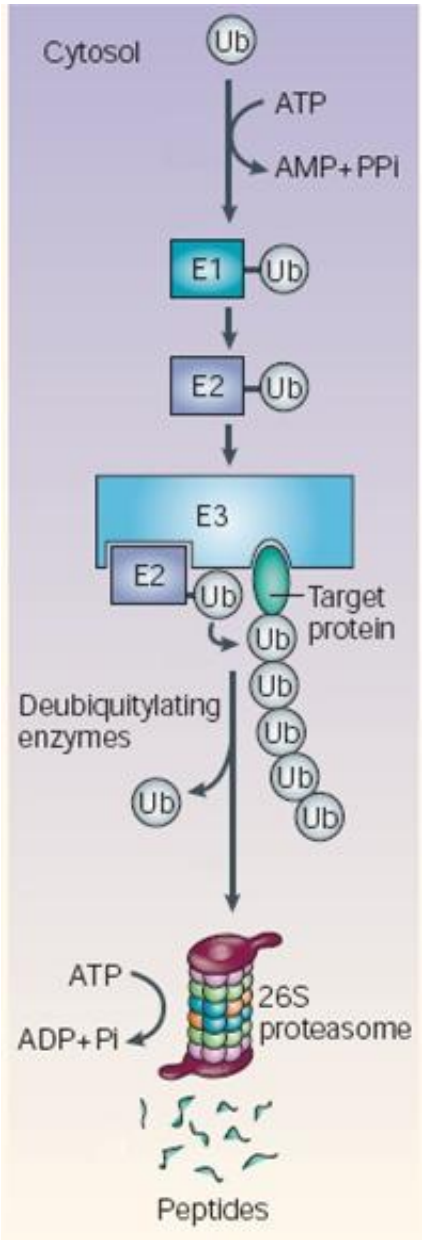

Figure 7. The ubiquitin-proteasomal pathway (Ciechanover, 2005).

CHAPTER III

MATERIALS AND METHODS

Materials

1. Cell culture

Human hair follicle dermal papilla cells (HFDPC) are obtained from PromoCell (Heidelberg, Germany). The cells were cultured in HFDPC cell growth medium (PromoCell) containing 100 units/ml of penicillin and 100 μg/ml of streptomycin (Gibco, Gaithersburg, MA, USA) in a 5% CO_2 environment at 37 °C. Human keratinocyte HaCaT cells were obtained from Cell Lines Service (Heidelberg, Germany) and maintained in Dulbecco's modified Eagle's medium (DMEM; Gibco, Gaithersburg, MA, USA) supplemented with 2 mmol/l L-glutamine and 10% fetal bovine serum (Gibco, Gaithersburg, MA, USA) in a 5% CO_2 at 37 °C.

2. Reagents

cis-diammine-dichloroplatinum II (CDDP, cisplatin), 3-(4,5-Dimethylthiazol-2-yl)-2,5-diphenyltetrazolium bromide (MTT), *N*-acetylcysteine (NAC), reduced glutathione (GSH), sodium formate, uric acid, lactacystin, and antibody for ubiquitin were obtained from Sigma Chemical, Inc. (St. Louis, MO, USA). Hoechst 33342, prodidium iodide (PI), dichlorofluorescein diacetate (H_2DCF-DA), dihydroethidium (DHE) and Mitosox^{TM} were obtained from Molecular Probes, Inc. (Eugene, OR, USA). Doxorubicin, Mn(III)tetrakis(4-benzoic acid)porphyrin chloride (MnTBAP), and concanamycin A, PD98059 (MAP kinase ERK1/2 inhibitor), SP600165 (c-Jun N-terminal kinase inhibitor), and SB203580 (p38 MAP kinase inhibitor) were obtained

from Calbiochem (EMD Biosciences, Inc., La Jolla, CA, USA). Caspase inhibitor benzyloxycarbonyl-Val-Ala-Asp-(OMe) fluoromethyl ketone (zVAD-fmk) was obtained from Alexis Biochemicals (San Diego, CA). Hydroxyphenyl fluorescein (HPF) was obtained from Cell Technology (Mountain View, CA). Antibody for Bcl-2 and protein G-conjugated agarose were obtained from Santa Cruz Biotechnology (Santa Cruz, CA). Antibodies for Bax, caspase-3, MAP kinase signaling; ERK1/2 (p44/p42 and phospho-p44/p42), p38 (p38 and phospho-p38), and JNK1/2 (JNK and phospho-JNK), β-actin, and peroxidase conjugated secondary antibodies were obtained from Cell Signaling Technology (Boston, MA).

3. Plasmids and transfection

Bcl-2 and manganese superoxide dismutase (MnSOD) plasmids were generously provided by Dr. C. Stehlik (Northwestern University, School of Medicine, Chicago, IL) and Dr. X. Shi (University of Kentucky, School of Medicine, Lexington, KY), respectively. Authenticity of the plasmid construct was verified by DNA sequencing. HaCaT cells were transfected with Bcl-2, MnSOD or pcDNA3 control plasmid by nucleofection using Amexa Biosystems Nucleofector (Cologne, Germany), according to the manufacturer's instruction. Briefly, cells were suspended in 100 μl of nucleofection solution with 2 μg of plasmid and nucleofected using the device program U020. The cells were then resuspended in 500 μl of complete medium and seeded in 60-mm cell culture dish. Cells were allowed to recover for 72 h before each experiment. The efficiency of transfection was determined by using a GFP reporter plasmid and was found to be approximately 85%.

Methods

1. Sample preparation

Stock solution of cisplatin was freshly prepared in PBS containing 5% dimethylsulfoxide (DMSO) at a concentration of 1 mg/ml prior to use. Doxorubicin was dissolved in the distilled water to prepare the stock solution of 150 μM. Stock solution of doxorubicin would be stable at 4°C for a month. As per calculation, stock solution was added into the cell culture medium to the desired final concentration.

2. Drug treatment

Cells at approximately 90% confluence were treated with cisplatin or doxorubicin for indicated time. To determine the role of apecific ROS in the process, cells were pretreated for 30 min with various specific ROS scavengers, including catalase (hydrogen peroxide scavenger), MnTBAP (MnSOD mimetic and superoxide anion scavenger), and sodium formate (hydroxyl radical scavenger) or dimethythiourea (hydroxyl radical scavenger), followed by the drug treatment.

3. Cytotoxicity assay

Cytotoxicity was determined by MTT colorimetric assay. After specific treatments, cells in 96-well plate were incubated with 500 μg/ml of MTT for 4 h at 37°C. The intensity of the formazan product was measured at 550 nm using a microplate reader. Relative cell viability was calculated by dividing the absorbance of treated cells by that of the non-treated cells in each experiment.

4. Apoptosis assay

Apoptosis was determined by Hoechst 33342 DNA fragmentation assay. Briefly, cells were incubated with 10 μg/ml of Hoechst 33342 for 30 min and analyzed for apoptosis by scoring the percentage of cells having intensely condensed chromatin and/or fragmented nuclei by fluorescence microscopy (Leica Microsystems, Bannockburn, IL). Approximately 1,000 nuclei from ten random fields were analyzed for each sample. The apoptotic index was calculated as the percentage of cells with apoptotic nuclei over total number of cells. Necrosis cells were determined by propodium iodide (PI) assay (5 μg/ml).

5. ROS detection

ROS generation was determined by flow cytometry using dichlorodihydrofluorescein diacetate (H_2DCF-DA) as a general oxidative probe and dihydroethidium (DHE) as a superoxide probe. Briefly, cells were incubated with the probe (10 μM) for 30 min at 37°C, after which they were washed and resuspended in phosphate-buffered saline (PBS) and immediately analyzed for dichlorofluorescein (DCF) intensity using a 485-nm excitation beam and a 538-nm band-pass filter, or for DHE intensity using a 488-nm excitation beam and a 610-nm band-pass filter (FACSort, Becton Dickinson, Rutherford, NJ). The mean fluorescence intensity was quantified by CellQuest software (Becton Dickinson) analysis of the recorded histograms. H_2DCF-DA and DHE dyes were also utilized in the ROS detection using fluorescence microplate reader (time course measurements) and fluorescence microscopy.

Generation of highly reactive oxygen species (hROS) was determined according to the method previously described (Setsukinai et al., 2003) using

hydroxyphenyl fluorescein (HPF) as a probe. Briefly, cells were incubated with the probe (10 μM) for 1 h at 37°C, after which they were washed, resuspended in Hank's buffered salt solution (HBSS) and analyzed for fluorescence intensity using a fluorescence plate reader at a 485-nm excitation and a 520-nm emission (FLUOstar OPTIMA, BMG Labtech, Durham, NC).

Electron spin resonance (ESR) measurements, using 5,5-dimethyl-1-pyrroline-N-oxide (DMPO) as a spin trapping agent, were performed to identify specific ROS. Cells were incubated with the DMPO (10 mM) for 5-10 min at 37°C in the presence or absence of specific ROS scavengers to aid characterization of the generated free radicals. The ESR signals were measured using a Bruker EMX spectrometer (Bruker Instruments, Billerica, MA) and a flat cell assembly. Hyperfine couplings were measured (to 0.1 G) directly from magnetic field separation using potassium tetraperoxochromate and 1,1-diphenyl-2-picrylhydrazyl as reference standards. An Acquisit program (Bruker Instruments) was used for data acquisition and analysis.

6. Mitochondrial superoxide detection

Mitochondrial superoxide anion was detected by fluorescence microscopy using MitoSOX^{TM} Red as a specific fluorescent probe. Briefly, cells were incubated with 5 μM of the probe for 30 min at 37°C in dark. They were then washed thoroughly with warm HBSS buffer and mounted for imaging. MitoSOX^{TM} Red was visualized under an excitation wavelength of 546 nm and an emitter band pass of 605 nm.

7. Caspase activity assays

Caspase activity was determined by using APO LOGIX carboxyfluorescein caspase detection kit (Cell Technologies, Minneapolis, MN), according to the manufacturer's instructions. After specific treatments, cells were incubated with 10 µl of 30x FAM-DEVD-fmk, FAM-LETD-fmk, or FAM-LEHD-fmk for 2 h in dark for caspase-3, -8, or -9 activity, respectively. Cells were washed with 1x Working Dilution Wash buffer which was supplied with the kit. The fluorescence signals were measured using a fluorescence microplate reader at the excitation and emission wavelengths of 488 and 520 nm, respectively. Caspase activity was expressed as the ratio of fluorescence signal from the treated and control samples.

8. Western blot analysis

After specific treatments, cells were incubated with lysis buffer containing 20 mM Tris-HCl (pH 7.5), 1% Triton X-100, 150 mM NaCl, 10% glycerol, 1 mM Na_3VO_4, 50 mM NaF, 100 mM phenylmethylsulfonyl fluoride, and a commercial protease inhibitor mixture (Roche Molecular Biochemicals) at 4°C for 20 min. Cell lysates were collected and determined for protein content using the Bradford method (Bio-Rad Laboratories, Hercules, CA). Proteins (40 µg) were resolved under denaturing conditions by 10% sodium dodecyl sulfate-polyacrylamide gel electrophoresis (SDS-PAGE) and transferred onto nitrocellulose membranes (Bio-Rad). The transferred membranes were blocked for 1 h in 5% nonfat dry milk in TBST (25 mM Tris-HCl, pH 7.4, 125 mM NaCl, 0.05% Tween-20) and incubated with appropriate primary antibodies at 4°C overnight. The membranes were washed twice with TBST for 10 min and incubated with horseradish peroxidase-conjugated secondary antibodies for 1 h at room temperature. The immune complexes were

detected by chemiluminescence detection system (Amersham Biosciences, Piscataway, NJ) and quantified using analyst/PC densitometry software (Bio-Rad Laboratories, Hercules, CA).

9. Immunoprecipitation

After specific treatments, cells were washed with PBS and lysed in lysis buffer at 4°C for 20 min. The lysates were collected and determined for protein content using the Bradford method. Cell lysates (60 μg protein) were incubated with anti-Bcl-2 antibody at 4°C for 14 h, followed by incubation with protein G-conjugated agarose for 4 h at 4°C. The immune complexes were washed 6 times with cold lysis buffer and resuspended in 2x Laemmli sample buffer. The immune complexes were separated by 10% SDS-PAGE and analyzed by Western blotting as described.

10. Statistical analysis

The data represent means ± S.D. from three or more independent experiments. ANOVA and unpaired Student's *t* test was used to determine differences between treatment groups. *p* value less than 0.05 indicated statisitical significance.

Experimental Design

To provide an overview of the study, scheme representing sequential experiments was first covered as below:

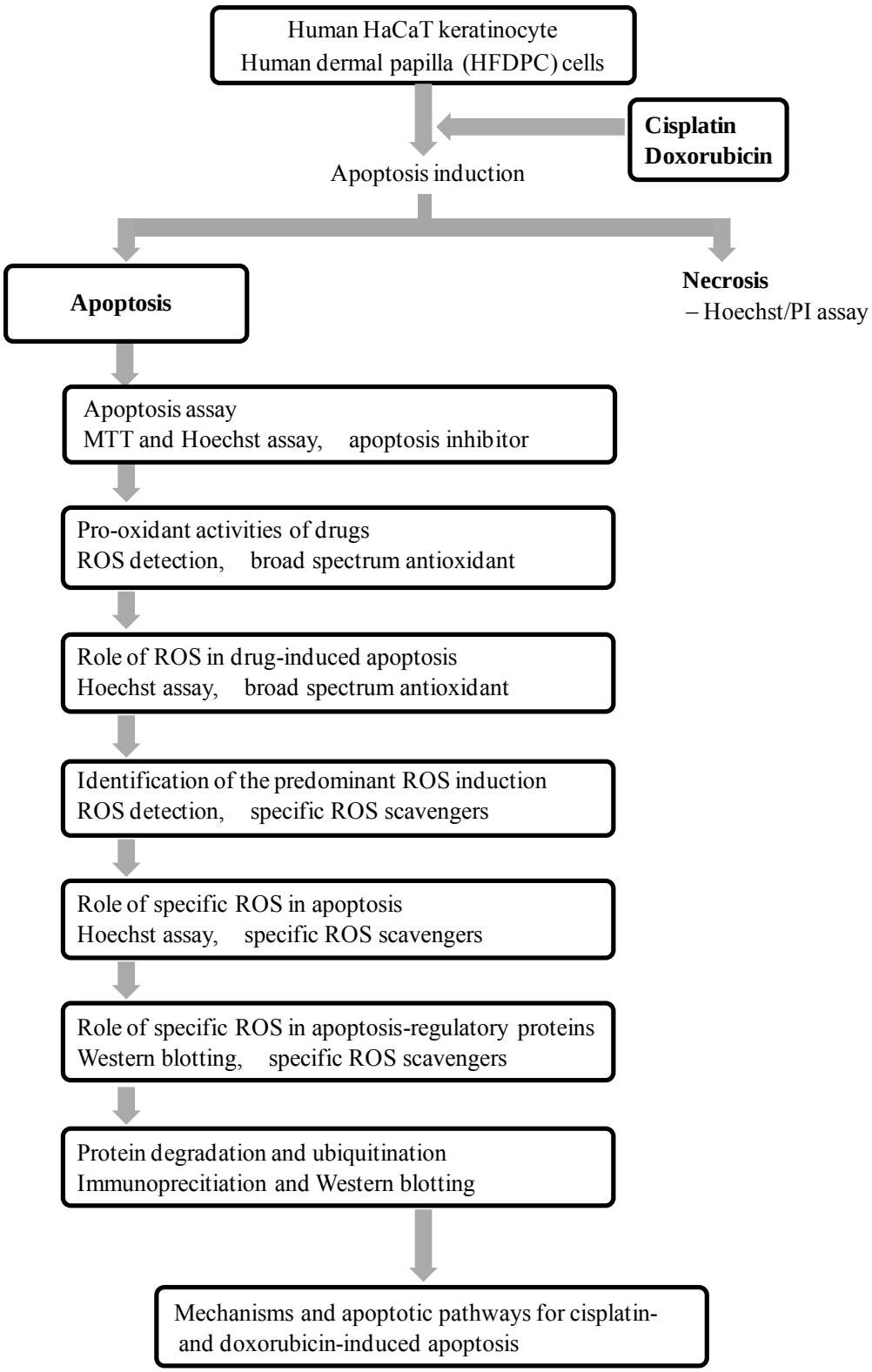

CHAPTER IV

RESULTS

This study determined the identity and role of reactive oxygen species in toxicity induced by cisplatin and doxorubicin in hair follicle dermal papilla cells and keratinocytes. To aid the understanding in molecular pathway of each drug, the effects of cisplatin and doxorubicin were shown separately.

Cisplatin

1. Cisplatin induces toxicity of hair follicle dermal papilla cells and keratinocytes

Cytotoxic effect of cisplatin on human hair follicle dermal papilla cells (HFDPC) and HaCaT keratinocytes were first evaluated. The cells were treated with various concentrations of cisplatin and their viability was determined by MTT assay. Figure 8 shows that cisplatin dose-dependently decreased the viability of both HFDPC and HaCaT cells. This effect of cisplatin was inhibited by pancaspase inhibitor, zVAD-fmk, in both cell types, suggesting caspase-dependent apoptosis as the mechanism of cisplatin-induced cytotoxicity.

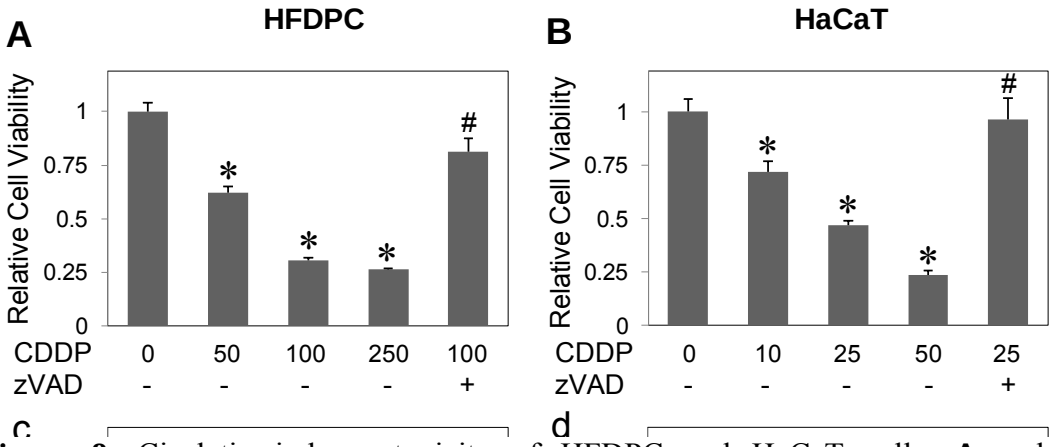

Figure 8. Cisplatin induces toxicity of HFDPC and HaCaT cells. **A** and **B** subconfluent monolayers (80%) of HFDPC and HaCaT cells were treated with various concentrations of cisplatin (CDDP; 0-250 μM and 0-50 μM in HFDPC and HaCaT cells, respectively) in the presence or absence of pan-caspase inhibitor (z-VAD-fmk; 10 μM) for 24 h. Cell toxicity was determined by MTT assay. Plots are mean ± S.D. (n = 4). *, $p < 0.05$ versus non-treated control. #, $p < 0.05$ versus cisplatin-treated control.

2. Cisplatin induces apoptosis of HFDPC and HaCaT cells

To confirm that apoptosis is the mechanism of cisplatin-induced cytotoxicity in HFDPC and HaCaT cells, cells were similarly treated with various concentrations of cisplatin and apoptosis was determined by Hoechst 33342 assay. Cisplatin was able to induce apoptosis of both HFDPC and HaCaT cells (Fig. 9, A and B). The induction of apoptosis by cisplatin was correlated with the observed reduction of cell viability. Figure 9, C and D, shows representative micrographs of the cells treated with cisplatin. Propidium iodide assay showed lack of necrosis in cisplatin-treated cells, as indicated by non-detectable PI fluorescence. Altogether with the ability of apoptosis (caspase) inhibitor, zVAD-fmk, to inhibit cisplatin-induced cell death (Fig. 8), apoptosis was found to be the primary mode of cell death in this study.

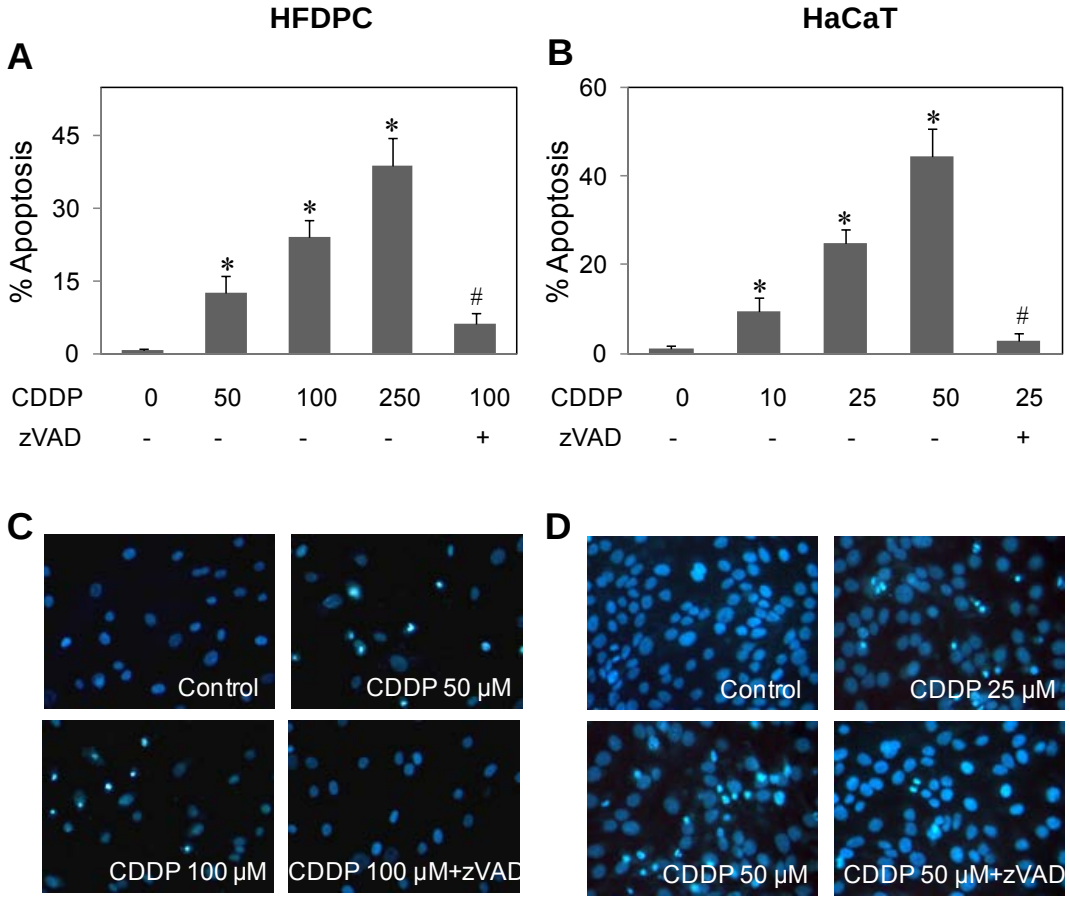

Figure 9. Cisplatin induces apoptosis of HFDPC and HaCaT cells. **A** and **B** subconfluent monolayers (80%) of HFDPC and HaCaT cells were treated with various concentrations of cisplatin (CDDP; 0-250 μM and 0-50 μM in HFDPC and HaCaT cells, respectively) in the presence or absence of pan-caspase inhibitor (z-VAD-fmk; 10 μM) for 24 h. Apoptosis was determined by Hoechst 33342 assay. **C** and **D** fluorescence micrographs of the treated cells stained with Hoechst dye. Apoptotic cells exhibited condensed and/or fragmented nuclei with bright nuclear fluorescence (original magnification, 400X). Plots are mean ± S.D. (n = 4). *, $p < 0.05$ versus non-treated control. #, $p < 0.05$ versus cisplatin-treated control.

3. Antioxidants protect cisplatin-induced apoptosis in HFDPC and HaCaT cells

Apoptosis assays show that cisplatin-induced apoptosis of HFDPC and HaCaT cells can be inhibited by co-treatment of the cells with antioxidants such as reduced glutathione (GSH) and *N*-acetyl cysteine (NAC) (Fig. 10, A and B). These results suggest the role of ROS in the apoptosis induction by cisplatin, which is confirmed in subsequent studies using specific ROS scavengers. Figure 10, C and D, shows representative micrographs of the cells treated with cisplatin in the presence or absence of NAC.

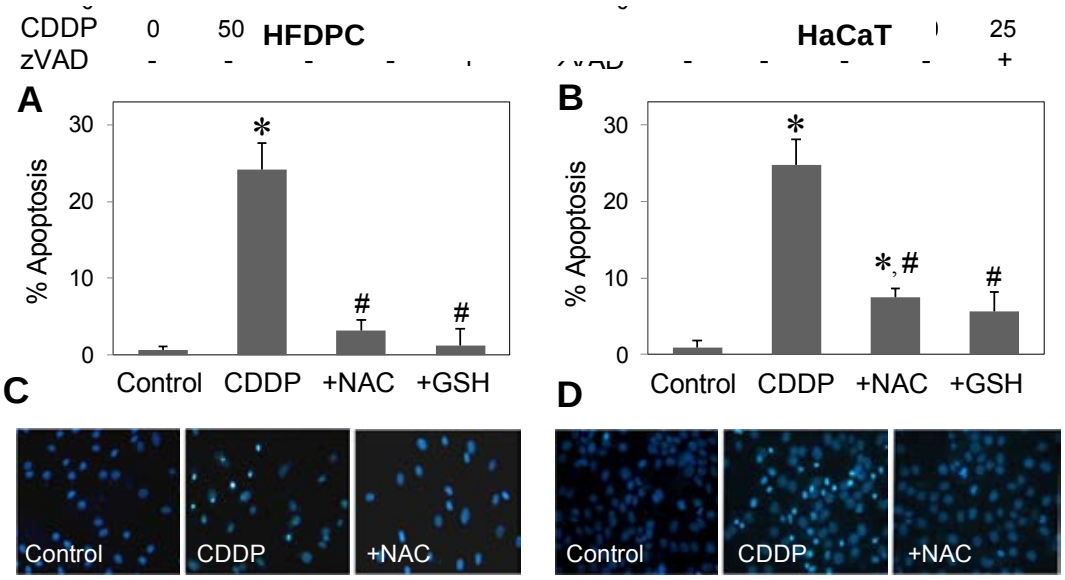

Figure 10. Antioxidants protect cisplatin-induced apoptosis of HFDPC and HaCaT cells. **A** and **B** HFDPC and HaCaT cells were pretreated for 30 min with NAC (2.5 mM) or GSH (2.5 mM) followed by cisplatin (100 μM and 25μM in HFDPC and HaCaT cells, respectively) for 24 h and analyzed for apoptosis by Hoechst 33342 assay. **C** and **D** fluorescence micrographs of the treated cells stained with Hoechst dye. Apoptotic cells exhibited condensed and/or fragmented nuclei with bright nuclear fluorescence (original magnification, 400X). Plots are mean ± S.D. (n = 4). *, $p < 0.05$ versus non-treated control. #, $p < 0.05$ versus cisplatin-treated control.

4. Cisplatin induces ROS generation in HFDPC and HaCaT cells

To provide evidence for cisplatin-induced ROS generation, HFDPC and HaCaT cells were treated with cisplatin in the presence or absence of antioxidant NAC, and cellular ROS levels were determined by flow cytometry and fluorescence microscopy using H_2DCF-DA as a fluorescent probe. Time course measurement for ROS generation were first analyzed and found the maximum response time of 2 h (Fig. 11). Figure 12, A and B, shows that cisplatin was able to induce ROS generation, as indicated by the increase in cellular DCF fluorescence intensity which was inhibited by the addition of antioxidant NAC. Figure 12, C and D, shows representative results of the flow cytometry and microscopy experiments which support the generation of ROS in cisplatin-treated HFDPC and HaCaT cells.

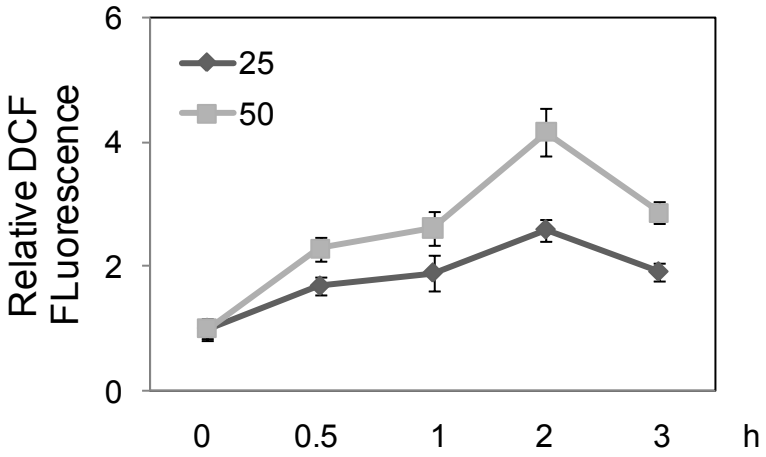

Figure 11. Time course measurements of cellular ROS generation by cisplatin. HaCaT cells were treated with cisplatin (25 and 50 μM) for various times (0-3 h), after which they were analyzed for ROS generation by fluorometry using H_2DCF-DA as a probe**.** Plots are mean ± S.D. (n = 3).

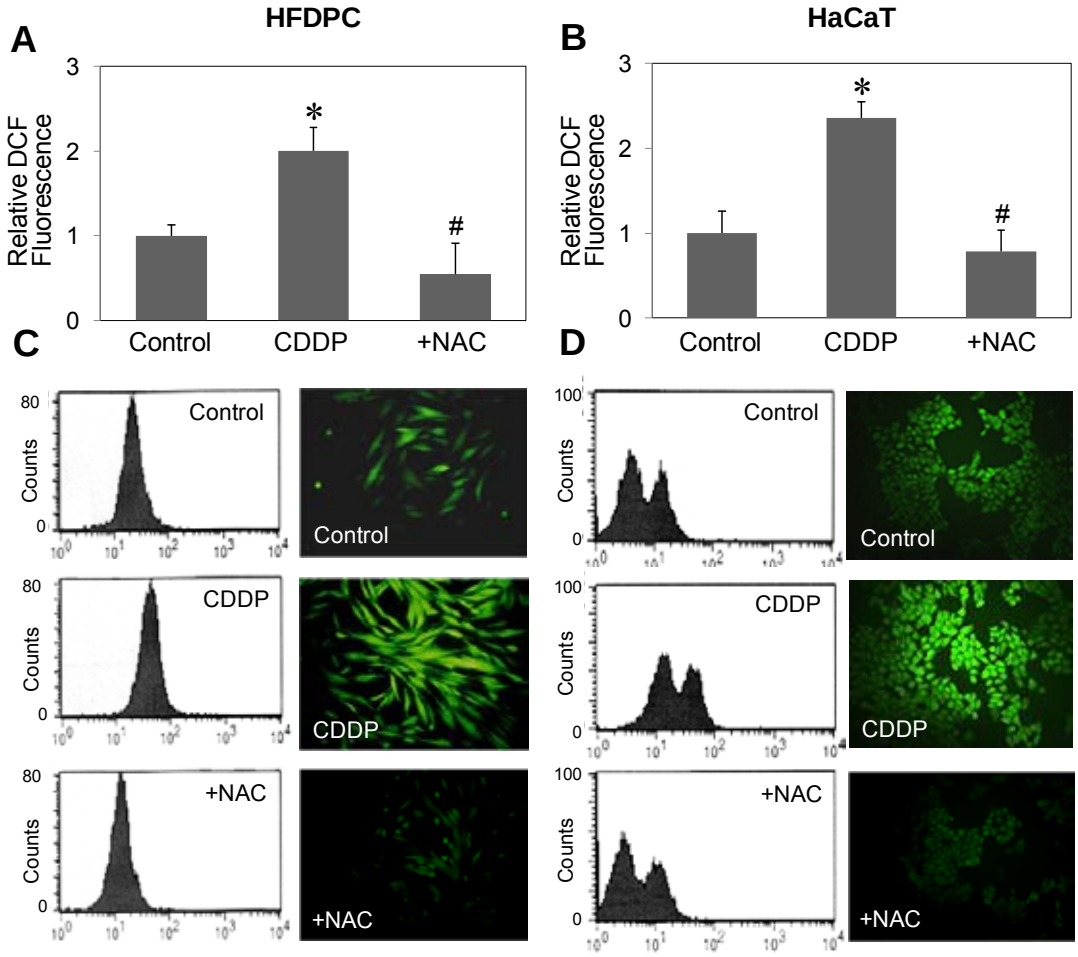

Figure 12. Effect of cisplatin on cellular ROS generation. **A** and **B** HFDPC and HaCaT cells were pretreated for 30 min with NAC (2.5 mM) for 2 h followed by cisplatin (100 μM and 25 μM in HFDPC and HaCaT cells, respectively), after which they were analyzed for ROS generation by flow cytometry using H_2DCF-DA as a fluorescent probe. **C** and **D** representative flow cytometric histograms (*left*) and fluorescence micrographs (*right*) of DCF measurements in the treated cells (original magnification, 400X). Plots are mean ± S.D. (n = 3). *, $p < 0.05$ versus non-treated control. #, $p < 0.05$ versus cisplatin-treated control.

5. Role of specific ROS in cisplatin-induced apoptosis

To determine the role of specific ROS in cisplatin-induced apoptosis, HFDPC and HaCaT cells were treated with cisplatin in the presence or absence of various specific ROS scavengers, including catalase (hydrogen peroxide scavenger), MnTBAP (MnSOD mimetic and superoxide anion scavenger) and sodium formate (hydroxyl radical scavenger), and apoptosis was determined by Hoechst 33342 assay. Figure 13 shows that catalase and MnTBAP had no significant effect on apoptosis induced by cisplatin, whereas sodium formate strongly inhibited the apoptosis. The role of hydroxyl radical on apoptosis by cisplatin was once again confirmed by the inhibition effect of another hydroxyl radical scavenger dimethylthiourea (data not shown).

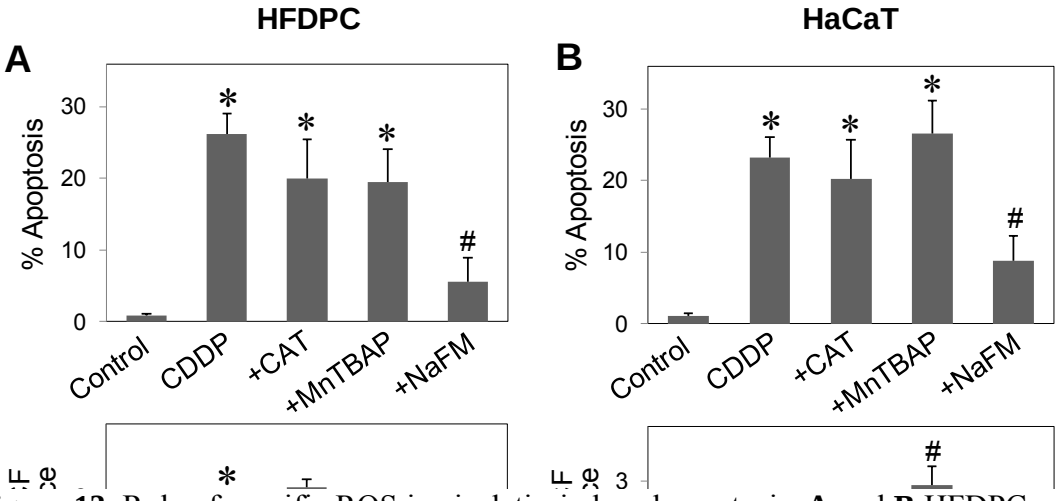

Figure 13. Role of specific ROS in cisplatin-induced apoptosis. **A** and **B** HFDPC and HaCaT cells were pretreated for 30 min with catalase (CAT, 7,500 U/ml), MnTBAP (50 μM), or sodium formate (NaFM, 2.5 mM) followed by cisplatin treatment (100 μM and 25 μM in HFDPC and HaCaT cells, respectively) for 24 h and analyzed for apoptosis by Hoechst 33342 assay. Plots are mean ± S.D. (n = 3). *, $p < 0.05$ versus non-treated control. #, $p < 0.05$ versus cisplatin-treated control.

6. Identification of specific ROS generation by cisplatin

In agreement with apoptosis assay, analysis of ROS generation by flow cytometry also indicated that sodium formate inhibited the generation of ROS induced by cisplatin, whereas catalase and MnTBAP had no significant inhibitory effect (Fig. 14). Altogether, these results suggest that hydroxyl radical is a major ROS produced by the cells in response to cisplatin treatment and that this oxidative species plays a key role in apoptosis induced by cisplatin.

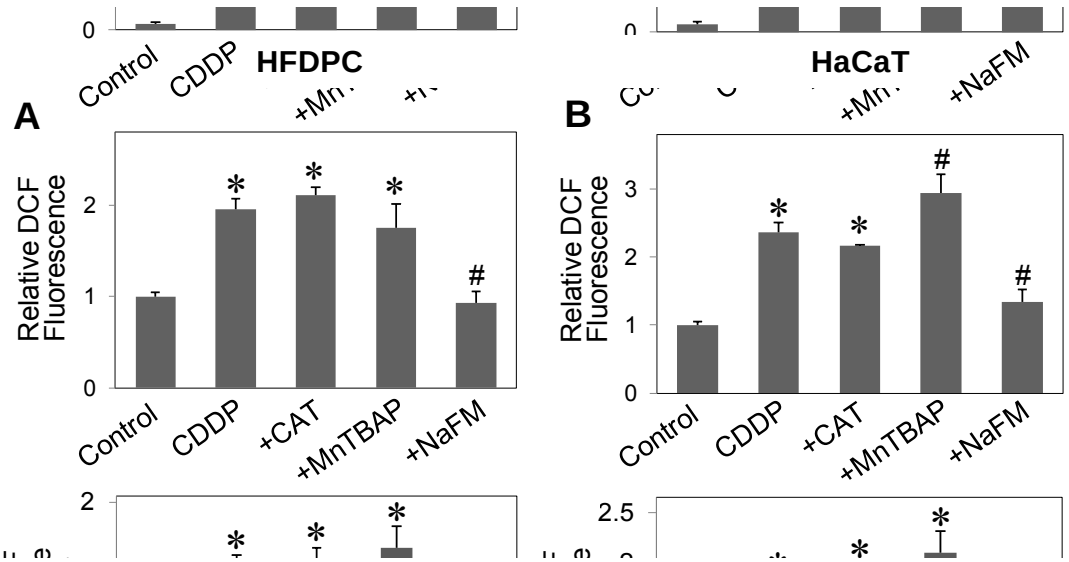

Figure 14. Specific ROS generation induced by cisplatin. **A** and **B** HFDPC and HaCaT cells were pretreated for 30 min with catalase (CAT, 7,500 U/ml), MnTBAP (50 μM), or sodium formate (NaFM, 2.5 mM) followed by cisplatin treatment (100 μM and 25 μM in HFDPC and HaCaT cells, respectively) and analyzed for ROS generation at the maximum response time of 2 h by flow cytometry using H_2DCF-DA as a fluorescent probe. Plots are mean ± S.D. (n = 3). *, $p < 0.05$ versus non-treated control. #, $p < 0.05$ versus cisplatin-treated control.

To confirm the formation of hydroxyl radicals in response to cisplatin treatment, two additional experiments were performed. Firstly, hydroxyphenyl fluorescein (HPF) was used as a probe to detect highly reactive oxygen species

(hROS) in the presence or absence of hydroxyl radical scavenger sodium formate. Upon treatment of the cells with cisplatin, cellular HPF fluorescence intensity was enhanced in a dose-dependent manner, the effect that was completely inhibited by sodium formate (Fig. 15). Secondly, ESR measurements using spin trapping agent DMPO were performed. In response to cisplatin treatment, an ESR signal consisting of a 1:2:2:1 quartet which is a characteristic of DMPO-OH$^{\bullet}$ adduct was observed (Fig. 16A). Addition of sodium formate, but not MnTBAP or catalase, to the treated cells inhibited the ESR signal, indicating the scavenging of hydroxyl radical under the test condition.

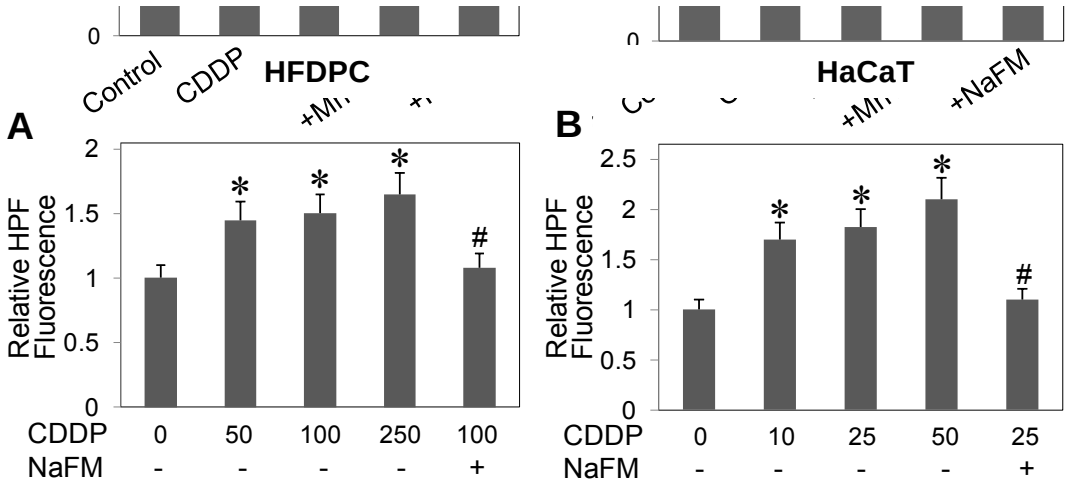

Figure 15. Highly reactive oxygen induction by cisplatin treatment. **A** and **B** HFDPC and HaCaT cells were treated with various concentration of cisplatin (0-250 μM and 0-50 μM in HFDPC and HaCaT cells, respectively) in the presence or absence of sodium formate (2.5 mM) for 30 min and cellular hROS generation was determined by fluorescence plate reader using HPF as a fluorescent probe as described in *Materials and Methods*. Plots are mean ± S.D. (n = 3). *, $p < 0.05$ versus non-treated control. #, $p < 0.05$ versus cisplatin-treated control.

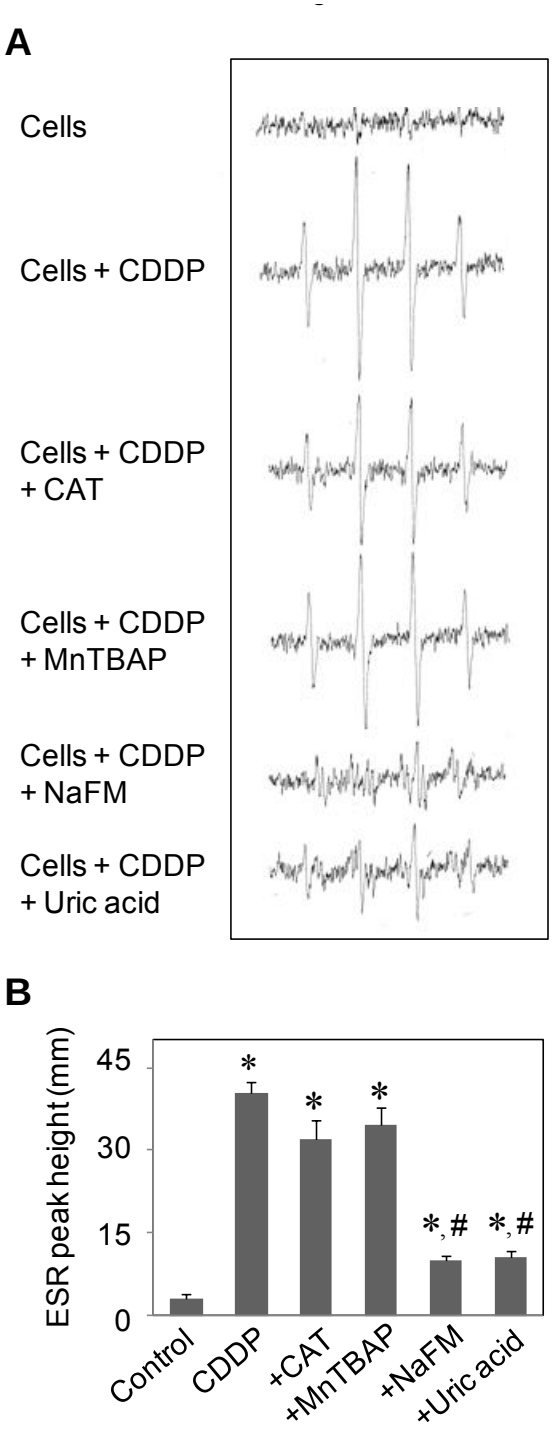

Figure 16. Hydroxyl radical induction by cisplatin treatment. **A** HaCaT cells (1x106 cells/ml) were incubated in PBS containing the spin trapper DMPO (10 mM) with or without cisplatin (25 μM), catalase (7,500 U/ml), MnTBAP (50 μM), sodium formate (NaFM, 2.5 mM), and uric acid (100 μM). ESR spectra were then recorded 30 min after the addition of the test agents. The spectrometer settings were as follows:

receiver gain at $1.5x10^5$, time constants at 0.3 sec, modulation amplitude at 1.0 G, scan time at 4 min, and magnetic field at 3,470 ± 100 G. **B** analysis of ESR measurements. Plots are mean ± S.D. (n = 3). *, $p < 0.05$ versus non-treated control (cells). #, $p < 0.05$ versus cisplatin-treated control.

7. Source of hydroxyl radical production

Since hydrogen peroxide is a major source of hydroxyl radical, the lack of inhibitory effect of catalase on cisplatin-induced hydroxyl radical formation (Fig. 16) is somewhat surprising and suggests other unknown sources of hydroxyl radical. Recently, it has been reported that hydroxyl radical could be formed from the decomposition of peroxynitrite (Beckman et al., 1997; Zhang et al., 2001). To test this possibility, we utilized a known specific scavenger of peroxynitrite, uric acid, and tested its effect on cisplatin-induced hydroxyl radical formation. Figure 16A (*lowest panel*) shows that uric acid was able to inhibit the ESR signal induced by cisplatin, suggesting peroxynitrite decomposition as a potential source for hydroxyl radical formation in the test system.

8. Cisplatin induces the activation of caspase-3

To further clarify the mechanism of apoptosis, activation of caspase-3 was measured by caspase-3 enzymatic activity. Figure 17 shows that cisplatin was able to induce the processing of inactive pro-caspase-3 to active caspase-3, as indicated by the significant increase in caspase-3 activity. Since activation of caspase-3 is a final execution of caspase-dependent apoptosis (Porter and Janicke, 1999; Elmore, 2007), the result of this study supports the induction of apoptosis by cisplatin through a caspase-dependent mechanism.

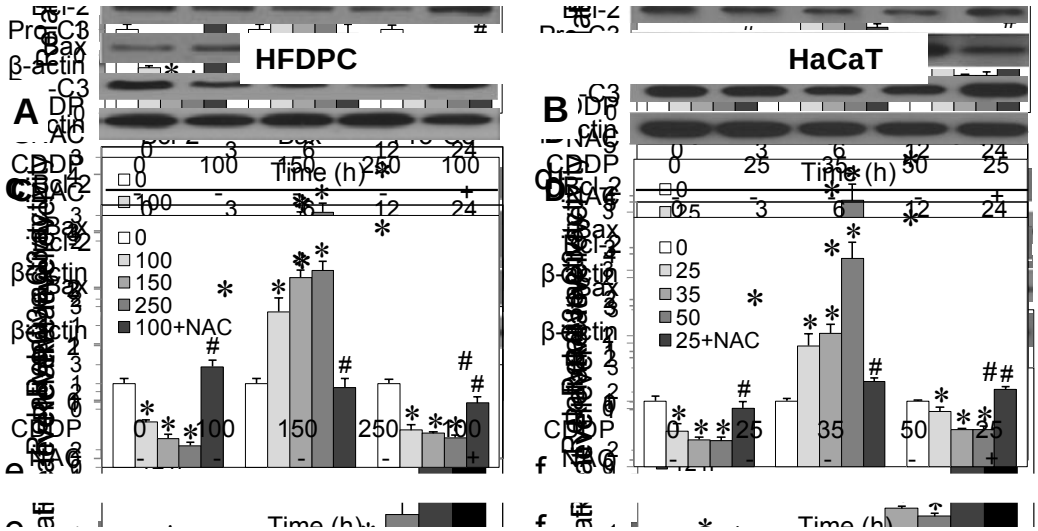

Figure 17. Cisplatin induces the activation of caspase-3. **A** and **B** HFDPC and HaCaT cells were treated with cisplatin (0-250 μM and 0-50 μM in HFDPC and HaCaT cells, respectively) in the presence or absence of NAC (2.5 mM) for 15 h (maximum response) and analyzed for caspase-3 activity using the fluorometric substrate FAM-DEVD-fmk. Plots are mean ± S.D. (n = 3). *, $p < 0.05$ versus non-treated control. #, $p < 0.05$ versus cisplatin-treated control.

9. Effects of cisplatin treatment on apoptosis-regulatory proteins

Cisplatin was previously shown to activate caspase 9 and induce apoptosis through the mitochondrial death pathway (Park et al., 2002; Wang et al., 2008). Since this pathway of apoptosis is known to be regulated by the balance of anti- and pro-apoptotic proteins in the Bcl-2 family (Mignotte and Vayssiere, 1998; Tsujimoto, 1998), The expression level of two key Bcl-2 family proteins, namely Bcl-2 and Bax, in response to cisplatin treatment in HFDPC and HaCaT cells was examined. Immunoblotting studies show that cisplatin induced down-regulation of the anti-apoptotic Bcl-2 protein and up-regulation of the pro-apoptotic Bax protein in a dose-dependent manner (Fig. 18). Additionally, proteolytic cleavage of pro-caspase-3 protein was also shown. The involvement of ROS in cisplatin-induced apoptosis was

confirmed by the observation that an addition of NAC strongly inhibited the effects of cisplatin on apoptosis-regulatory proteins Bcl-2, Bax, and pro-caspase-3.

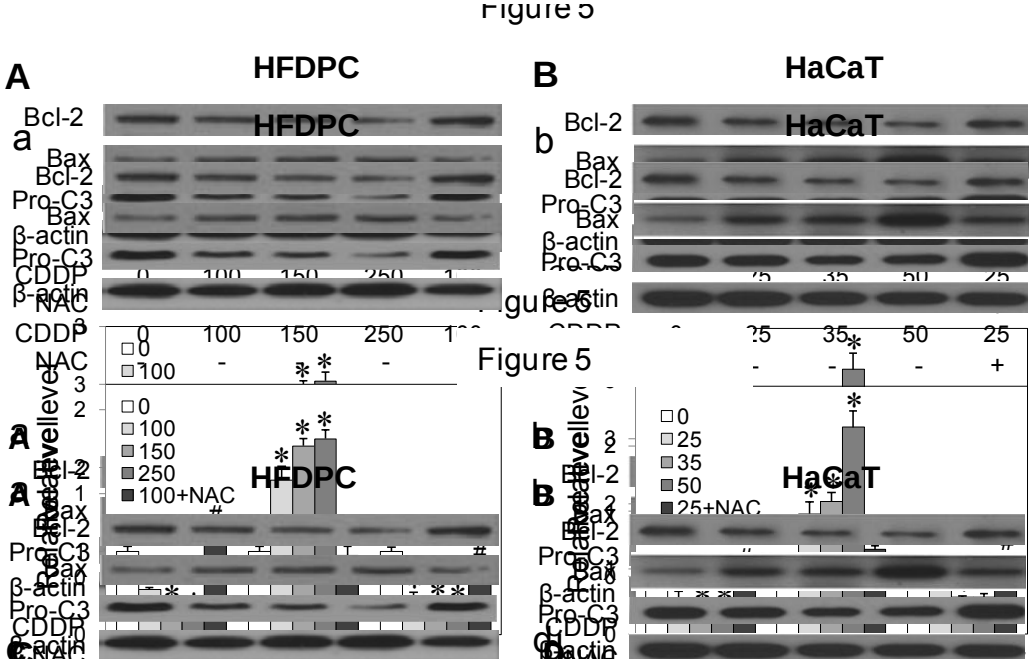

Figure 18. Effect of cisplatin treatment on apoptosis-regulatory proteins. **A** and **B** HFDPC and HaCaT cells were treated with cisplatin (0-250 μM and 0-50 μM in HFDPC and HaCaT cells, respectively) in the presence or absence of NAC (2.5 mM) for 24 h. Cell lysates were prepared and analyzed for Bcl-2, Bax, and pro-caspase 3 (Pro-C3) expression by Western blotting. Blots were reprobed with β-actin antibody to confirm equal loading of samples. Immunoblot signals were quantified by densitometry, and mean data from three independent experiments (one of which is shown here) was normalized to the result obtained in cells without treatment (control). Plots are mean ± S.D. (n = 3). *, $p < 0.05$ versus non-treated control. #, $p < 0.05$ versus cisplatin-treated control.

The effect of cisplatin on p53 and its active phosphorylated form was also determined. Cisplatin markedly up-regulated p53 phosphorylated form at low dose in both types of cells (Fig. 19). Since the activation of p53 decreased at high dose where

it induced more apoptosis, cisplatin-induced apoptosis was likely mediated through p53-independent mechanism.

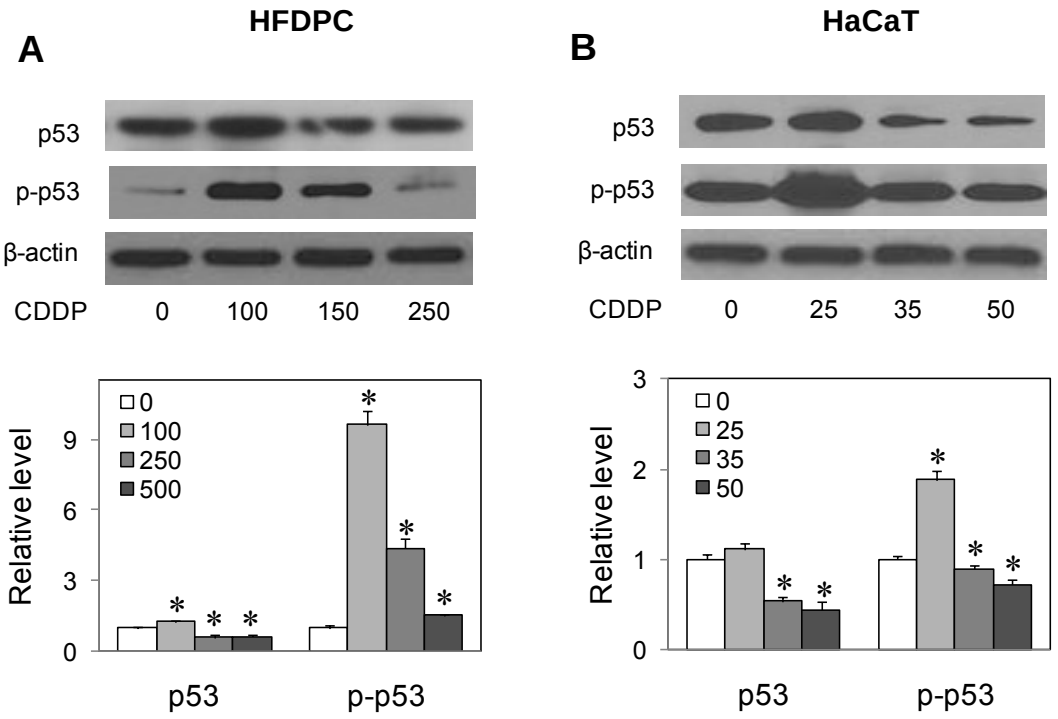

Figure 19. Effect of cisplatin on p53 and its active phosphorylated form. **A** and **B** HFDPC and HaCaT cells were treated with cisplatin (0-250 μM and 0-50 μM in HFDPC and HaCaT cells, respectively), p53 and phospho-p53 expression was determined by Western blotting. β-actin was used as a loading control. Plots are mean ± S.D. (n = 3). *, $p < 0.05$ versus non-treated control.

10. Time course measurements on apoptosis-regulatory proteins

Time dependence studies of the effect of cisplatin on Bcl-2 and Bax show that cisplatin induced a significant change in the protein levels at approximately 6 h after the treatment (Fig. 20).

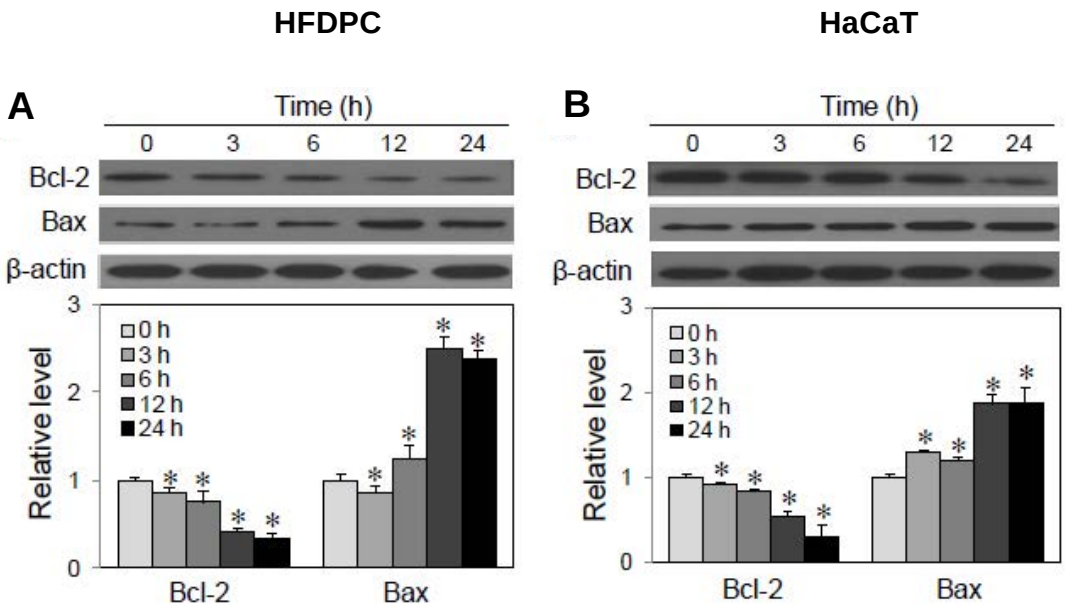

Figure 20. Time course measurements on apoptosis-regulatory proteins. **A** and **B** HFDPC and HaCaT cells were treated with cisplatin (100 μM and 25 μM in HFDPC and HaCaT cells, respectively) for various times (0-24 h), and Bcl-2 and Bax expression was determined by Western blotting. β-actin was used as a loading control. Plots are mean ± S.D. (n = 3). *, $p < 0.05$ versus non-treated control.

11. Cisplatin regulates Bcl-2 and Bax through hydroxyl radical

To determine the role of specific ROS in Bcl-2 and Bax regulation, the expression level of Bcl-2 and Bax after cisplatin treatment was determined in the presence or absence of NAC, catalase, MnTBAP, and sodium formate. In agreement with the apoptosis assay (Fig. 13), Western blot analysis of Bcl-2 expression showed that the down-regulation of Bcl-2 by cisplatin was inhibited by the addition of sodium formate or NAC, but not by catalase or MnTBAP (Fig. 21). Sodium formate also inhibited the effect of cisplatin on Bax, whereas catalase had no significant effect and MnTBAP had variable effect. Together, these results suggest the role of hydroxyl

radical as a key ROS involved in the alteration of Bcl-2 and Bax after cisplatin treatment.

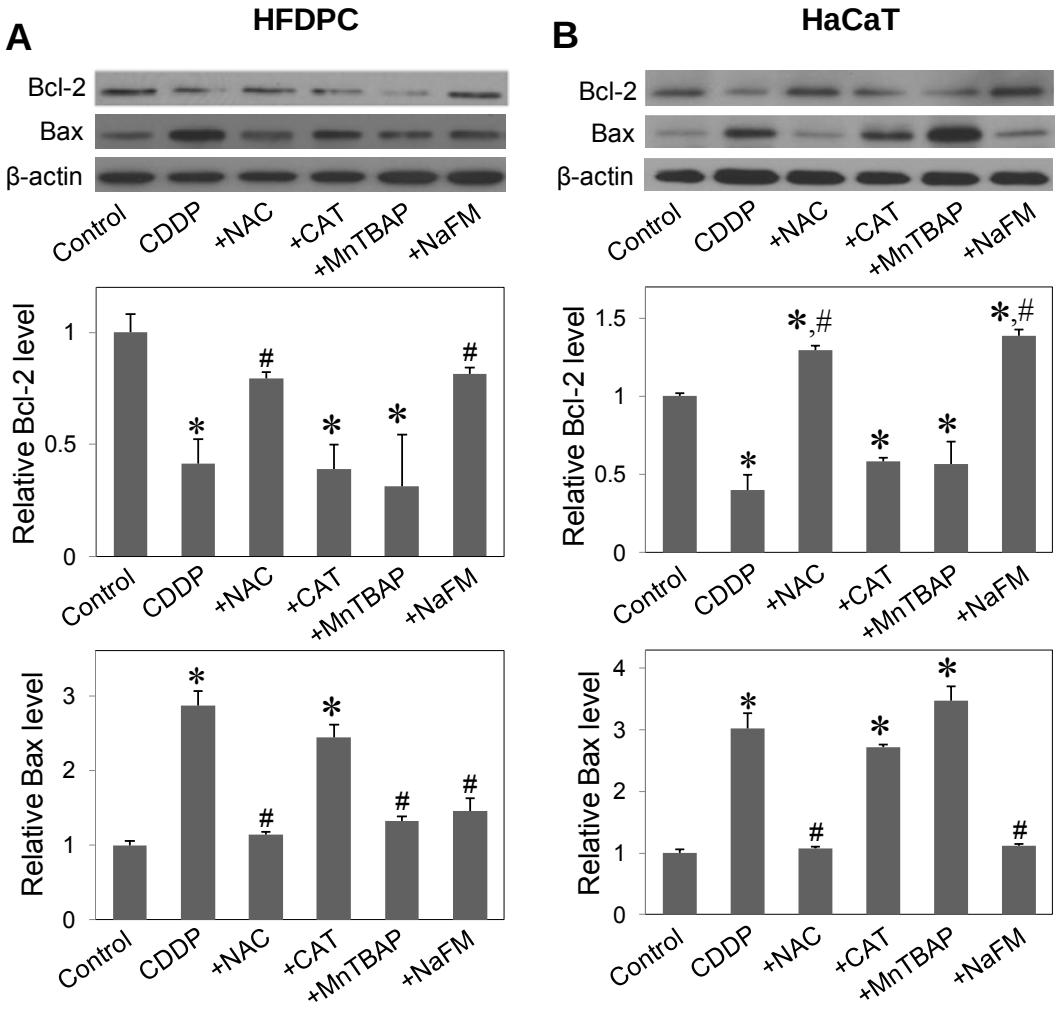

Figure 21. Effects of cisplatin and ROS scavengers on Bcl-2 and Bax expression. **A** and **B** HFDPC and HaCaT cells were treated with cisplatin (100 μM and 25 μM in HFDPC and HaCaT cells, respectively) in the presence or absence of NAC (2.5 mM), catalase (CAT, 7,500 U/ml), MnTBAP (50 μM), or sodium formate (NaFM, 2.5 mM). Cell lysates were prepared and analyzed for Bcl-2 and Bax expression by Western blotting using Bcl-2 and Bax antibodies. β-actin was used as a loading control. Plots are mean ± S.D. (n = 3). *, $p < 0.05$ versus non-treated control. #, $p < 0.05$ versus cisplatin-treated control.

Since the fate of cells is determined by the balance of pro- and anti-apoptotic proteins, the Bcl-2-to-Bax ratio was also reported (Fig. 22).

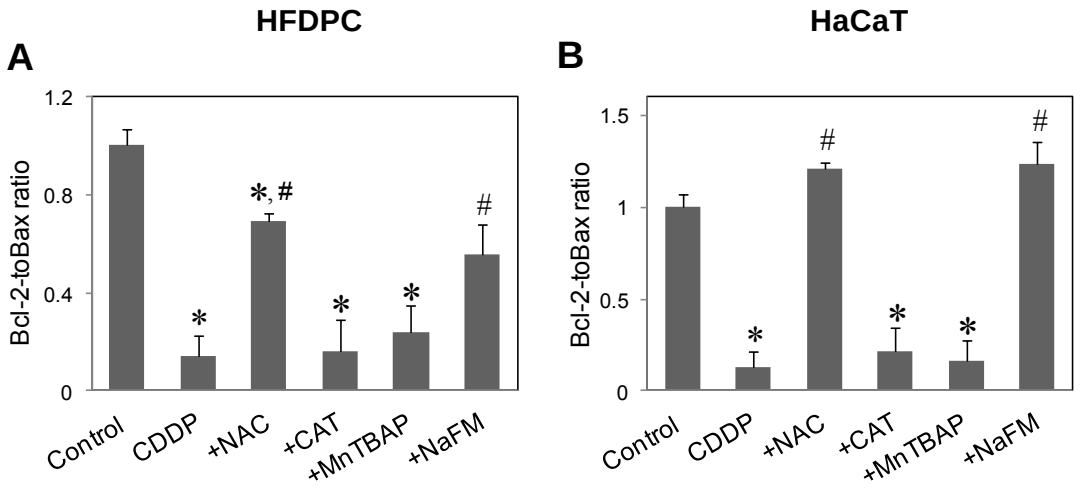

Figure 22. Effects of cisplatin and ROS scavengers on Bcl-2-to-Bax ratio. **A** and **B** HFDPC and HaCaT cells were treated with cisplatin (100 μM and 25 μM in HFDPC and HaCaT cells, respectively) in the presence or absence of NAC (2.5 mM), catalase (CAT, 7,500 U/ml), MnTBAP (50 μM), or sodium formate (NaFM, 2.5 mM). Cell lysates were prepared and analyzed for Bcl-2 and Bax expression by Western blotting using Bcl-2 and Bax antibodies. Histogram represents ratio of Bcl-2 and Bax expression. Plots are mean ± S.D. (n = 3). *, $p < 0.05$ versus non-treated control. #, $p < 0.05$ versus cisplatin-treated control.

12. Cisplatin down-regulates Bcl-2 through proteasomal degradation

Bcl-2 has been shown to be regulated by ubiquitin-proteasomal degradation pathway under diverse apoptosis conditions (Chanvorachote et al., 2006; Azad et al., 2008; Wang et al., 2008). To determine whether this pathway is involved in the down-regulation of Bcl-2 by cisplatin in the test cell systems, HFDPC and HaCaT cells were treated with lactacystin, a highly specific proteasome inhibitor, and its

effects on cisplatin-induced Bcl-2 down-regulation was determined by Western blotting. As lysosomal degradation is another possible pathway of protein degradation (Ciechanover, 2005), cells were also treated with cisplatin in the presence or absence concanamycin A, a known lysosome inhibitor. Figure 23 shows that lactacystin inhibited the down-regulation of Bcl-2 by cisplatin both in HFDPC and HaCaT cells, whereas concanamycin A had no significant effect, suggesting proteasomal degradation as the primary mechanism of cisplatin-induced Bcl-2 down-regulation.

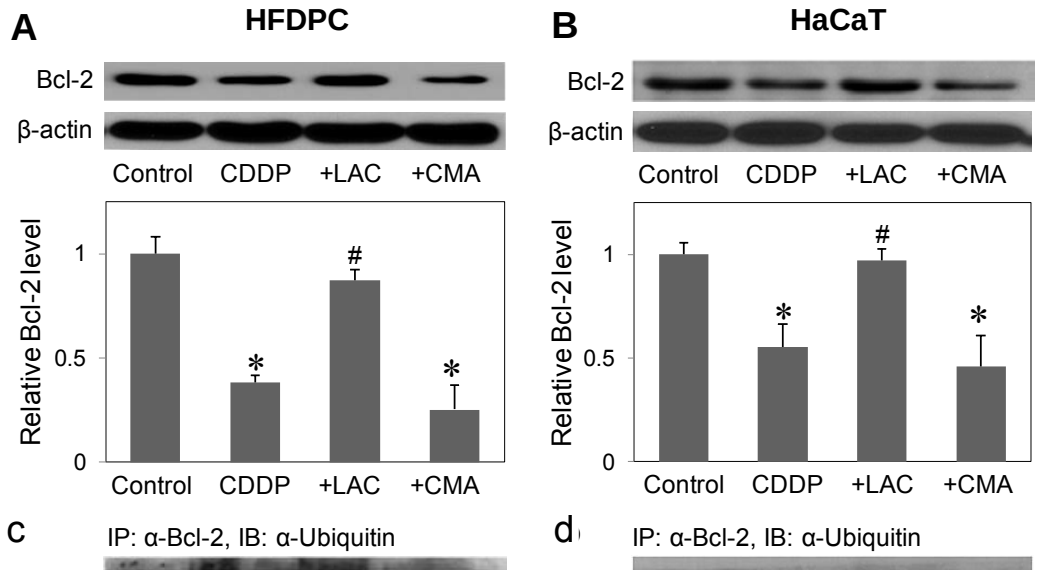

Figure 23. Cisplatin down-regulates Bcl-2 through proteasomal degradation. **A** and **B** HFDPC and HaCaT cells were pretreated with proteasome inhibitor lactacystin (LAC, 10 μM) or with lysosome inhibitor concanamycin A (CMA, 1 μM) for 1 h, and then treated with cisplatin (100 μM and 25 μM in HFDPC and HaCaT cells, respectively) for 24 h. Bcl-2 expression was determined by Western blots using anti-Bcl-2 antibody. Plots are mean ± S.D. (n = 3). *, $p < 0.05$ versus non-treated control. #, $p < 0.05$ versus cisplatin-treated control.

13. Cisplatin induces Bcl-2 ubiquitination

Ubiquitination is a major cellular process for selective removal of proteins via proteasomal degradation (Lecker et al., 2006). To test whether cisplatin could induce Bcl-2 ubiquitination in the test cell systems, cells were treated with cisplatin for various time (0-3 h), and cell lysates were prepared and immunoprecipitated using anti-Bcl-2 antibody. The resulting immune complexes were then analyzed for ubiquitination using anti-ubiquitin antibody. Cisplatin induced Bcl-2 ubiquitination was observed as early as 1 h and peaked at approximately 2 h after treatment (Fig. 24).

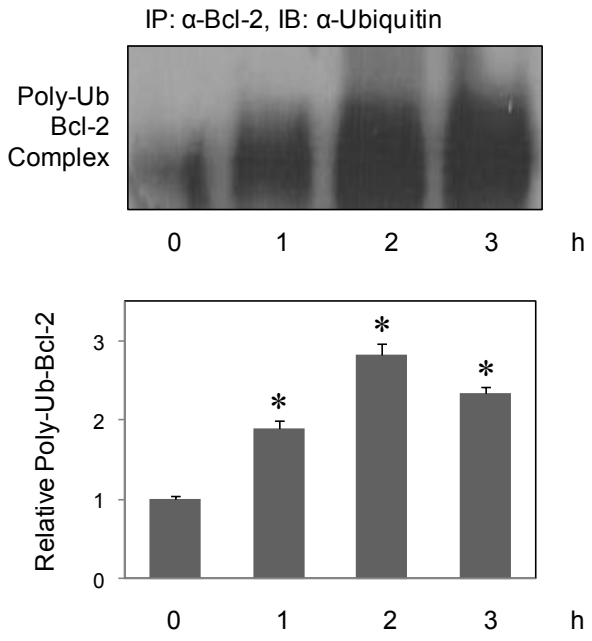

Figure 24. Cisplatin induces Bcl-2 ubiquitination. HaCaT cells were pretreated with LAC (10 μM) for 1 h (to prevent proteasomal degradation of Bcl-2) and then treated with cisplatin (25 μM) for various times (0-3 h). Cell lysates were immunoprecipitated with anti-Bcl-2 antibody and the immune complexes were analyzed for ubiquitin by Western blotting. Plots are mean ± S.D. (n = 3). *, $p < 0.05$ versus non-treated control.

14. Cisplatin induces dephosphorylation of Bcl-2

Bcl-2 ubiquitinaiton has been reported to be regulated by its phosphorylation. Certain apoptotic agents such as lipopolysaccharide and tumor necrosis factor-α have been shown to induce Bcl-2 dephosphorylation that triggers its ubiquitination (Dimmeler et al., 1999; Breitschopf et al., 2000). To test whether cisplatin can induce this process in HFDPC and HaCaT cells, cells were treated with cisplatin and its effect on Bcl-2 phosphorylation were examined. Figure 25 shows that cisplatin induces Bcl-2 dephosphorylation in a dose-dependent manner.

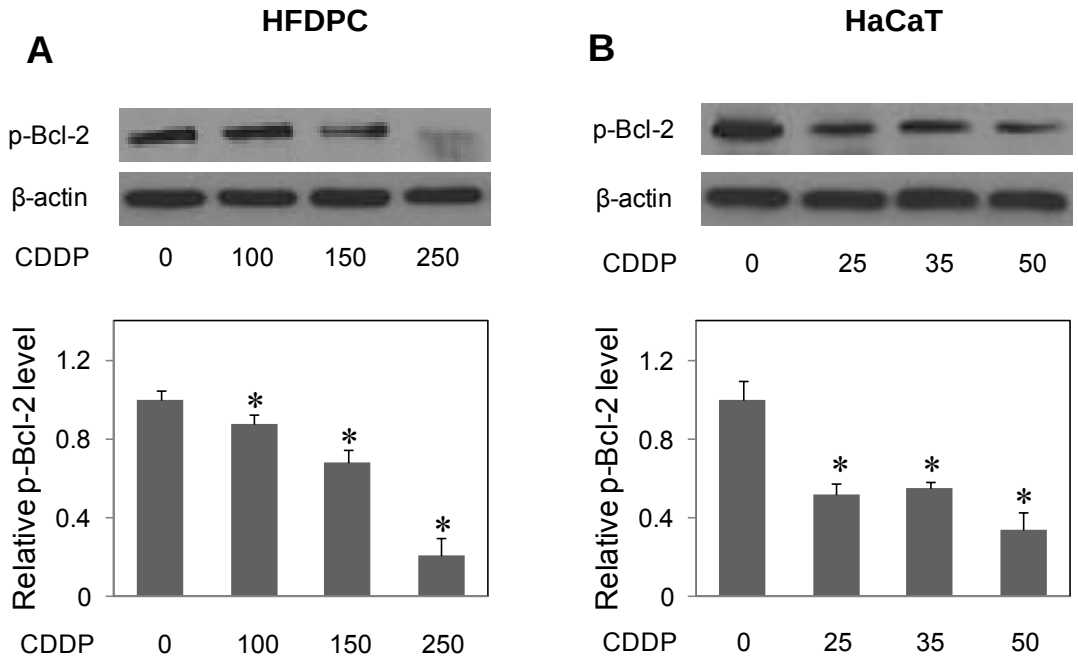

Figure 25. Dephosphorylation of Bcl-2 by cisplatin. **A** and **B** HFDPC and HaCaT cells were treated with cisplatin (0-250 μM and 0-50 μM in HFDPC and HaCaT cells, respectively) for 24 h. Cell lysates were prepared and analyzed for phospho-Bcl-2 expression by Western blotting using phospho-Bcl-2 antibody. β-actin was used as a loading control. Plots are mean ± S.D. (n = 3). *, $p < 0.05$ versus non-treated control.

15. Cisplatin induces Bcl-2 ubiquitination through hydroxyl radical

To test whether ROS play the role in Bcl-2 ubiquitination, cells were treated with cisplatin in the presence or absence of various ROS scavengers, and cell lysates were prepared and immunoprecipitated using anti-Bcl-2 antibody. The resulting immune complexes were then analyzed for ubiquitination using anti-ubiquitin antibody. The results show cisplatin-induced Bcl-2 ubiquitination was able to be inhibited by the general antioxidant NAC or the hydroxyl scavenger sodium formate (Fig. 26). Neither catalase nor MnTBAP was effective in inhibiting the ubiquitination, indicating that hydroxyl radical is the major oxidative species involved in the ubiquitination process.

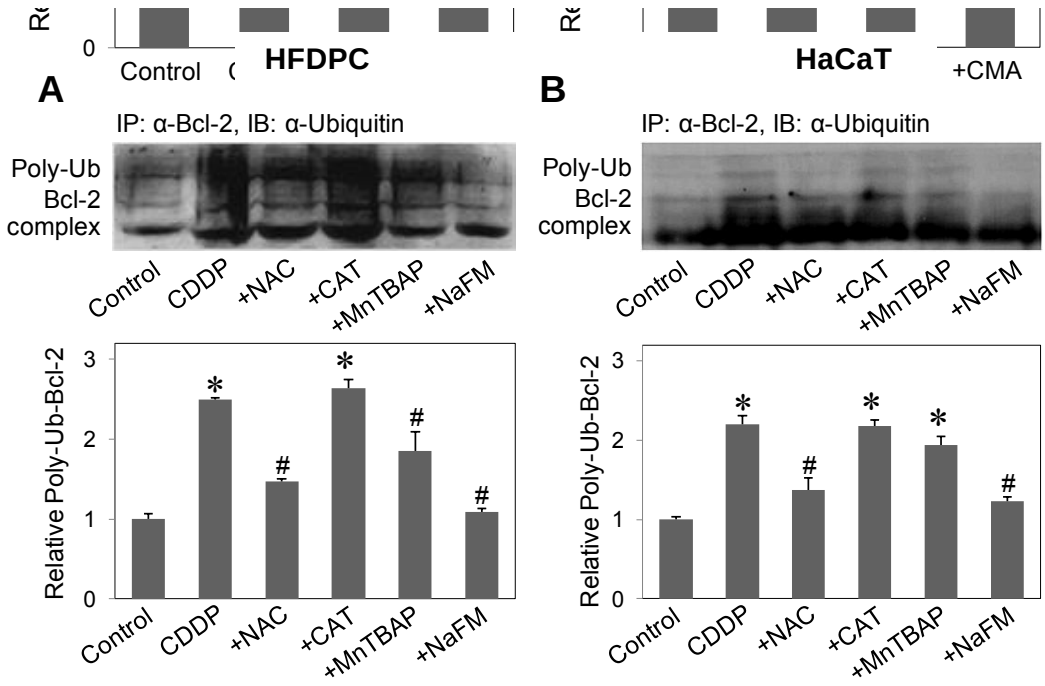

Figure 26. Effect of cisplatin and ROS scavengers on Bcl-2 ubiquitination. **A** and **B** HFDPC and HaCaT cells were pretreated with LAC (10 μM) for 1 h (to prevent proteasomal degradation of Bcl-2) and then treated with cisplatin in the presence or absence of NAC (2.5 mM), catalase (CAT, 7,500 U/ml), MnTBAP (50 μM), or sodium formate (NaFM, 2.5 mM) for 2 h. Cell lysates were immunoprecipitated with

anti-Bcl-2 antibody and the immune complexes were analyzed for ubiquitin by Western blotting. Analysis of ubiquitin was performed at 2 h posttreatment where ubiquitination was found to be maximal. Plots are mean ± S.D. (n = 3). *, $p < 0.05$ versus non-treated control. #, $p < 0.05$ versus cisplatin-treated control.

16. Comparison of apoptotic response in HFDPC and HaCaT cells

Although a similar pattern of apoptosis was observed in HFDPC and HaCaT cells, the apoptotic response to cisplatin treatment in HFDPC cells was much lower than that in HaCaT cells (Fig. 27).

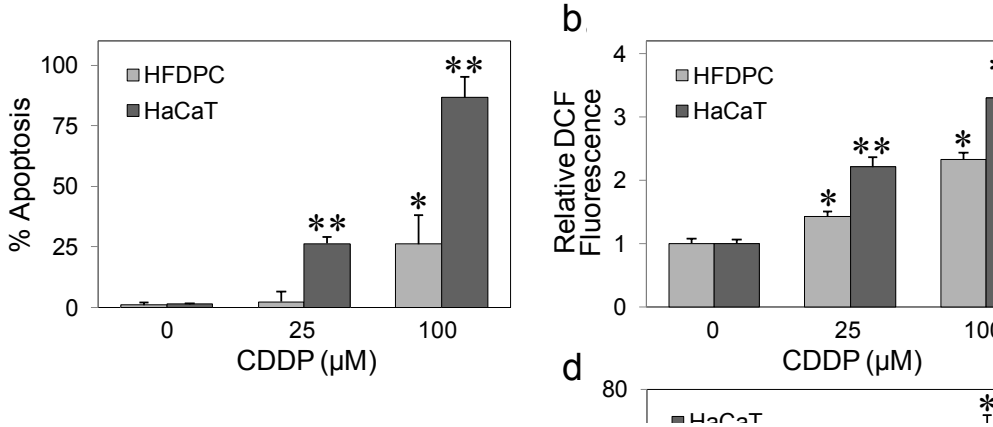

Figure 27. Comparison of apoptosis by cisplatin in HFDPC and HaCaT cells. HFDPC and HaCaT cells were treated with various concentrations of cisplatin (0-100 μM) for 24 h, and analyzed for apoptosis by Hoechst 33342 assay. Plots are mean S.D. (n = 3). *, $p < 0.05$ versus non-treated control. **, $p < 0.05$ versus cisplatin-treated HFDPC cells.

17. Effect of ROS generation on cisplatin-induced apoptosis

As ROS was earlier shown to be required for the induction of apoptosis by cisplatin, the level of ROS generation in the two cell types after cisplatin treatment was compared. Figure 28 shows that at the same treatment concentrations, HFDPC

cells produced less ROS than HaCaT cells. However, at the IC_{25} concentration of cisplatin (about 100 μM in HFDPC cells and 25 μM in HaCaT cells), the cellular ROS level was about the same in the two cell types, suggesting a correlation between the ROS and apoptotic responses.

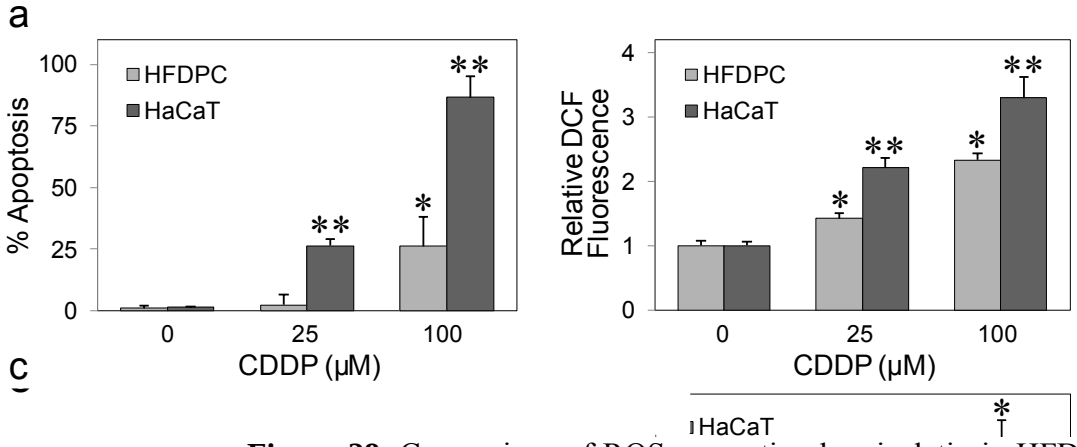

Figure 28. Comparison of ROS generation by cisplatin in HFDPC and HaCaT cells. HFDPC and HaCaT cells were treated with cisplatin (0-100 μM) and analyzed for ROS generation by flow cytometry at 2 h post-treatment. Plots are mean ± S.D. (n = 3). *, $p < 0.05$ versus non-treated control. **, $p < 0.05$ versus cisplatin-treated HFDPC cells.

18. Effect of Bcl-2 expression on cisplatin-induced apoptosis

Bcl-2 was previously shown to be a key regulator of apoptosis induced by cisplatin in cancer cells (Wang et al., 2008). To determine whether Bcl-2 also plays a role in the apoptosis regulation of non-cancer hair follicular cells, the cells were transfected with Bcl-2 or control plasmid, and their effect on cisplatin-induced apoptosis was examined. Because primary HFDPC cells were refractory to gene transfection, only HaCaT cells were used to study the role of Bcl-2 in the apoptosis. Figure 29 shows that Bcl-2-transfected HaCaT cells expressed a higher level of Bcl-2

protein and exhibited less susceptibility to apoptosis induction by cisplatin than vector-transfected control cells.

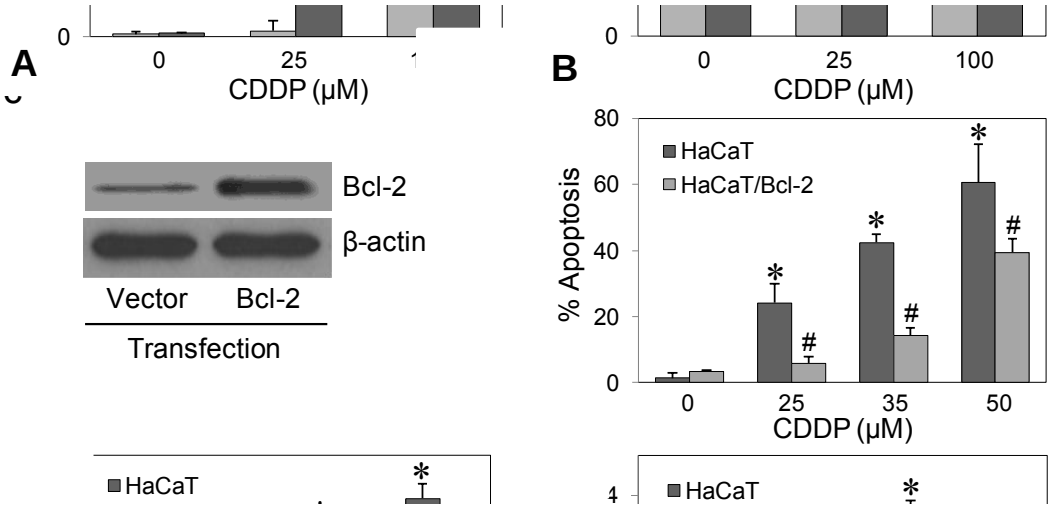

Figure 29. Effect of Bcl-2 expression on cisplatin-induced apoptosis. **A** HaCaT cells were transiently transfected with Bcl-2 or control pcDNA3 plasmid as described under *Materials and Methods*. Transfected cells were analyzed for Bcl-2 expression by Western blotting. **B** transfected cells were treated with cisplatin (0-50 μM) for 24 h and analyzed for apoptosis by Hoechst 33342 assay. Plots are mean ± S.D. (n = 3). *, $p < 0.05$ versus non-treated control. #, $p < 0.05$ versus cisplatin-treated vector-transfected HaCaT cells.

19. Effect of Bcl-2 expression on cisplatin-induced ROS generation

Bcl-2 and ROS are key mediators of apoptosis by cisplatin. The observation that, upon cisplatin treatment, HFDPC cells produced less ROS than HaCaT cells (Fig. 25) whilst expressed higher Bcl-2 (Fig. 30) posed a question whether Bcl-2 affects ROS level. Analysis of ROS generation in Bcl-2-transfected cells shows that these cells produced less ROS than the control cells (Fig. 31).

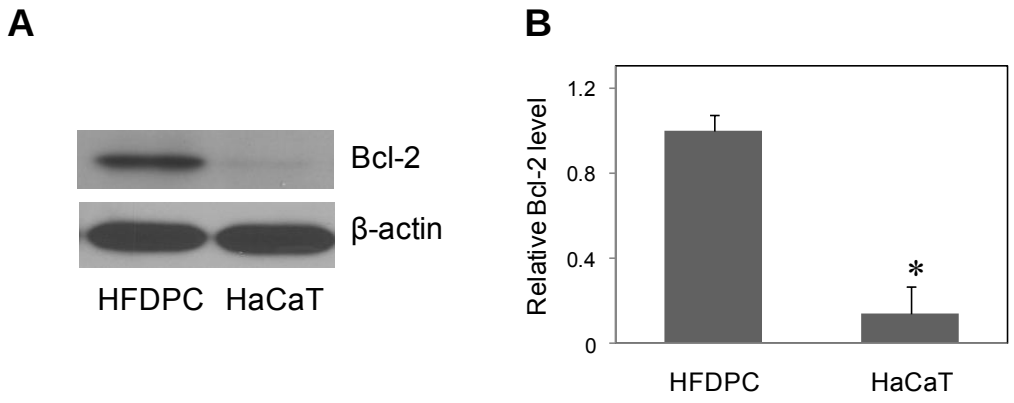

Figure 30. Comparison of Bcl-2 expression in HFDPC and HaCaT cells. HFDPC and HaCaT cell lysates were prepared and analyzed for Bcl-2 by Western blotting. β-actin was used as a loading control. Plots are mean ± S.D. (n = 3). *, $p < 0.05$ versus HFDPC cells.

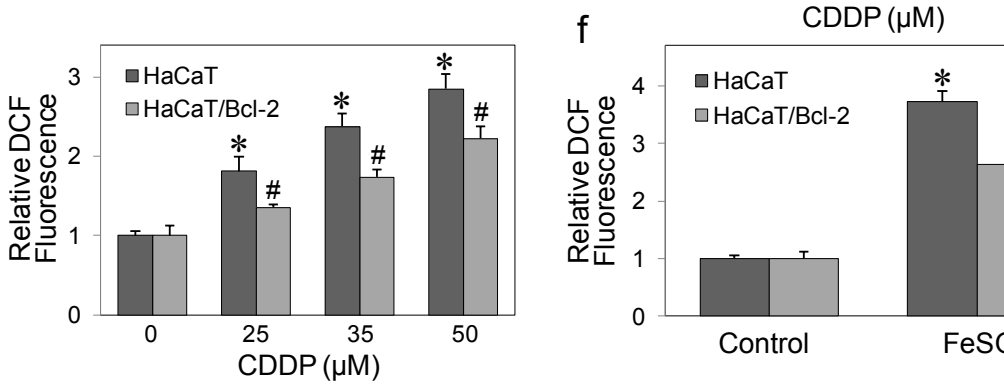

Figure 31. Bcl-2 suppresses ROS generation by cisplatin. HaCaT cells were transiently transfected with Bcl-2 or control pcDNA3 plasmid as described under *Materials and Methods*. Transfected cells were treated with cisplatin (0-50 μM) and analyzed for ROS generation by flow cytometry at 2 h after the treatment. Plots are mean ± S.D. (n = 3). *, $p < 0.05$ versus non-treated control. #, $p < 0.05$ versus cisplatin-treated vector-transfected HaCaT cells.

20. Effect of Bcl-2 expression on hydroxyl radical generation

Since hydroxyl radical was shown to be a key mediator of cisplatin-induced apoptosis, we further evaluated the potential antioxidant effect of Bcl-2 on hydroxyl radical generation in a well defined system using ferrous sulfate as a source of hydroxyl radical generation through Fenton reaction (Luanpitpong et al., 2010). Figure 32 shows that treatment of the cells with ferrous sulfate resulted in a substantial increase in ROS generation. However, this effect was less pronounced in Bcl-2-transfected cells as compared to vector-transfected cells. Together, these results support the role of Bcl-2 as a suppressor of cisplatin-induced apoptosis and as a negative regulator of hydroxyl radical generation.

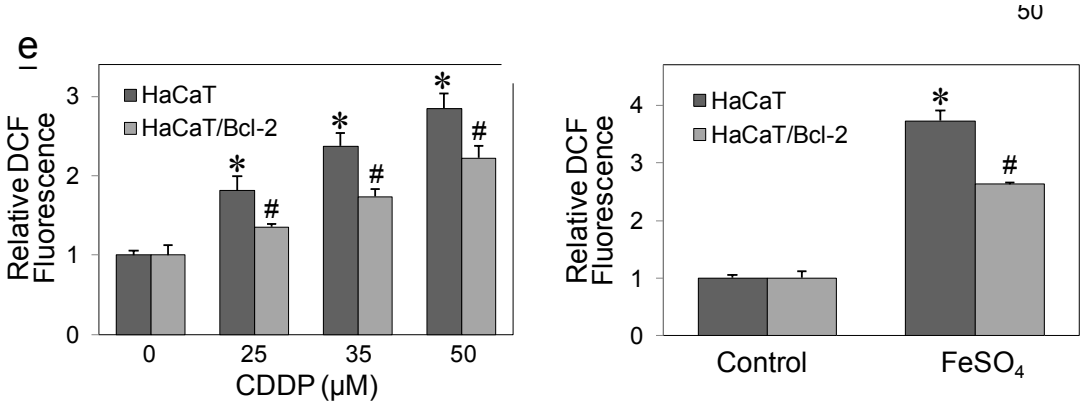

Figure 32. Bcl-2 negatively regulates hydroxyl radical generation. HaCaT cells were transiently transfected with Bcl-2 or control pcDNA3 plasmid as described under *Materials and Methods*. Transfected cells were treated with ferrous sulfate ($FeSO_4$, 100 μM) and ROS generation was similarly determined after 2 h. Plots are mean ± S.D. (n = 3). *, $p < 0.05$ versus non-treated control. #, $p < 0.05$ versus ferrous sulfate-treated vector-transfected HaCaT cells.

Doxorubicin

1. Doxorubicin induces toxicity of hair follicle dermal papilla cells and keratinocytes

Cytotoxic effect of doxorubicin on human hair follicle dermal papilla cells (HFDPC) and HaCaT keratinocytes were first evaluated. The cells were treated with various concentrations of doxorubicin and their viability was determined by MTT assay. Figure 33 shows that doxorubicin dose-dependently decreased the viability of both HFDPC and HaCaT cells. This effect of doxorubicin was inhibited by pancaspase inhibitor, zVAD-fmk, in both cell types, suggesting caspase-dependent apoptosis as the mechanism of doxorubicin-induced cytotoxicity.

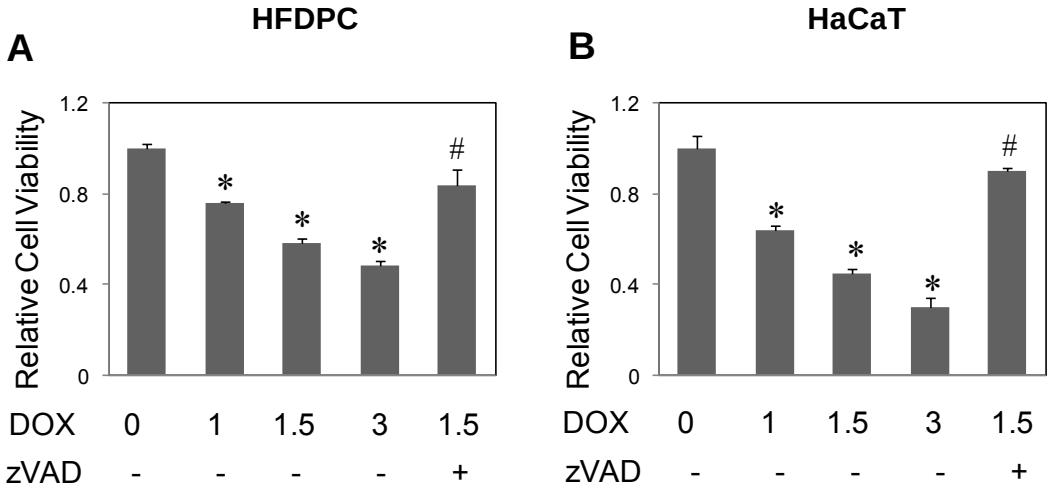

Figure 33. Doxorubicin induces toxicity of HFDPC and HaCaT cells. **A** and **B** subconfluent monolayers (80%) of HFDPC and HaCaT cells were treated with various concentrations of doxorubicin (DOX; 0-3 μM) in the presence or absence of pan-caspase inhibitor (z-VAD-fmk; 10 μM) for 24 h. Cell toxicity was determined by MTT assay. Plots are mean ± S.D. (n = 4). *, $p < 0.05$ versus non-treated control. #, $p < 0.05$ versus doxorubicin-treated control.

2. Doxorubicin induces apoptosis of HFDPC and HaCaT cells

To characterize the apoptosis response to doxorubicin treatment, HFDPC and HaCaT cells were treated with various concentrations of doxorubicin (0-3 μM) and apoptosis was determined after 24 h by Hoechst 33342 assay. Doxorubicin treatment caused a dose-dependent increase in apoptosis, the effect that was inhibited by co-treatment of the cells with pan-caspase inhibitor, zVAD-fmk (Fig. 34, A and B). The apoptotic cells exhibited shrunken nuclei and chromatin condensation with intense nuclear fluorescence (Fig. 34, C and D).

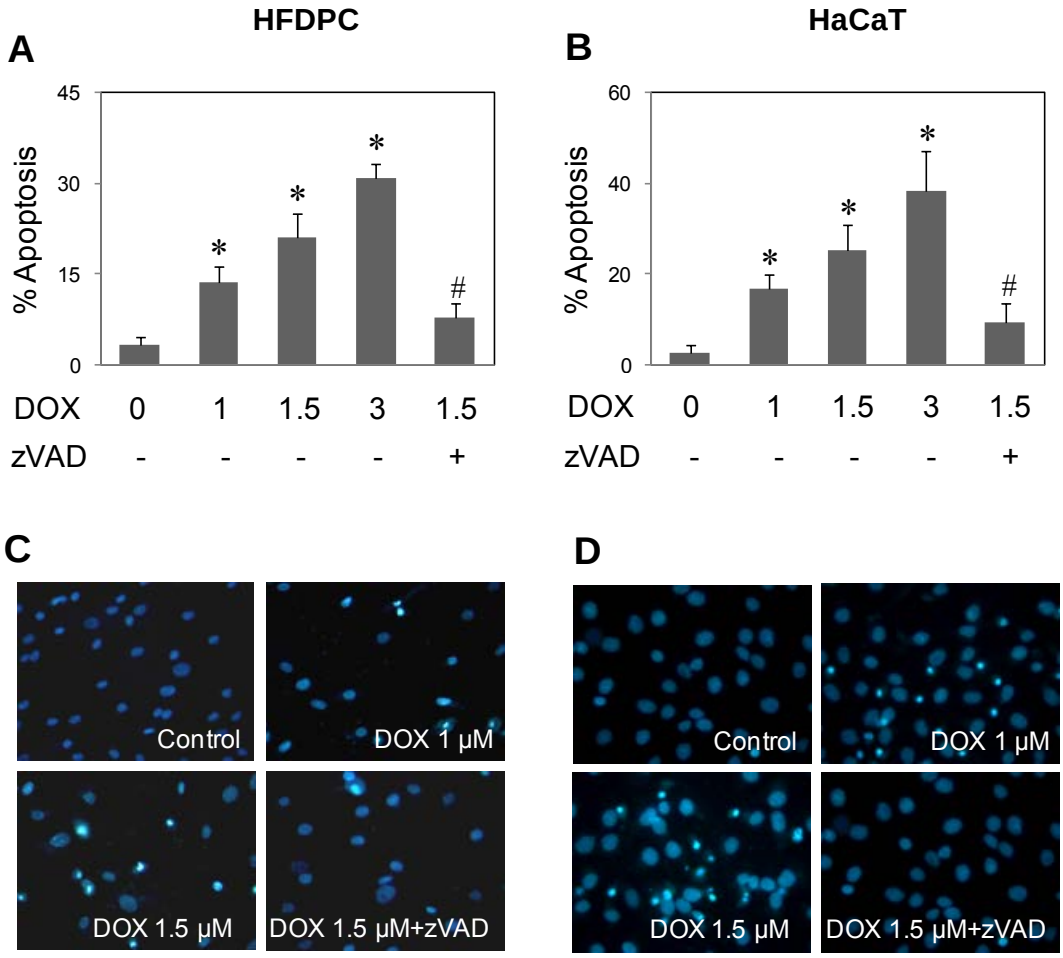

Figure 34. Doxorubicin induces apoptosis of HFDPC and HaCaT cells. **A** and **B** subconfluent monolayers (80%) of HFDPC and HaCaT cells were treated with various concentrations of doxorubicin (DOX; 0-3 μM) in the presence or absence of

pan-caspase inhibitor (z-VAD-fmk; 10 μM) for 24 h. Apoptosis was determined by Hoechst 33342 assay. **C** and **D** fluorescence micrographs of the treated cells stained with Hoechst dye (original magnification, 400X). Plots are mean ± S.D. (n = 4). *, $p < 0.05$ versus non-treated control. #, $p < 0.05$ versus doxorubicin-treated control.

3. Doxorubicin induces the activation of caspase-3

To further clarify the mechanism of apoptosis, activation of caspase-3, as indicated by the proteolytic cleavage of inactive (full length) pro-caspase-3 into activated (cleaved) fragment, was evaluated by Western blotting. Figure 35 shows that doxorubicin induced caspase-3 activation in a dose-dependent manner in concomitant with the nuclear morphological changes (Fig. 34), supporting the caspase-dependent apoptosis induced by doxorubicin in these cell types.

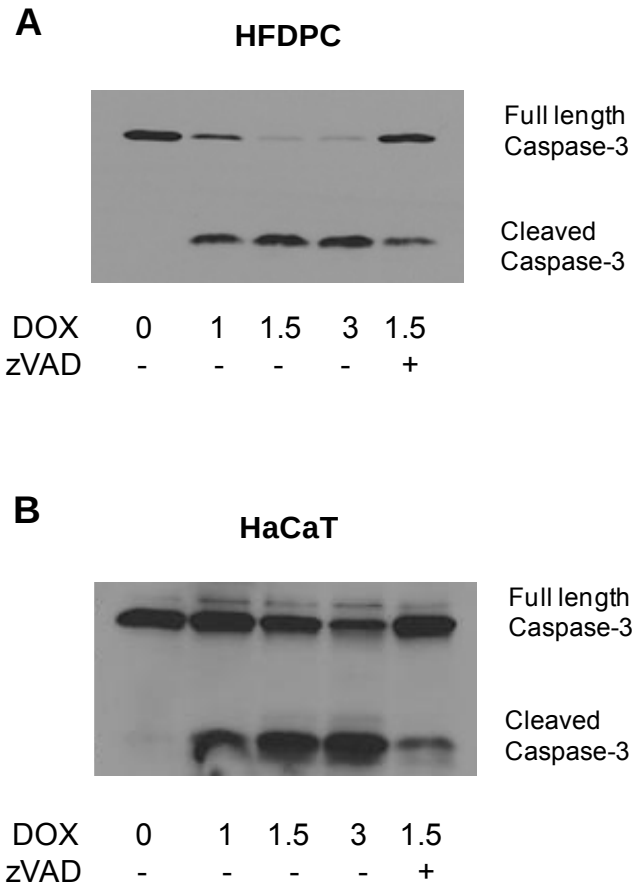

Figure 35. Doxorubicin induces caspase-3 activation. **A** and **B** HFDPC and HaCaT cells were treated with various concentrations of doxorubicin (DOX; 0-3 μM) in the presence or absence of pan-caspase inhibitor (z-VAD-fmk; 10 μM) for 24 h. Caspase-3 activation was determined by Western blotting using caspase-3 antibody.

4. Doxorubicin induces apoptosis through mitochondrial pathway

Because caspase-9 serves as the apical caspase of the intrinsic death pathway and caspase-8 represents the apical caspase of the extrinsic pathway (Li et al., 1997; Gupta, 2003), we analyzed caspase-8 and -9 activities in doxorubicin-treated cells to identify the apoptosis pathway. Figure 36 shows that doxorubicin induced caspase-9 activation in a dose-dependent manner whereas it had no effect on caspase-8 activity, indicating that the mitochondrial pathway is the major pathway of apoptosis induced by doxorubicin.

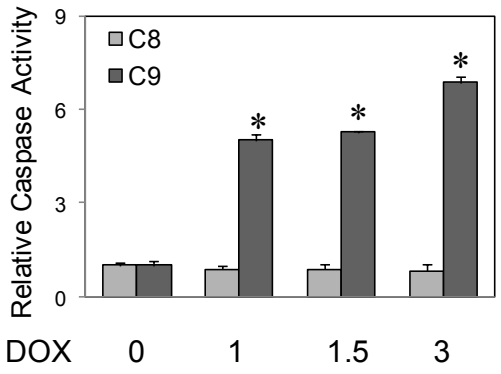

Figure 36. Doxorubicin induces caspase-9 activation. HaCaT cells were treated with various concentrations of doxorubicin (DOX; 0-3 μM) for 12 h and were analyzed for caspase-8 and -9 activity using the fluorometric substrate FAM-LETD-fmk and FAM-LEHD-fmk, respectively. Plots are mean ± S.D. (n = 3). *, $p < 0.05$ versus non-treated control.

5. Doxorubicin induces ROS generation in HFDPC and HaCaT cells

To determine whether doxorubicin could induce ROS generation in HFDPC an HaCaT cells which may link to their apoptosis, cellular ROS levels in response to doxorubicin treatment were determined by flow cytometry using H_2DCF-DA as a fluorescent probe. H_2DCF-DA is a general oxidative probe that can detect multiple ROS. Figure 37, A and B, shows that doxorubicin was able to increase ROS fluorescence intensity in a dose dependent manner. Figure 37, C and D, shows representative results of the flow cytometry and microscopy experiments which support the generation of ROS in doxorubicin-treated HFDPC and HaCaT cells.

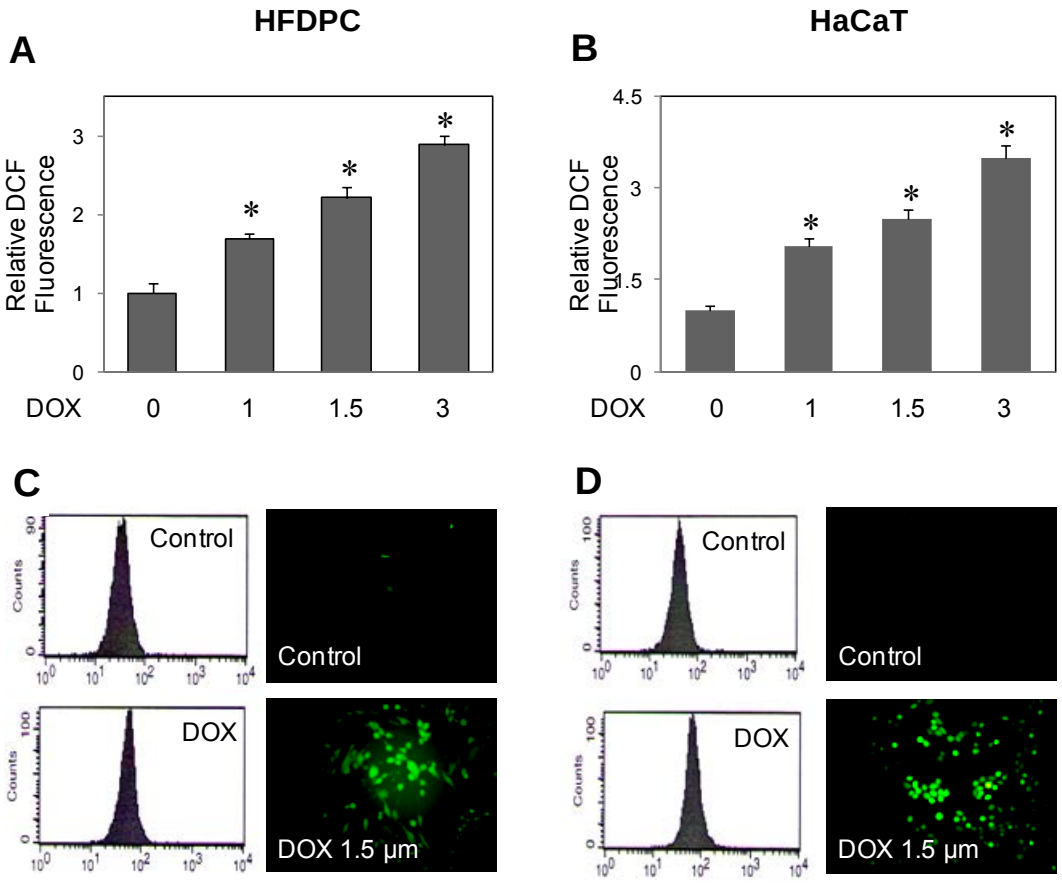

Figure 37. Effect of doxorubicin on cellular ROS generation. **A** and **B** HFDPC and HaCaT cells were treated with doxorubicin (0-3 µM) for 2 h, after which they were analyzed for ROS generation by flow cytometry using H_2DCF-DA as a fluorescent

probe. **C** and **D** representative flow cytometric histograms (*left*) and fluorescence micrographs (*right*) of DCF measurements in the treated cells (original magnification, 400X). Plots are mean ± S.D. (n = 3). *, $p < 0.05$ versus non-treated control.

6. Role of specific ROS in doxorubicin-induced apoptosis

To determine the role of specific ROS in doxorubicin-induced apoptosis, HFDPC and HaCaT cells were treated with doxorubicin in the presence or absence of various specific ROS scavengers, including MnTBAP (MnSOD mimetic and superoxide scavenger), catalase (hydrogen peroxide scavenger) and DMTU (hydroxyl radical scavenger), and apoptosis was determined by Hoechst 33342 assay. Figure 38 shows that MnTBAP but not catalase or DMTU was able to inhibit DOX-induced apoptosis.

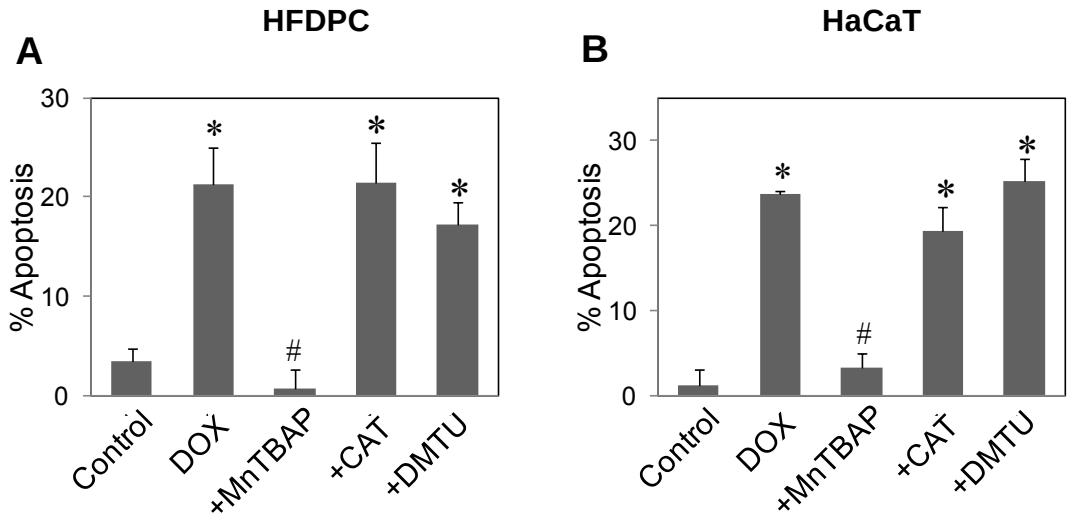

Figure 38. Role of specific ROS in doxorubicin-induced apoptosis. **A** and **B** HFDPC and HaCaT cells were pretreated for 30 min with MnTBAP (50 μM), catalase (CAT, 7,500 U/ml), or DMTU (5 mM) followed by doxorubicin treatment (1.5 μM) for 24 h and analyzed for apoptosis by Hoechst 33342 assay. Plots are mean ± S.D. (n = 3). *, $p < 0.05$ versus non-treated control. #, $p < 0.05$ versus doxorubicin-treated control.

7. Identification of specific ROS generation by doxorubicin

To further investigate the specific ROS generated, HFDPC and HaCaT cells were treated with doxorubicin in the presence or absence of various specific ROS scavengers, including MnTBAP, catalase and DMTU, and cellular ROS generation were determined as above. Consistent with apoptosis data, Figure 39 shows that pretreatment of the cells with MnTBAP but not with catalase or DMTU completely inhibited the generation of ROS induced by doxorubicin. The results suggest that superoxide is the primary ROS produced by HFDPC and HaCaT cells in response to doxorubicin treatment and that this oxidative species play a key role in apoptosis induced by doxorubicin.

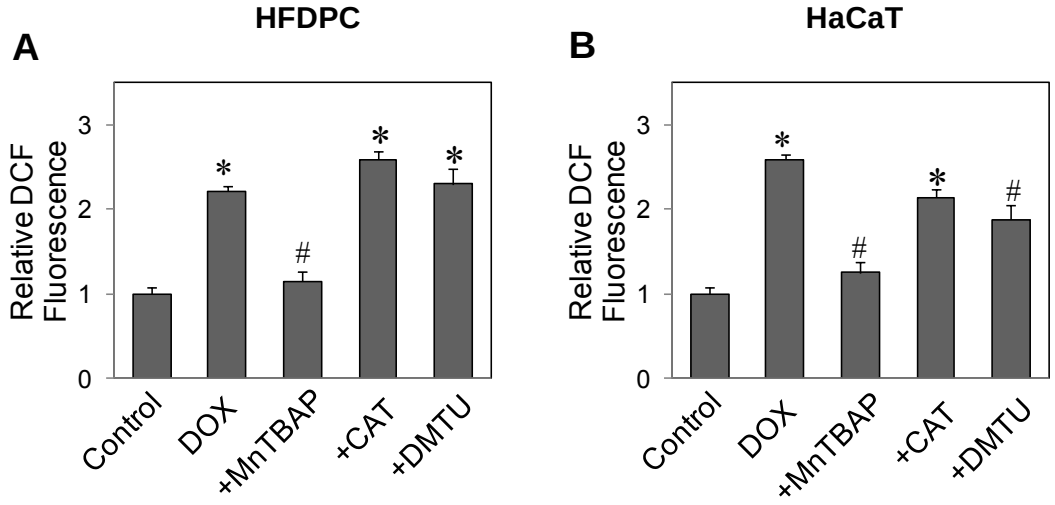

Figure 39. Specific ROS generation induced by doxorubicin. **A** and **B** HFDPC and HaCaT cells were pretreated for 30 min with MnTBAP (50 μM), catalase (CAT, 7,500 U/ml), or DMTU (5 mM) followed by doxorubicin treatment (1.5 μM) for 2 h and analyzed for ROS generation at 2 h by flow cytometry using H_2DCF-DA as a fluorescence probe. Plots are mean ± S.D. (n = 3). *, $p < 0.05$ versus non-treated control. #, $p < 0.05$ versus doxorubicin-treated control.

To confirm the generation of ROS in treated cells, ESR measurements were performed using DMPO as a spin trapping agent. The ESR technique was used because it allows more accurate identification of the specific ROS involved. The hyperfine coupling of the spin adduct is generally characteristic of the original trapped radical. Cells were treated with doxorubicin in the presence or absence of specific ROS scavengers and analyzed for free radical generation. Non-treated cells with DMPO were used as a negative control. In the presence of added doxorubicin, a clear positive signal was observed (Fig. 40). Based on the line shape and hyperfine splitting, the spectrum observed is indicative of superoxide anion. The observation that MnTBAP, but not other ROS scavengers, totally inhibited the ESR signal further indicates the specificity of superoxide detection. This finding indicates superoxide anion as the major ROS generated by doxorubicin.

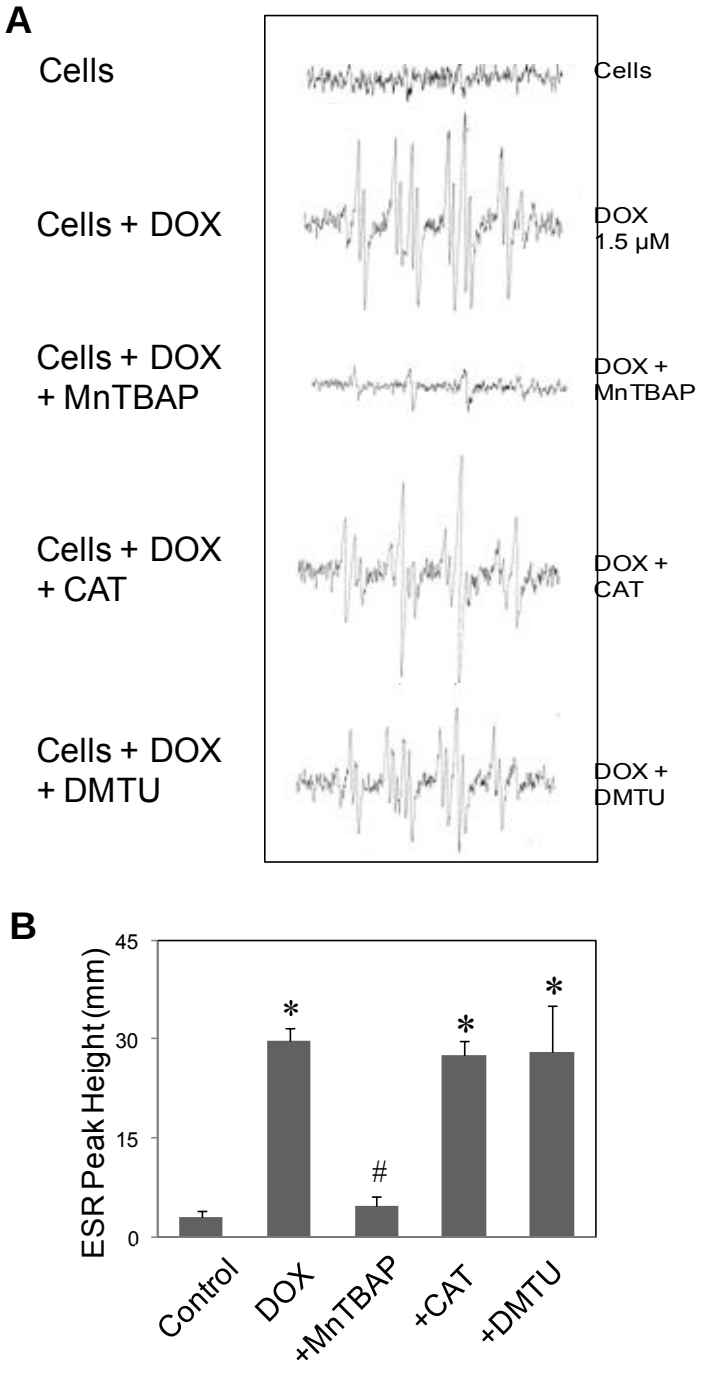

Figure 40. Superoxide induction by doxorubicin treatment. **A** HaCaT cells ($1x10^6$ cells/ml) were incubated in PBS containing the spin trapper DMPO (10 mM) with or without doxorubicin (1.5 µM), MnTBAP (50 µM), catalase (CAT, 7,500 units/ml), and DMTU (5 mM). ESR spectra were then recorded 5 min (peak response time) after the addition of the test agents. The spectrometer settings were as follows: receiver gain at $1.5x10^5$, time constants at 0.3 sec, modulation amplitude at 1.0 G, scan time at

4 min, and magnetic field at 3,470 ± 100 G. Plots are mean ± S.D. (n = 3). *, $p < 0.05$ versus non-treated control (cells). #, $p < 0.05$ versus doxorubicin-treated control.

8. Doxorubicin induces mitochondrial superoxide generation

The induction of superoxide generation by doxorubicin was confirmed by flow cytometry using dihydroethidium (DHE) as a fluorescent probe. The result showed a dose dependent increase in DHE fluorescence in doxorubicin-treated cells (Fig. 41). Next, mitochondria-targeted hydroethidium (MitoSOX^{TM} Red) was used to further investigate whether mitochondria is a possible source of superoxide generation. Figure 42 shows an increase in mitochondrial fluorescence of MitoSOX in doxorubicin-treated cells, which was completely inhibited by MnTBAP. This result strongly supports the role of mitochondria in doxorubicin-induced superoxide generation.

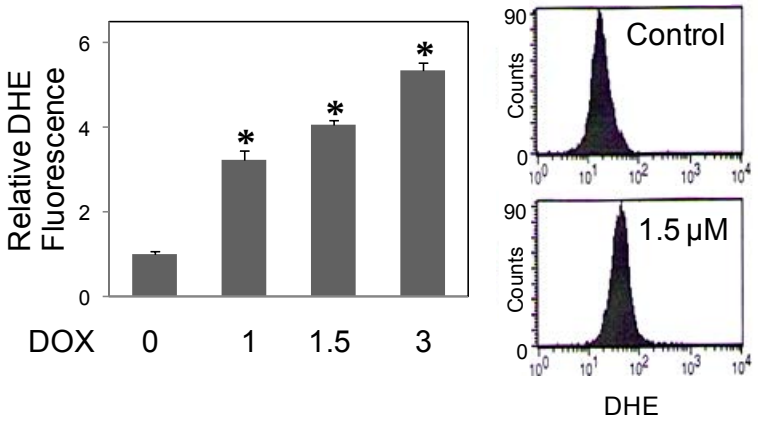

Figure 41. Effect of doxorubicin on cellular superoxide generation. HaCaT cells were treated with various concentrations of doxorubicin (0-3 μM) for 2 h, after which they were analyzed for superoxide generation by flow cytometry using DHE as a fluorescent probe. Representative flow cytometric histograms were shown in the *right* panel. Plots are mean ± S.D. (n = 3). *, $p < 0.05$ versus non-treated control.

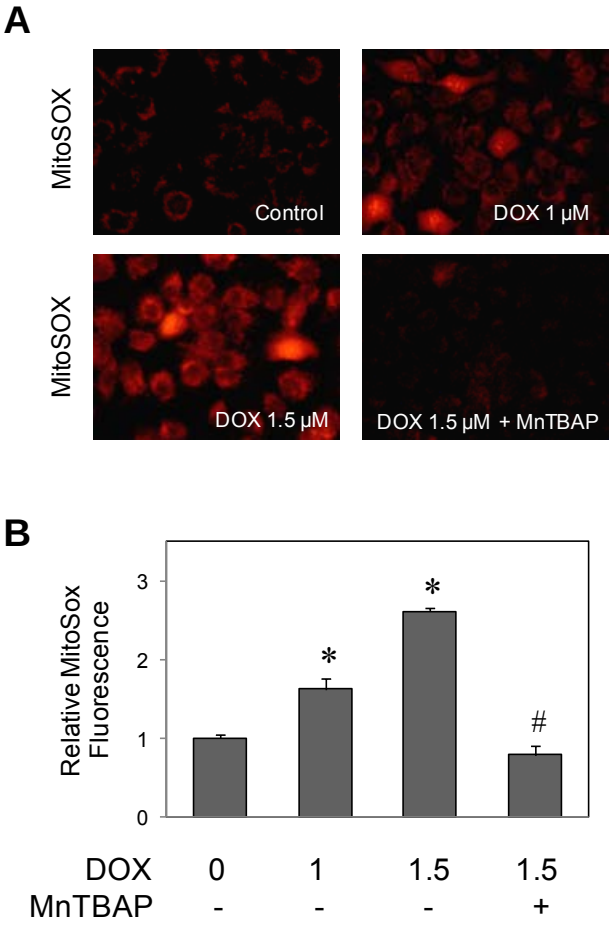

Figure 42. Effect of doxorubicin on mitochondrial superoxide generation. HaCaT cells were treated with DOX in the presence or absence of MnTBAP (50 μM) for 2 h, and analyzed for mitochondrial superoxide generation by fluorescence microscopy using MitoSOX^{TM} Red as a fluorescent probe. **A** representative fluorescence micrographs demonstrating dose-dependent increase in mitochondrial MitoSOX^{TM} fluorescence were shown. **B** analysis of fluorescence micrographs. Plots are mean ± S.D. (n = 3). *, $p < 0.05$ versus non-treated control. #, $p < 0.05$ versus doxorubicin-treated control.

9. Mitochondrial superoxide mediates doxorubicin-induced apoptosis

To test the role of mitochondrial superoxide in the apoptotic process, cells were ectopically transfected with MnSOD (mitochondrial SOD) or control plasmid,

and their effect on doxorubicin-induced apoptosis was determined. Western blot analysis of MnSOD-transfected cells showed an increase in MnSOD protein expression over vector-transfected control (Fig. 43A). The MnSOD overexpressing cells showed a strong reduction in apoptotic response to doxorubicin treatment as compared to control cells (Fig. 43B). Overexpression of MnSOD also caused a substantial reduction in doxorubicin-induced superoxide generation (Fig. 44). These results indicate mitochondrial superoxide as a key contributor to doxorubicin-induced apoptosis.

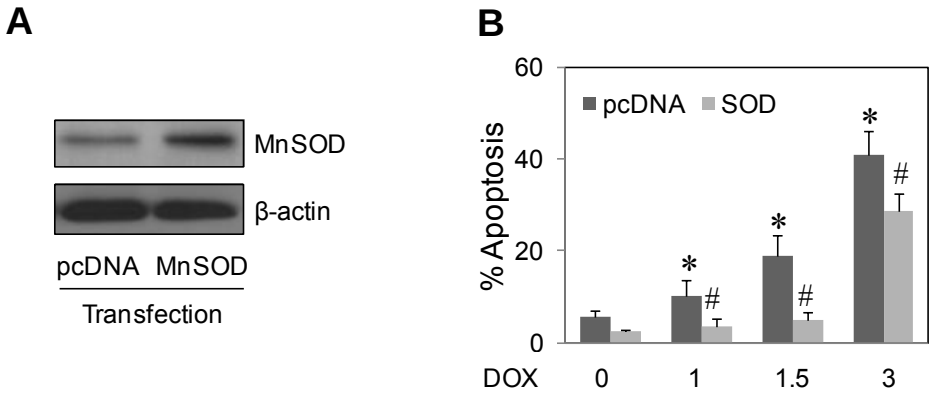

Figure 43. MnSOD overexpression inhibits doxorubicin-induced apoptosis. HaCaT cells were transiently transfected with mitochondrial superoxide scavenging enzyme MnSOD or control pcDNA3 plasmid as described under *Materials and Methods*. **A** MnSOD expression of transfected cells were analyzed by Western blotting. **B** transfected cells were treated with doxorubicin (0-3 μM) for 24 h and analyzed for apoptosis by Hoechst 33342 assay. Plots are mean ± S.D. (n = 3). *, $p < 0.05$ versus vector-transfected cells. #, $p < 0.05$ versus doxorubicin-treated vector transfected cells.

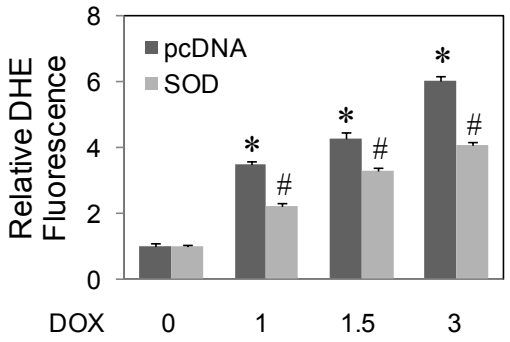

Figure 44. MnSOD overexpression inhibits doxorubicin-induced superoxide induction. HaCaT cells were transiently transfected with mitochondrial superoxide scavenging enzyme MnSOD or control pcDNA3 plasmid as described under *Materials and Methods*. Transfected cells were treated with DOX (0-3 μM) and analyzed for superoxide generation by flow cytometry at 2 h after the treatment. *, $p < 0.05$ versus vector-transfected cells. #, $p < 0.05$ versus doxorubicin-treated vector transfected cells.

10. Effects of doxorubicin treatment on apoptosis-regulatory proteins

The mitochondrial pathway of apoptosis is regulated by the balance of pro- and anti-apoptotic proteins, particularly in the Bcl-2 family. Two key apoptosis-regulatory proteins in the Bcl-2 family, namely Bax and Bcl-2, were examined and evaluated their response to doxorubicin treatment. Immunoblot studies showed that doxorubicin induced a down-regulation of the anti-apoptotic Bcl-2 protein in a dose-dependent manner and caused an up-regulation of the pro-apoptotic Bax protein in HFDPC and HaCaT cells (Fig. 45).

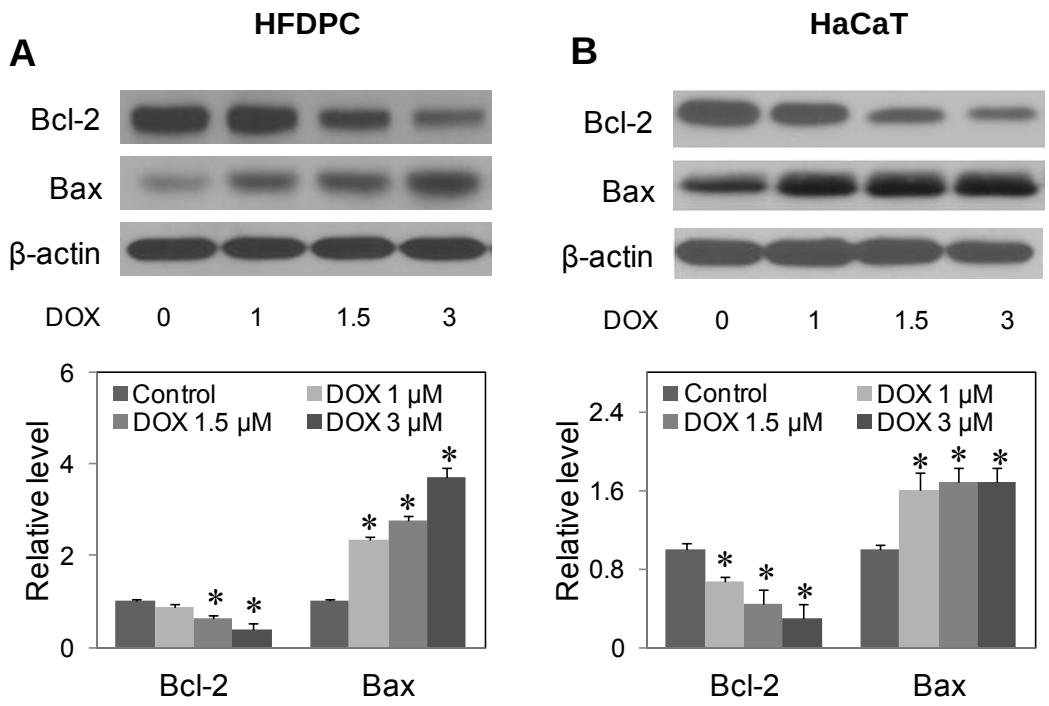

Figure 45. Effect of doxorubicin treatment on apoptosis-regulatory proteins. **A** and **B** HFDPC and HaCaT cells were treated with doxorubicin (0-3 μM) for 24 h. Cell lysates were prepared and analyzed for Bcl-2 and Bax expression by Western blotting using Bcl-2 and Bax antibodies. Blots were reprobed with β-actin antibody to confirm equal loading of samples. Immunoblots signals were quantified by densitometry, and mean data from three independent experiments (one of which is shown here) was normalized to the result obtained in cells without treatment (control). Plots are mean ± S.D. (n = 3). *, $p < 0.05$ versus non-treated control.

In addition, p53 and its active phosphorylated form were also examined. Doxorubicin surprisingly down-regulated the pro-apoptotic p53 protein, but up-regulated its phosphorylated form at low doxorubicin doses (Fig. 46). Since the expression of p53 and its active form showed no correlation with the apoptosis

response, we concluded that doxorubicin-induced apoptosis was mediated through Bcl-2-dependent but p53-independent mechanisms.

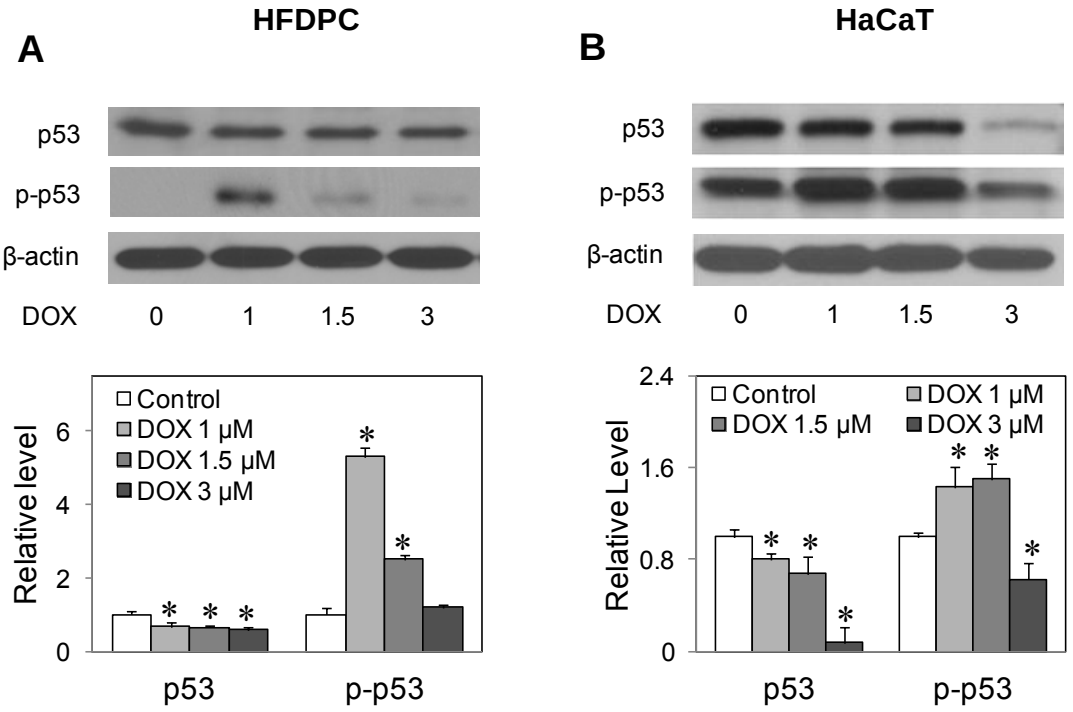

Figure 46. Effect of doxorubicin on p53 and its active phosphorylated form. **A** and **B** HFDPC and HaCaT cells were treated with doxorubicin (0-3 μM) for 24 h. Cell lysates were prepared and analyzed for p53 and phospho-p53 expression by Western blotting using p53 and phosphor-p53 antibodies. β-actin was used as a loading control. Plots are mean ± S.D. (n = 3). *, $p < 0.05$ versus non-treated control.

11. Doxorubicin regulates Bcl-2 and Bax through superoxide

To determine the potential role of ROS in Bcl-2 and Bax regulation, the expression levels of Bcl-2 and Bax after doxorubicin treatment were determined. To identify the specific ROS involved, HFDPC and HaCaT cells were co-treated with MnTBAP, catalase, or DMTU. In agreement with the apoptosis results (Fig. 38), doxorubicin down-regulation of Bcl-2 was found to be inhibited by MnTBAP, but not

by catalase or DMTU (Fig. 47). MnTBAP also inhibited the effect of doxorubicin on Bax, whereas catalase and DMTU had no effect.

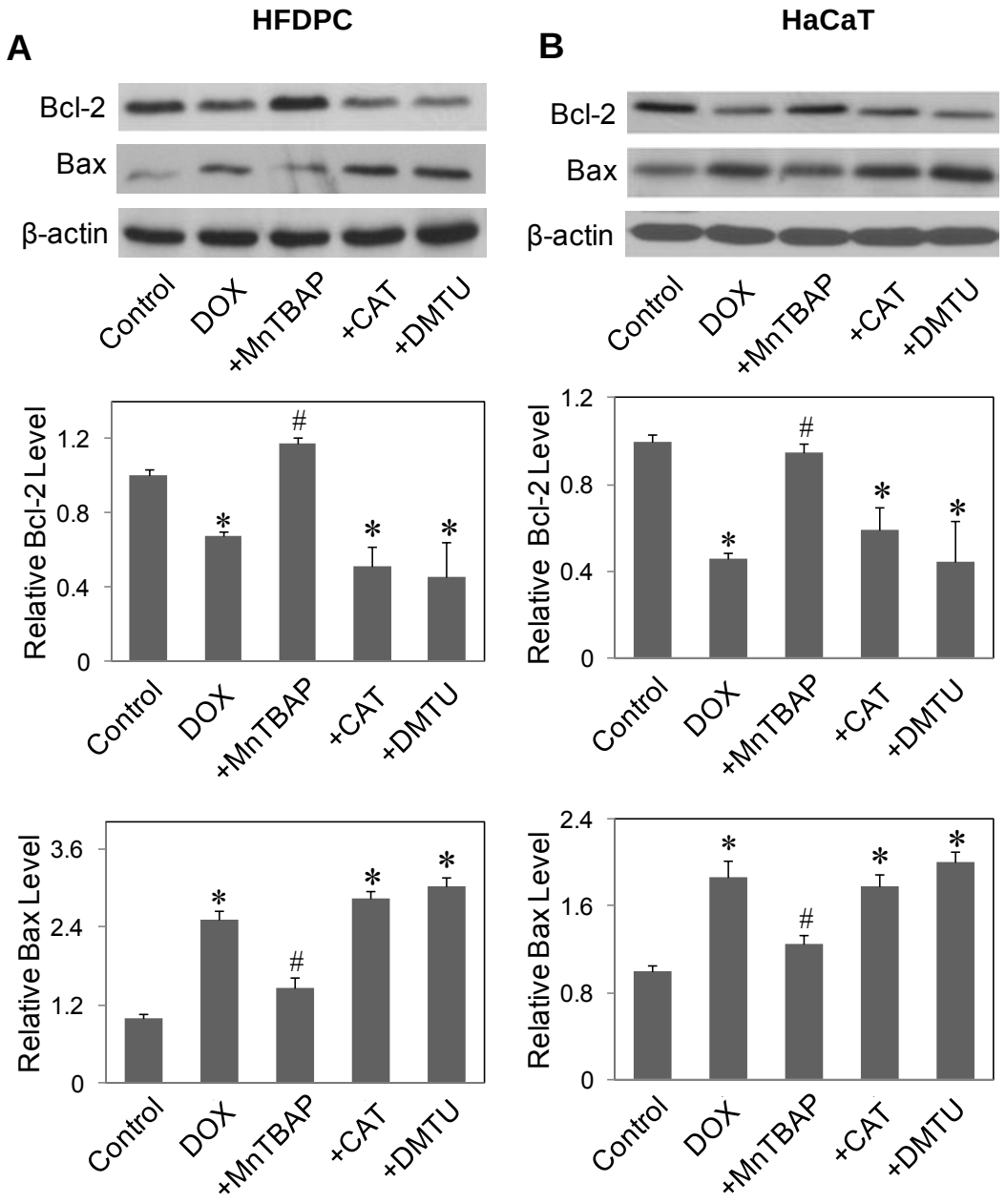

Figure 47. Effects of doxorubicin and ROS scavengers on apoptotic proteins. **A** and **B** HFDPC and HaCaT cells were pretreated for 30 min with MnTBAP (50 μM), catalase (CAT, 7,500 units/ml), or DMTU (5 mM) followed by doxorubicin (DOX, 1.5 μM) for 24 h. Cell lysates were prepared and analyzed for Bcl-2 and Bax expression by Western blotting using Bcl-2 and Bax antibodies. β-actin was used as a

loading control. Plots are mean ± S.D. (n = 3). *, $p < 0.05$ versus non-treated control. #, $p < 0.05$ versus doxorubicin-treated control.

Since the fate of cells is determined by the balance of pro- and anti-apoptotic proteins, the Bcl-2-to-Bax ratio was reported (Fig. 48).

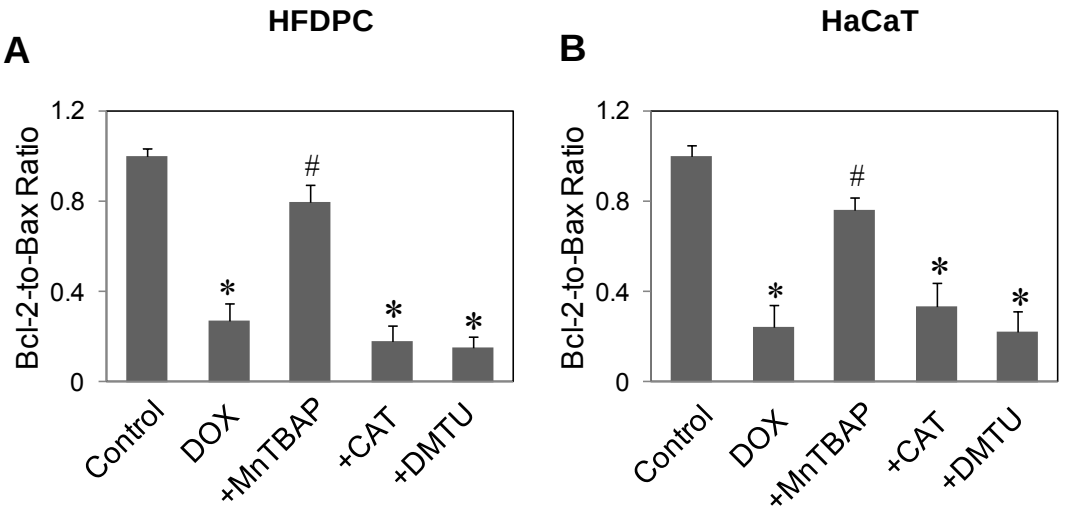

Figure 48. Effects of doxorubicin and ROS scavengers on Bcl-2-to-Bax ratio. **A** and **B** HFDPC and HaCaT cells were pretreated for 30 min with MnTBAP (50 μM), catalase (CAT, 7,500 units/ml), or DMTU (5 mM) followed by doxorubicin (DOX, 1.5 μM) for 24 h. Cell lysates were prepared and analyzed for Bcl-2 and Bax expression by Western blotting using Bcl-2 and Bax antibodies. Histograms represents ratio of Bcl-2 and Bax expression. Plots are mean ± S.D. (n = 3). *, $p < 0.05$ versus non-treated control. #, $p < 0.05$ versus doxorubicin-treated control.

12. Doxorubicin down-regulates Bcl-2 through proteasomal degradation

Bcl-2 has been shown to be regulated by ubiquitin-proteasomal degradation pathway under diverse apoptosis conditions (Chanvorachote et al., 2006; Azad et al.,

2008; Wang et al., 2008). To determine whether this pathway is involved in the down-regulation of Bcl-2 by cisplatin in the test cell systems, HFDPC and HaCaT cells were treated with lactacystin, a highly specific proteasome inhibitor, and its effects on doxorubicin-induced Bcl-2 down-regulation was determined by Western blotting. As lysosomal degradation is another possible pathway of protein degradation (Ciechanover, 2005), cells were also treated with doxorubicin in the presence or absence concanamycin A, a known lysosome inhibitor. Figure 49 shows that lactacystin inhibited the down-regulation of Bcl-2 by doxorubicin both in HFDPC and HaCaT cells, whereas concanamycin A had no significant effect, suggesting proteasomal degradation as the primary mechanism of doxorubicin-induced Bcl-2 down-regulation.

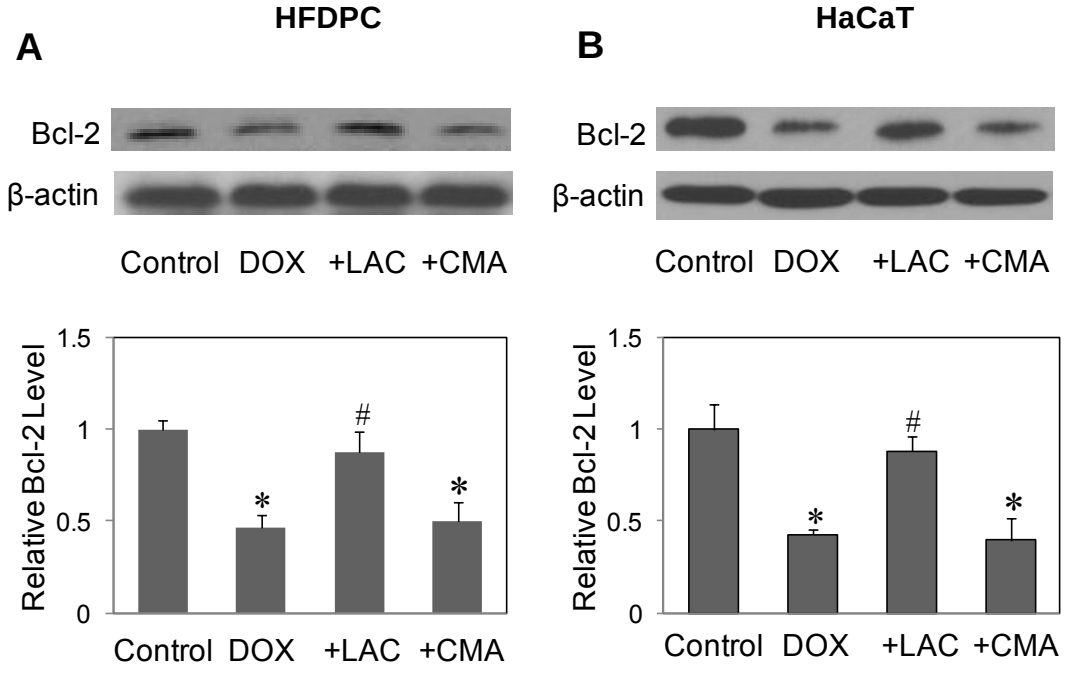

Figure 49. Doxorubicin down-regulates Bcl-2 through proteasomal degradation. **A** and **B** HFDPC and HaCaT cells were pretreated with proteasome inhibitor lactacystin (LAC, 10 μM) or with lysosome inhibitor concanamycin A (CMA, 1 μM) for 1 h, and then treated with doxorubicin (1.5 μM) for 24 h. Bcl-2 expression was determined by

Western blots using anti-Bcl-2 antibody. Plots are mean ± S.D. (n = 3). *, $p < 0.05$ versus non-treated control. #, $p < 0.05$ versus doxorubicin-treated control.

13. Doxorubicin induces Bcl-2 ubiquitination

Ubiquitination is a major cellular process for selective removal of proteins via proteasomal degradation (Lecker et al., 2006). To test whether doxorubicin could induce Bcl-2 ubiquitination in the test cell systems, cells were treated with doxorubicin for various time (0-3 h), and cell lysates were prepared and immunoprecipitated using anti-Bcl-2 antibody. The resulting immune complexes were then analyzed for ubiquitination using anti-ubiquitin antibody. Doxorubicin induced Bcl-2 ubiquitination was observed as early as 1 h and peaked at approximately 2 h after treatment (Fig. 50).

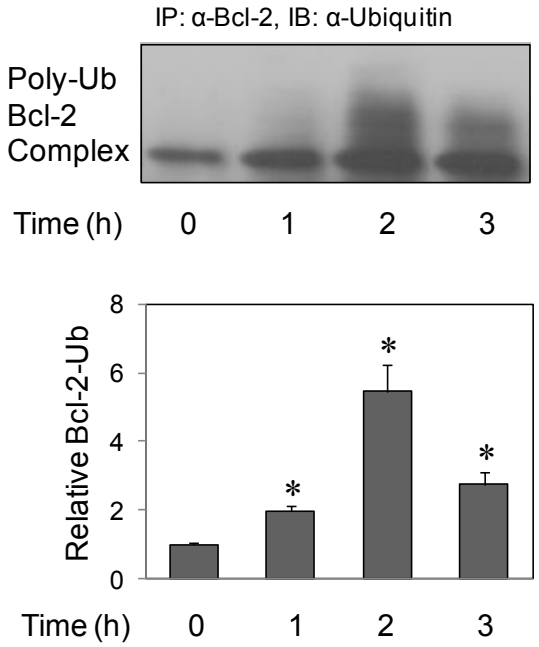

Figure 50. Doxorubicin induces Bcl-2 ubiquitination. HaCaT cells were pretreated with LAC (10 μM) for 1 h (to prevent proteasomal degradation of Bcl-2) and then treated with doxorubicin (1.5 μM) for various times (0-3 h). Cell lysates were

immunoprecipitated with anti-Bcl-2 antibody and the immune complexes were analyzed for ubiquitin by Western blotting. Plots are mean ± S.D. (n = 3). *, $p < 0.05$ versus non-treated control.

14. Doxorubicin induces Bcl-2 ubiquitination through superoxide

To test whether ROS play the role in Bcl-2 ubiquitination, HFDPC and HaCaT cells were treated with doxorubicin in the presence or absence of various ROS scavengers, and cell lysates were prepared and analyzed for Bcl-2 ubiquitination by immunoprecipitation. Pretreatment of the cells with MnTBAP completely inhibited the ubiquitination of Bcl-2 by doxorubicin (Fig. 51). Neither catalase nor DMTU was able to significantly inhibit the ubiquitination, indicating that superoxide is the major oxidative species involved in the ubiquitination.

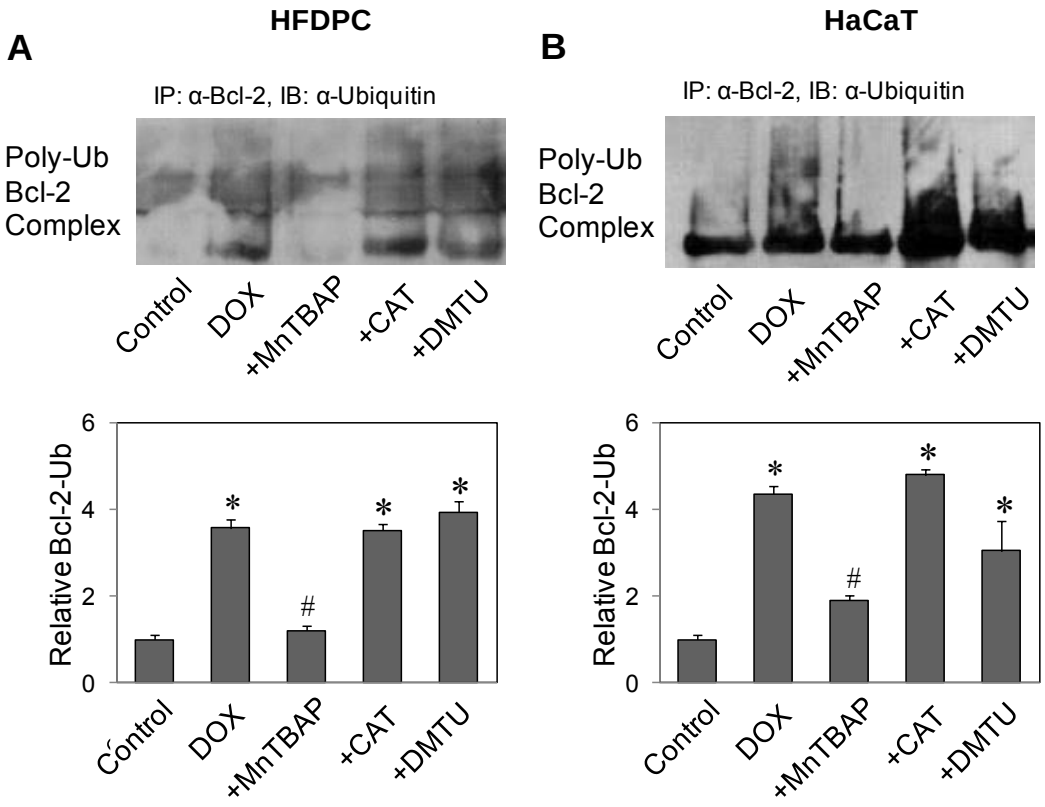

Figure 51. Effect of doxorubicin and ROS scavengers on Bcl-2 ubiquitination. **A** and **B** HFDPC and HaCaT cells were pretreated with LAC (10 μM) for 1 h (to prevent proteasomal degradation of Bcl-2) and then treated with doxorubicin in the presence or absence of MnTBAP (50 μM), catalase (CAT, 7,500 units/ml), or DMTU (5 mM) for 2 h. Cell lysates were immunoprecipitated with anti-Bcl-2 antibody and the immune complexes were analyzed for ubiquitin by Western blotting. Analysis of ubiquitin was performed at 2 h posttreatment where ubiquitination was found to be maximal. Plots are mean ± S.D. (n = 3). *, $p < 0.05$ versus non-treated control. #, $p < 0.05$ versus doxorubicin-treated control.

15. Doxorubicin induces dephosphorylation of Bcl-2

Bcl-2 ubiquitinaiton has been reported to be regulated by its phosphorylation. Certain apoptotic agents such as lipopolysaccharide and cisplatin have been shown to

induce Bcl-2 dephosphorylation that triggers its ubiquitination (Dimmeler et al., 1999; Wang et al., 2008). To test whether doxorubicin can induce this process in HFDPC and HaCaT cells, cells were treated with doxorubicin and its effect on Bcl-2 phosphorylation were examined. Figure 52 shows that doxorubicin induces Bcl-2 dephosphorylation in a dose-dependent manner.

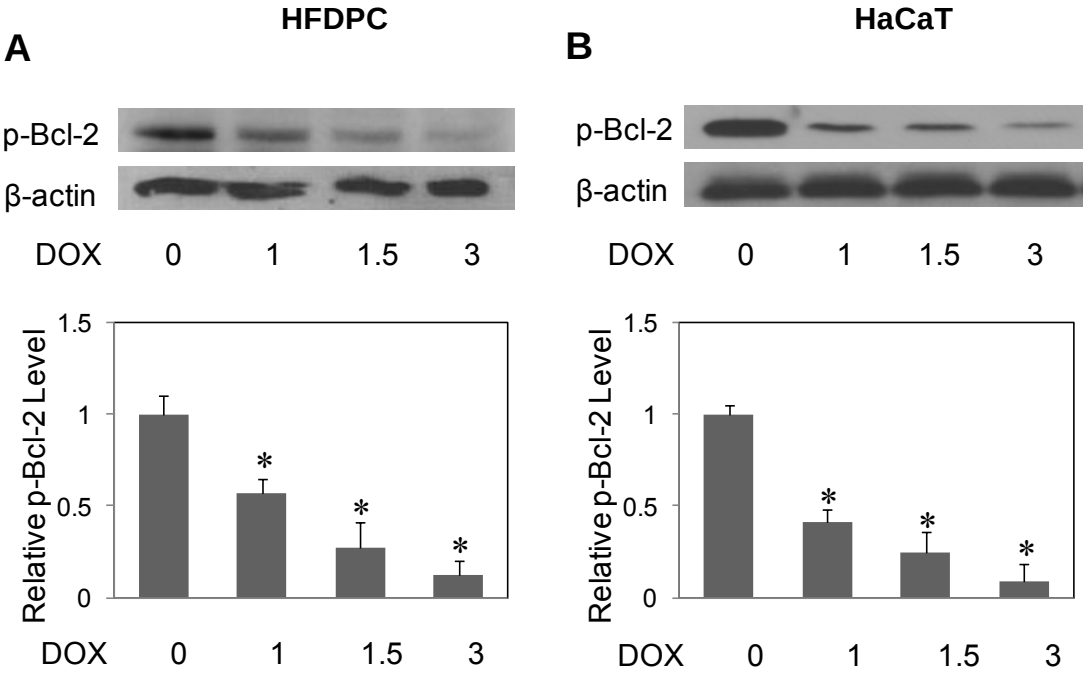

Figure 52. Dephosphorylation of Bcl-2 by doxorubicin. **A** and **B** HFDPC and HaCaT cells were treated with doxorubicin (0-3 μM) for 24 h. Cell lysates were prepared and analyzed for phospho-Bcl-2 expression by Western blotting using phospho-Bcl-2 antibody. β-actin was used as a loading control. Plots are mean ± S.D. (n = 3). *, $p <$ 0.05 versus non-treated control.

16. Identification of Bcl-2 kinases

One of the primary phosphorylation-dephosphorylation signaling cascades is mitogen-activated protein (MAP) kinases, including p44/p42 extracellular signal-related kinases (ERK1/2), c-Jun-NH2-terminal protein kinase (JNKs), and p38 kinase

(Su and Karin, 1996; Ruvolo et al., 2001). Accordingly, one or more of the MAP kinases may serve as Bcl-2 kinases. Cells were treated with doxorubicin in the presence or absence of various known kinase inhibitors including PD98059 (ERK1/2 inhibitor), SB203580 (p38 inhibitor), and SP600125 (JNK inhibitor), and their effects on Bcl-2 phosphorylation were examined. Figure 53 shows that PD98059 was able to enhance doxorubicin-induced dephosphorylation, whereas SB203580 had minor effects. SP600125 sustained the Bcl-2 phosphorylation, attributable to an observed activation of ERK1/2 by this inhibitor (Fig. 54).

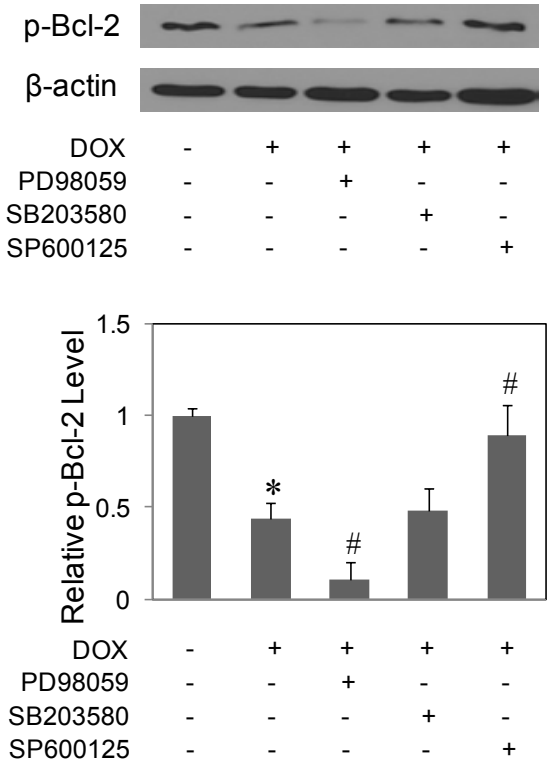

Figure 53. Effects of MAP kinases inhibitors on Bcl-2 phosphorylation. HaCaT cells were treated with DOX (1.5 μM) in the presence or absence of PD98059 (ERK1/2 inhibitor, 25 μM), SB203580 (p38 inhibitor, 10 μM), and SP600125 (JNK inhibitor, 10 μM) and p-Bcl-2 was determined. β-actin was used as a loading control. Plots are

mean ± S.D. (n = 3). *, $p < 0.05$ versus non-treated control. #, $p < 0.05$ versus doxorubicin-treated control.

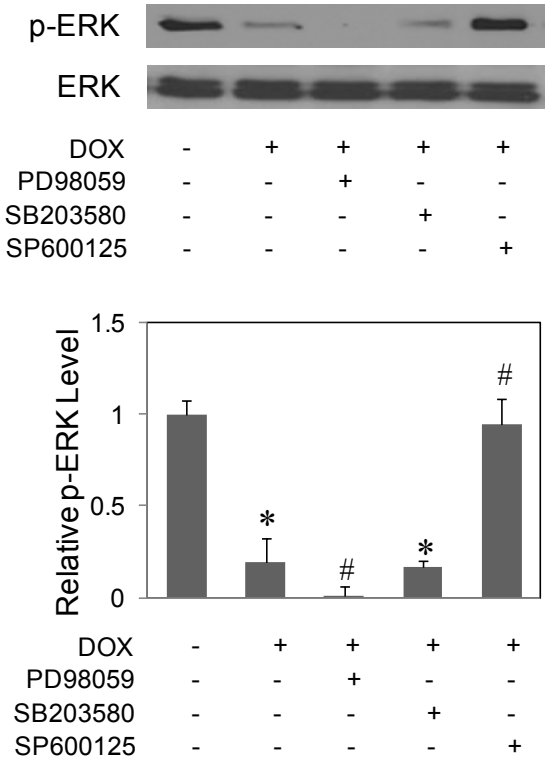

Figure 54. Effects of MAP kinases inhibitors on ERK1/2 phosphorylation. HaCaT cells were treated with DOX (1.5 μM) in the presence or absence of PD98059 (ERK1/2 inhibitor, 25 μM), SB203580 (p38 inhibitor, 10 μM), and SP600125 (JNK inhibitor, 10 μM) and p-ERK1/2 was determined. Blots were reprobed with ERK1/2 antibody to confirm equal loading of samples. Plots are mean ± S.D. (n = 3). *, $p < 0.05$ versus non-treated control. #, $p < 0.05$ versus doxorubicin-treated control.

To confirm the role of inactivation (dephosphorylation) of ERK1/2 in Bcl-2 dephosphorylation, cells were treated with various concentration of doxorubicin (0-3 μM) and its effect on ERK1/2 phosphorylation was evaluated by Western blotting. Figure 55 shows that doxorubicin dose-dependently induced ERK1/2 inactivation in a

close association with Bcl-2 dephosphorylation (Fig. 52). Both JNK1 and p38 kinase were oppositely activated (phosphorylated) following doxorubicin treatment, while phospho-JNK2 was not detected in the test system. These findings suggested that ERK1/2, but not JNKs and p38 kinase, is a potential Bcl-2 kinase.

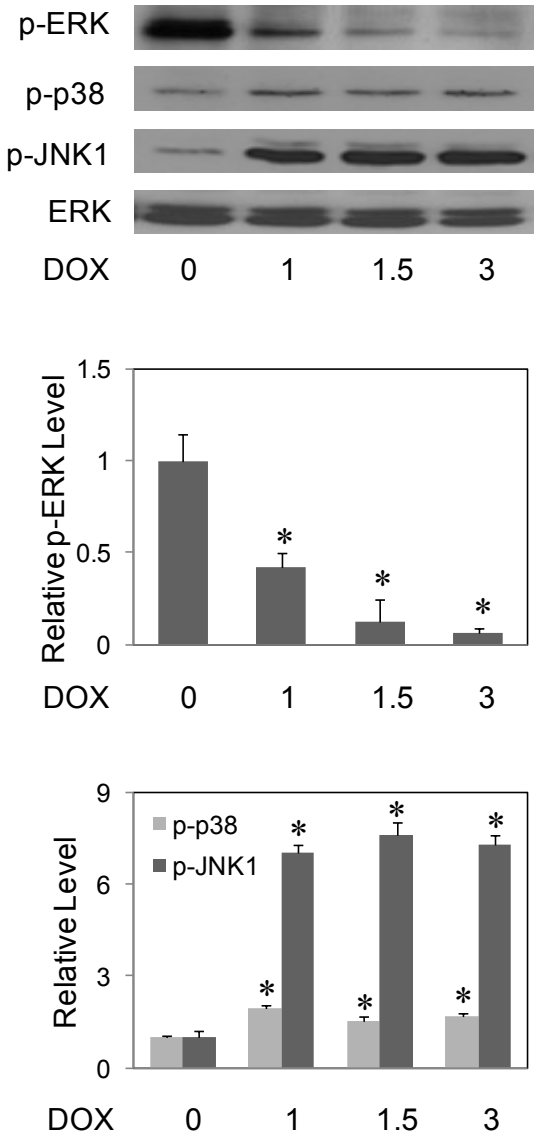

Figure 55. Doxorubicin induces ERK1/2 inactivation. HaCaT cells were treated with doxorubicin (0-3 μM) for 24 h. Cell lysates were prepared and analyzed for phospho-ERK1/2, phospho-p38, and phospho-JNK expression by Western blotting using phospho-ERK1/2, phospho-p38, and phospho-JNK antibodies. Blots were reprobed

with ERK1/2 antibody to confirm equal loading of samples. Plots are mean ± S.D. (n = 3). *, $p < 0.05$ versus non-treated control.

To further confirm the role of ERK1/2 and other kinases on Bcl-2 ubiquitination, cells were treated with DOX in the presence or absence of various known kinase inhibitors including PD98059, SB203580, and SP600125, and their effects on Bcl-2 ubiqutination were examined. Consistency with the effect on Bcl-2 dephosphorylation, PD98059 was able to induce doxorubicin-induced ubiquitination, (Fig. 56).

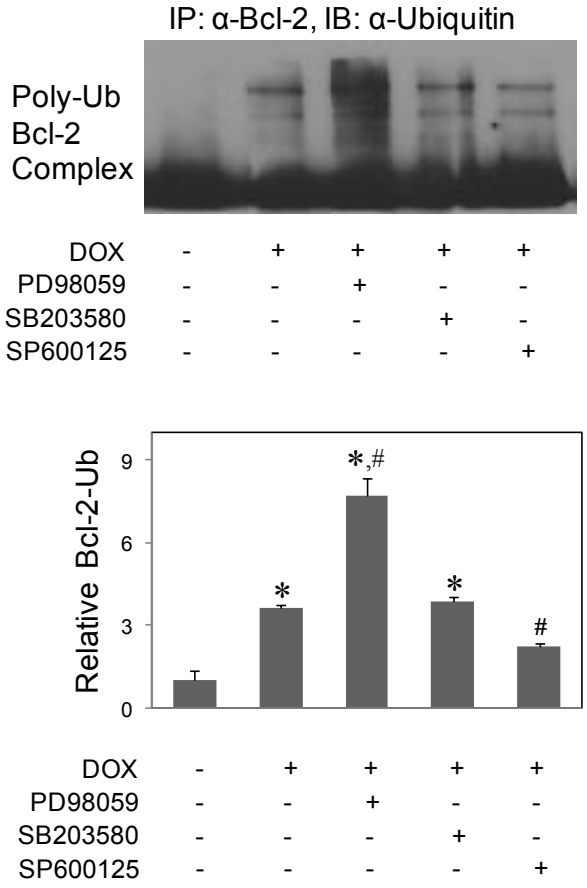

Figure 56. Effects of MAP kinases inhibitors on Bcl-2 ubiquitination. HaCaT cells were treated with DOX (1.5 μM) in the presence or absence of PD98059 (ERK1/2 inhibitor, 25 μM), SB203580 (p38 inhibitor, 10 μM), and SP600125 (JNK inhibitor,

10 μM). Analysis of Bcl-2 ubiquitination was performed as described at 2 h post-treatment where it was found to be maximal. Plots are mean ± S.D. (n = 3). *, $p < 0.05$ versus non-treated control. #, $p < 0.05$ versus doxorubicin-treated control.

17. Superoxide mediates dephosphorylation of Bcl-2 and inactivation of ERK1/2

Bcl-2 ubiquitination induced by doxorubicin was shown to be dependent on ROS. To test whether ROS might mediate its effect through ERK1/2 inactivation and Bcl-2 dephosphorylation, cells were treated with doxorubicin in the presence or absence of various ROS scavengers including MnTBAP, catalase and DMTU, and analyzed for ERK1/2 and Bcl-2 phosphorylation. Figure 57 shows that treatment of the cells with MnTBAP, but not by catalase or DMTU, completely inhibited doxorubicin-induced ERK1/2 and Bcl-2 dephosphorylation. These results are consistent with the apoptosis (Fig. 38) and Bcl-2 ubiquitination (Fig. 51) data, and indicate that superoxide mediates the Bcl-2 destabilizing effect of doxorubicin by inactivating ERK1/2, which promotes dephosphorylation and subsequent ubiquitin-proteasomal degradation of Bcl-2.

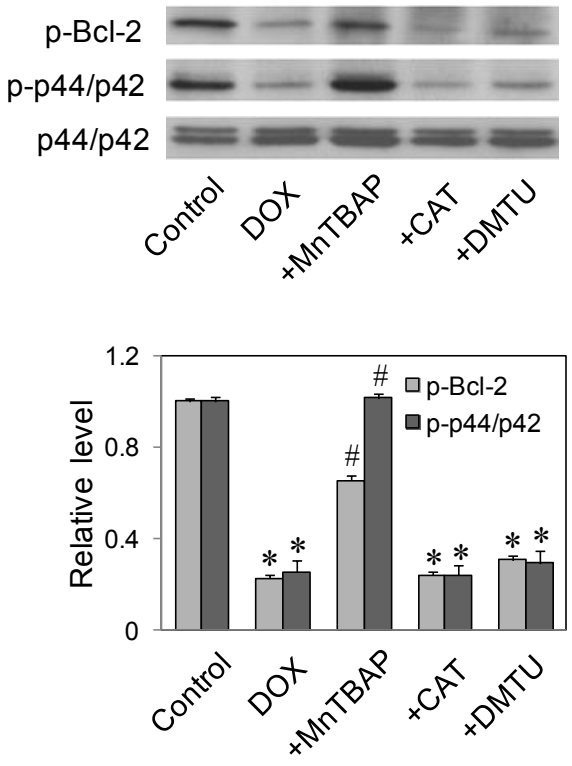

Figure 57. Effects of ROS scavengers on Bcl-2 and ERK1/2 dephosphorylation. HaCaT cells were pretreated for 30 min with MnTBAP (50 μM), catalase (CAT, 7,500 units/ml), or DMTU (5 mM) followed by doxorubicin (DOX, 1.5 μM) for 24 h. Cell lysates were analyzed for phospho-Bcl-2 and phospho-ERK1/2 by Western blotting using phospho-Bcl-2 and phospho-ERK1/2 antibodies. Blots were reprobed with ERK1/2 antibody to confirm equal loading of samples. Plots are mean ± S.D. (n = 3). *, $p < 0.05$ versus non-treated control. #, $p < 0.05$ versus doxorubicin-treated control.

CHAPTER V

DISCUSSION AND CONCLUSION

Chemotherapy-induced alopecia (CIA) is a major clinical problem associated with most cancer chemotherapies. Despite improvements in CIA management and active research in recent years, effective treatment of CIA has yet to be developed and the mechanisms underlying the disease process remain poorly understood. It is generally accepted that CIA develops as a result of massive cell death of hair follicle cells after chemotherapy. Strategic intervention of this cell death, i.e., by localized treatment, may prevent or alleviate CIA without negatively affecting chemotherapy efficacy.

The present study demonstrated that cisplatin and doxorubicin induced toxicity of human hair follicle dermal papilla cells and keratinocytes through a mechanism that involves ROS-dependent apoptosis. Time course measurements indicate that ROS is upstream of caspase-3 activation and apoptosis. In dermal HFDPC and HaCaT cells, the underlying ROS signaling of these cells by cisplatin and doxorubicin are strikingly similar, but the predominant ROS responsible for the apoptotic effect varies, depending on the drug stimuli.

The findings that ROS were generated in HFDPC and HaCaT cells in response to cisplatin treatment and that inhibition of ROS by antioxidant NAC or hydroxyl radical scavenger sodium formate effectively inhibited apoptosis induced by cisplatin supported the role of ROS, particularly hydroxyl radical, in the process. Although hydrogen peroxide was previously shown to be a key mediator of apoptosis induced by cisplatin in human lung cancer cells (Wang et al., 2008), the same effect was not

observed in the dermal cell systems. These results suggest that the specific ROS and apoptosis response to cisplatin treatment is cell type-specific and may be determined by the phenotypic characteristics of cells, i.e., their expression of antioxidant enzymes. It is worth noting that normal cells and cancer cells appear to have differential susceptibility to cisplatin-induced ROS generation and apoptosis, which may be exploited for selective killing strategies of cancer cells while sparing normal cells, for example, pharmacological or genetic modulations that possess hydroxyl radical scavenging action without interfering with peroxide production. The mechanism by which cisplatin induces ROS generation is incompletely understood. The present study showed that while hydroxyl radical plays a predominant role, peroxynitrite decomposition is suggested as a likely source of hydroxyl radical production. Generally, peroxynitrite ($ONOO^-$/ONOOH) is expected to be formed *in vivo* from the interaction between superoxide ($O_2^{-\bullet}$) and nitric oxide ($^\bullet NO$). Recently, a further source of endogenous peroxynitrite has been reported from the interaction of nitroxyl anion (NO^-) with oxygen. Nitroxyl anion is generated from the reduction of nitric oxide by Cu(I),Zn-SOD, hemoglobin, and cytochrome C^{2+} as well as the NOS-catalyzed oxidation of L-arginine and the reaction of S-nitrosothiols with thiols (Kirsch and de Groot, 2002).

Superoxide anion is responsible for the apoptotic effect of doxorubicin in HFDPC and HaCaT cells, as concluded by a strong association of superoxide induction and apoptosis. Inhibition of superoxide by superoxide scavenger MnTBAP completely inhibited doxorubicin-induced apoptosis. High degree of superoxide specificity in the test system was demonstrated by detected ESR spectrum induced by doxorubicin. Using the mitochondrial-targeted hydroethidium, the present study reported mitochondria as the likely source of doxorubicin-induced superoxide

generation. Consistent with the ROS inhibitions, overexpression of mitochondrial superoxide scavenging enzyme MnSOD lowered superoxide generation and apoptosis induction by doxorubicin, indicating the role of mitochondrial superoxide as a key mediator of doxorubicin-induced apoptosis.

Apoptosis induced by cisplatin and doxorubicin is mediated through mitochondrial death pathway. It is well documented that Bcl-2 family proteins are important in regulating mitochondrial membrane permeability and apoptotic cell death through this pathway (Handcock et al., 2001; Martin and Vouri, 2004; Fruehauf and Meyskens, 2007). Both cisplatin and doxorubicin induced down-regulation of Bcl-2 and up-regulation of Bax in concomitant with apoptosis, the effects that are dependent on ROS generation. Since p53 was reported to regulate Bcl-2 family proteins through transcription-dependent and -independent processes (Hemann and Lowe, 2006), p53 activation was evaluated to address whether it is responsible for apoptosis induced by cisplatin and doxorubicin in HFDPC and HaCaT cells. The results show that although p53 is activated (phosphorylated) by cisplatin and doxorubicin treatment, such activation did not play a significant role in the apoptotic process. This conclusion is supported by the observation that cisplatin and doxorubicin did not induce p53 activation at high doses where it induced extensive apoptosis. These results indicate that cisplatin- and doxorubicin-induced apoptosis in HFDPC and HaCaT cells was through a p53-independent pathway but dependent on Bcl-2 family proteins.

The anti-apoptotic function of Bcl-2 is closely associated with its expression level, which is controlled by various mechanisms depending on the apoptotic stimuli (Haendeler et al., 1996; Chanvorachote et al., 2006). The results show that down-regulation of Bcl-2 by cisplatin and doxorubicin is mediated primarily through the

ubiquitin-proteasomal degradation pathway. Such ubiquitination is dependent on ROS generation. For cisplatin, inhibition of ROS by sodium formate but not by catalase or MnTBAP inhibited the ubiquitination of Bcl-2, indicating the dominant role of hydroxyl radical in the process. For doxorubicin, Bcl-2 ubiquitination is dependent on superoxide generation since it is inhibited by the superoxide scavenger MnTBAP but not by other ROS scavengers.

Bcl-2 ubiquitinaiton has been reported to be regulated by its phosphorylation (Dimmeler et al., 1999; Breitschopf et al., 2000). Certain apoptotic agents such as lipopolysaccharide and tumor necrosis factor-α have been shown to induce Bcl-2 dephosphorylation that triggers its ubiquitination. In HFDPC and HaCaT cells, cisplatin and doxorubicin induced Bcl-2 dephosphorylation. The mechanisms underlying the Bcl-2 dephosphorylation was investigated in HaCaT cells upon receiving doxorubicin. One of the primary phosphorylation-dephosphorylation signaling cascades is mitogen-activated protein (MAP) kinases, including p44/p42 extracellular signal-related kinases (ERK1/2), c-Jun-NH2-terminal protein kinase (JNKs), and p38 kinase (Su and Karin, 1996; Ruvolo et al., 2001). In the present study, dephosphorylation of Bcl-2 was found to be mediated by the MAP kinase ERK1/2 pathway. This pathway is inactivated (dephosphorylated) by doxorubicin which promotes Bcl-2 dephosphorylation. Further inactivation of ERK1/2 by its inhibitor (PD98059) enhanced Bcl-2 dephosphorylation and ubiquitination. Thus, it is likely that ERK1/2 is Bcl-2 kinase in this cell system.

Overview of pathways for cisplatin- and doxorubicin-induced apoptosis has been proposed in Figure 58. Cisplatin and doxorubicin induced ROS that inhibited (dephosphorylated) Bcl-2 kinase ERK1/2 and subsequent Bcl-2 phosphorylation. The dephosphorylation of Bcl-2 triggered Bcl-2 ubiquitination which guided Bcl-2

degradation through proteasomal pathway. The imbalance of pro- and anti-apoptotic Bcl-2 family proteins activated caspase cascade, cytochrome C release and apoptosis thorugh mitochondrial pathway.

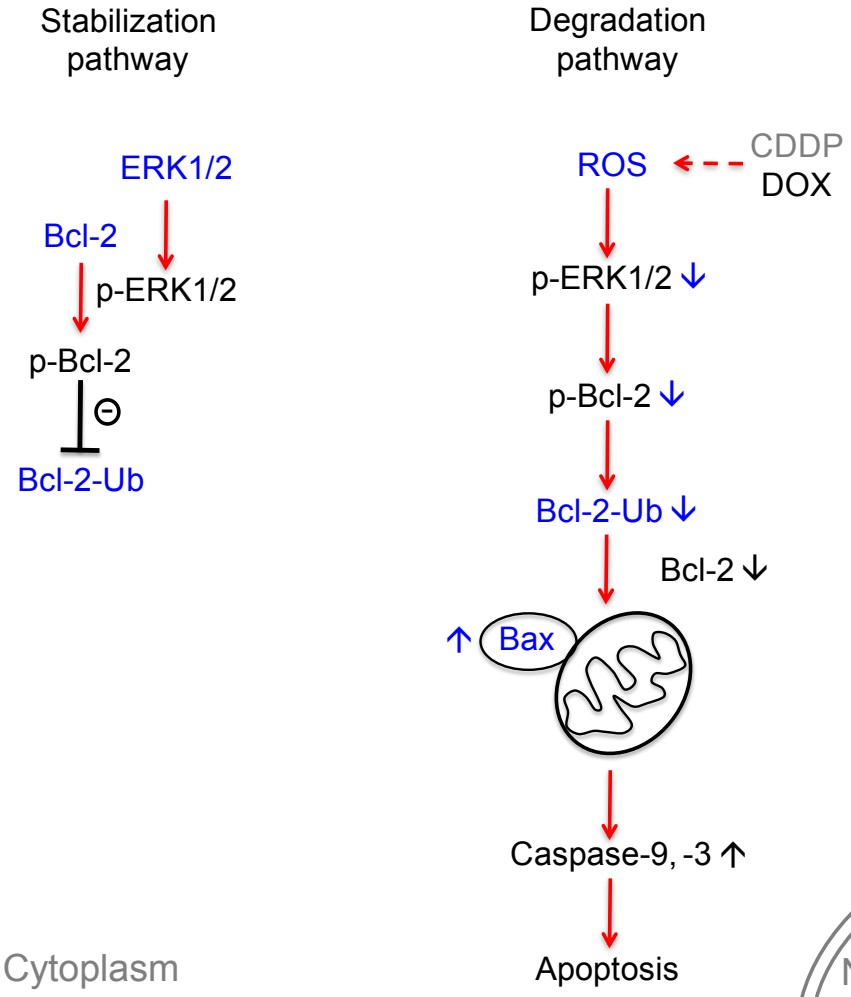

Figure 58. Proposed pathways of cisplatin- and doxorubicin-induced apoptosis in keratinocytes and dermal papilla cells.

One of the important observations in this study is the difference in apoptotic response to cisplatin treatment in HFDPC and HaCaT cells. The keratinocyte HaCaT cells were substantially more responsive than the dermal papilla HFDPC cells, suggesting that keratinocytes are the major target of cisplatin toxicity in hair follicle

cells. Although apoptosis is controlled by several regulatory proteins, and down-regulation of Bcl-2 itself may be insufficient to induce apoptosis, overexpression of Bcl-2 protects the cells from cisplatin-induced apoptosis. Furthermore, ROS induction by cisplatin was lower in Bcl-2-overexpressing cells as compared to vector-transfected cells, suggesting the potential antioxidant function, particularly against hydroxyl radical formation, of Bcl-2. The expression level of Bcl-2 was found to be higher in HFDPC cells as compared to HaCaT cells. Thus, Bcl-2 might contribute to some extent to the hydroxyl radical scavenging of HFDPC cells. A similar finding with regard to different apoptotic response was not observed in doxorubicin-treated HFDPC and HaCaT cells. Fate of the cells is determined by the balance of pro- and anti-apoptotic response, which normally considered as Bcl-2-to-Bax ratio as is the case of cell death through mitochondrial pathway (Raisova et al., 2001; Salakou et al., 2007). While doxorubicin effect was less pronounced on Bcl-2 down-regulation in HFDPC cells as compared to HaCaT cells, Bax expression was intensively up-regulated (~ 2.5-fold *versus* < 2-fold at doxorubicin 1.5 μM). In clinical practice, the incidence of CIA induced by doxorubicin is approximately 80% of all patients (Wang et al., 2006). According to the *in vitro* findings of this study, such high incidence of doxorubicin might be attributable to the high sensitivity of two key functional hair follicle populations; keratinocytes and dermal papilla cells, to the treatment.

In conclusion, the present study provided evidence that ROS is a key mediator of apoptosis induced by cisplatin and doxorubicin in keratinocytes and dermal papilla cells through a p53-independent pathway but dependent on Bcl-2 family proteins and caspase activation. With regard to the specific ROS induction upon treatment, hydroxyl radical is responsible for the down-regulation of Bcl-2 by cisplatin via ubiquitin-proteasomal degradation and superoxide is responsible for the same process

induced by doxorubicin. We identify the source of hydroxyl radical by cisplatin as peroxynitrite degradation and superoxide by doxorubicin as from mitochondrial production. The initial reactors and how drugs initially induce the process are not known and likely not a simple process, which need further investigations. Because chemotherapy-induced ROS generation is not limited to cisplatin and doxorubicin but also caused by a wide variety of agents including cyclophosphamide and etoposide (Conklin, 2004), and the relationship between ROS level and toxic side effects has been suggested, the findings on the mechanisms of apoptosis regulation by ROS in the hair follicle cells could be important in the understanding of CIA by other drugs and in the development of novel therapeutic and preventive approaches for CIA.

REFERENCES

Alonso, L., and Fuchs, E. 2006. The hair cycle. Journal of Cell Science 119: 391-393.

Aosh, S., Ohtsu, T., and Ohta, S. 2000. The super anti-apoptotic factor Bcl-xFNK constructed by disturbing intramolecular polar interactions in rat Bcl-xL. The Journal of Biological Chemistry 275: 37240-37245.

Apisarnthanarax, N., and Duvic, M. Dermatologic complications of cancer chemotherapy. In R. C. Bast, D. W. Kufe, R. E. Pollock, R. R. Weichsellbaum, J. F. Holland, and E. Frei (eds.), Frei Cancer Medicine, pp. 2271-2278. London: BC Decker Inc, 2003.

Arriagada, R., Bergman, B., Dunant, A., Le Chevalier, T., Pignon, J.P., and Vansteenkiste, J. 2004. Cisplatin-based adjuvant chemotherapy in patients with completely resected non-small-cell lung cancer. New England Journal of Medicine 350: 351-60.

Ashkenazi, A., and Dixit, V.M. 1998. Death Receptors: Signaling and modulation. Science 281: 1305-1308.

Azad, N., Iyer, A. K. V., Manosroi, A., Wang, L., and Rojanasakul, Y. 2008. Superoxide-mediated proteasomal degradation of Bcl-2 determines cell susceptibility to Cr(VI)-induced apoptosis. Carcinogenesis 29: 1538-1545.

Beckman, J. C., Beckman, T. W., Chen, J., Marshall, P. A., and Freeman, B. A. 1997. Apparent hydroxyl radical production by peroxynitrite: implications for endothelial injury from nitric oxide and superoxide. Proceedings of the National Academy of Sciences of United States of America 87: 1620-1624.

Baek, S.M., Kwon, C.H., Kim, J.H., Woo, J.S., Jung, J.S., and Kim, Y.K. 2003. Differential roles of hydrogen peroxide and hydroxyl radical in cisplatin-induced cell death in renal proximal tubular epithelial cells. The Journal of Laboratory and Clinical Medicine 142: 178-186.

Balsari, A. L., Morelli, D., Menard, S., Veronesi, U., and Colnagho, M. I. 1994. Protection against doxorubicin-induced alopecia in rats by liposome-entrapped monoclonal antibodies. The FASEB Journal 8: 226-230.

Batchelor, D. 2001. Hair and cancer chemotherapy: consequences and nursing care—a literature study. European Journal of Cancer Care 10: 147-163.

Bodo, E., Tobin, D.J., Kamenisch, Y., Biro, T., Berneburg, M., Funk, W., and Paus, R. 2007. Dissecting the impact of chemotherapy on the human hair follicle. The American Journal of Pathology 171: 1153-1167.

Botchkarev, V.A., Komarova, E.A., Siebenhaar, F., Botchkareva, N.V., Komarov, P.G., Maurer, M., Gilchrest, B.A., and Gudkov, A.V. 2000. p53 is essential for chemotherapy-induced hair loss. Cancer Research 60: 5002-5006.

Botchkarev, V.A., Komarova, E.A., Siebenhaar, F., Botchkareva, N.V., Sharov, A.A., Komarov, P.G., Maurer, M., Gudkov, A.V., and Gilchrest, B.A. 2001. p53 involvement in the control of murine hair follicle regression. The American Journal of Pathology 158: 1913-1919.

Botchkarev, V.A. 2003. Molecular mechanisms of chemotherapy-induced hair loss. Journal of Investigative Dermatology Symposium Proceedings 8: 72-75.

Botchkareva, N.V., Ahluwalia, G., and Shander, D. 2006. Apoptosis in the hair follicle. Journal of Investigative Dermatology 126: 258-264.

Braun, S., Krampert, M., Bodo, E., Kumin, A., Born-Berclaz, C., Paus, R., and Werner, S. 2006. Keratinocyte growth factor protects epidermis and hair follicles from cell death induced by UV irradiation, chemotherapeutic or cytotoxic agents. Journal of Cell Science 110: 4841-4849.

Breitschopf, K., Haendeler, J., Malchow, P., Zeiher, A. M., and Dimmeler, S. 2000. Posttranslational modification of Bcl-2 facilitates its proteasome-dependent degradation: molecular characterization of the involved signaling pathway. Molecular and Cellular Biology 20: 1886-1896.

Carelle, N., Piotto, E., Bellanger, A., Germanaud, J., Thuillier, A., and Khayat, D. 2002. Changing patient perceptions of the side effects of cancer chemotherapy. Cancer 95: 155-163.

Chanvorachote, P., Nimmannit, U., Stehlik, C., Wang, L., Jiang, B. H., Ongpipatanakul, B., and Rojanasakul, Y. 2006. Nitric oxide regulates cell sensitivity to cisplatin-induced apoptosis through S-nitrosylation and inhibition of Bcl-2 ubiquitination. Cancer Research 66: 6353-6360.

Chen, Y., Jungsuwadee, P., Vore, M., Butterfield, D.A., and St. Clair, D.K. 2007. Colleteral damage in cancer chemotherapy: oxidative stress in nontargeted tissues. Molecular Interventions 7: 147-156.

Ciechanover, A. 2005. Proteolysis: from the lysosome to ubiquitin and the proteasome. Nature Reviews Molecular Cell Biology 6: 79-86.

Conklin, K.A. 2004. Chemotherapy-associated with oxidative stress: impact on chemotherapeutic effectiveness. Integrative Cancer Therapies 3: 294-300.

Corsarelis, G., and Millar, S.E. 2001. Towards a molecular understanding of hair loss and its treatment. TRENDS in Molecular Medicine 7: 293-301.

Cutts, S.M., Nudelman, A., Rephaeli, A., and Philips, D.R. 2005. The power and potential of doxorubicin-DNA adducts. IUBMB Life 57: 73-81.

Danilenko, D. M., Ring, B. D., Yanagihara, D., Benson, W., Wiemann, B., Starnes, C. O., and Pierce, G. F. 1995. Keratinocyte growth factor is an important endogenous mediator of hair follicle growth, development, and differentiation. Normalization of the nu/nu follicular differentiation defect and amelioration of chemotherapy-induced alopecia. The American Journal of Pathology 147: 145-154.

Davis, S. T., Benson, B. G., Bramson, H. N., Chapman, D. E., Dickerson, S. H., Dold, K. M., Eberwein, D. J., Edelstein, M., Frye, S. V., Gampe Jr., R. T., Griffin, R. J., Harris, P. A., Hassel, A. M., Holmes, W. D., Hunter, R. N., Knick, V. B., Lackey, K., Lovejoy, B., Luzzio, M. J., Murray, D., Parker, P., Rocque, W. J., Shewchuk, L., Veal, J. M., Walker, D. H., and Kuyper, L. F. 2001. Prevention of chemotherapy-induced alopecia in rats by CDK inhibitors. Sciences 291: 134-137.

Davis, S. T., Benson, B. G., Bramson, H. N., Chapman, D. E., Dickerson, S. H., Dold, K. M., Eberwein, D. J., Edelstein, M., Frye, S. V., Gampe Jr., R. T., Griffin, R. J., Harris, P. A., Hassel, A. M., Holmes, W. D., Hunter, R. N., Knick, V. B., Lackey, K., Lovejoy, B., Luzzio, M. J., Murray, D., Parker, P., Rocque, W. J., Shewchuk, L., Veal, J. M., Walker, D. H., and Kuyper, L. F. 2002. Retraction. Sciences 298: 2327.

Dean, J. C., Salmon, S. E., and Griffiith, K. S. 1979. Prevention of doxorubicin-induced hair loss with scalp hypothermia. New England Journal of Medicine 301: 1427-1429.

Dimmeler, S., Breitschopf, K., Haendeler, J., amd Zeiher, A. M. 1999. Dephosphorylationtargets Bcl-2 for ubiquitin-dependent degradation: a link between the apoptosome and the proteasome pathway. Journal of Experimental Medicine 189: 1815-1822.

Droge, W. 2002. Free radicals in the physiological control of cell function. Physiological Reviews 82: 47-95.

Duvic, M., Lemak, N. A., Valero, V., Hymes, S. R., Farmer, K. L., Hortobagyi, G. N., Trancik, R. J., Bandstra, B. A., and Compton, L. D. 1996. A randomized trial of minoxidil in chemotherapy-induced alopecia. Journal of the American Academy of Dermatology 35: 74-78.

Elliott, K., Stephenson, T.J., and Messenger, A.G. 1999. Differences in hair follicle dermal papilla volume are due to extracellular matrix volume and cell number: implications for the control of hair follicle size and androgen responses. The Journal of Investigative Dermatology 113: 873-877.

Elmore, S. 2007. Apoptosis: a review of programmed cell death. Toxicologic Pathology 35: 495-516.

Freedman, T. G. 1994. Social and cultural dimensions of hair loss in women treated for breast cancer. Cancer Nursing 17: 334-341.

Fruehauf, J.P., and Meyskens, J.L., Jr. 2007. Reactive oxygen species: a breath of life or death? Clinical Cancer Research 13: 789-794.

Grevelman, E. G., and Breed, W. P. M. 2005. Prevention of chemotherapy-induced hair loss by scalp cooling. Annals of Oncology 16: 352-358.

Gupta, S. 2003. Molecular signaling in death receptor and mitochondrial pathways of apoptosis. International Journal of Oncology 22: 15-20.

Haendeler, J., Messmer, U. K., Brune, B., Neugebauer, E., and Dimmeler, S. 1996. Endotoxic shock leads to apoptosis in vivo and reduces Bcl-2. Shock 6:405-409.

Han, J. H., Kwon, O. S., Chung, J. H., Cho, K. H., Eun, H. C., and Kim, K. H. 2004. Effect of minoxidil on proliferation and apoptosis in dermal papilla cells of human hair follicle. Journal of Dermatological Science 34: 91-98.

Hancock, J.T., Desikan, R., and Neill, S.J. 2001. Role of reactive oxygen species in cell signalling pathways. Biochemical Society Transaction 29: 345-350.

Hardy, M.H. 1992. The secret life of the hair follicle. Trends in Genetics 8: 55-61.

Hemann, M.T., and Lowe, S.W. 2006. The p53–Bcl-2 connection. Cell Death and Differentiation 13: 1256-1259.

Hideshima, T., Bradner, J.E., Chauhan, D., and Anderson, K.C. 2005. Intracellular protein degradation and its therapeutic implications. Clinical Cancer Research 11: 8530-8533.

Huges, M. D., Hussain, M., Nawaz, Q., Sayyed, P., and Akhtar, S. 2001. The cellular delivery of antisense oligonucleotides and ribozymes. Drug Discovery Today 6: 305-315.

Hussein, A. M. 1993. Chemotherapy-induced alopecia: New developments. Southern Meidcal Journal 86: 489-496.

Hussein, A. M., Stuart, A., and Peters, W. P. 1995. Protection against chemotherapy-induced alopecia by cyclosporine A in the newborn rat animal model. Dermatology 190: 192-196.

Inui, S., Itami, S., Pan, H.J., and Chang, C. 2000. Lack of androgen receptor transcriptional activity in human keratinocytes. Journal of Dermatological Science 23: 87-92.

Ishino, A., Uzuka, M., Tsuji, Y., Nakanishi, J., Hanzawa, N., and Imamura S. 1997. Progressive decrease in hair diameter in Japanese with male pattern baldness. Journal of Dermatology 24: 758-764.

Jiang, M., Wei, Q., Pabla, N., Dong, G., Wang, C.Y., Yang, T., Smith, S.B., and Dong, Z. 2007. Effects of hydroxyl radical scavenging on cisplatin-induced p53 activation, tubular cell apoptosis, and nephrotoxicity. Biochemical Pharmacology 73: 1499-1510.

Jimenez, J. J., and Yuniz A. A. 1992. Protection from chemotherapy-induced alopecia by 1,25-dihydroxyvitamind D3. Cancer Research 52: 5123-5125.

Jimenez, J. J., and Yunis, A. A. 1996. Vitamin D3 and chemotherapy-induced alopecia. Nutrition 12: 448-449.

Jimenez, J. J., Roberts, S. M., Mejia, J., Mauro, L. M., Munson, J. W., Elgart, G. W., Connelly, E. A., Chen, Q., Zou, J., Goldenberg, C., and Voellmy, R. 2008. Prevention of chemotherapy-induced alopecia in rodent models. Cell Stress and Chaperones 13, No.1: 31-38.

Khopde, S.M., Indira Priyadarsini, K., Mohan, H., Gawandi, V.B., Satav, J.G., Yakhmi, J.V., Banavaliker, M.M., Biyani, M.K., and Mittal, J.P. 2001. Characterizing the antioxidant activity of amla (*Phyllanthus emblica*) extract. Current Sciences 81: 185-190.

Kirsch, M., and de Groot, H. 2002. Formation of peroxynitrite from reaction of nitroxyl anion with molecular oxygen. The Journal of Biological Chemistry 277: 13379-13388.

Kobayashi, T., Okumura, H., Hashimoto, K., Asada, H., Inui, S., and Yoshikawa, K. 1998. Synchronization of normal human keratinocytes in culture: its application to the analysis of 1,25-dihydroxyvitamin D3 effects on cell cycle. Journal of Dermatological Science 17: 108-114.

Krause, K., and Foitzik, K. 2006. Biology of the hair follicle. Seminars in Cutaneous Medicine and Surgery 25: 2-10.

Lecker, S.W., Goldberg, A.L., and Mitch, W.E. 2006. Protein degradation by the ubiquitin-proteasomal pathway in normal and disease states. Journal of the American Society of Nephrology 17: 1807-1819.

Li, P., Nijhawan, D., Budihardjo, I., Srinivasula, S. M., Ahmad, M., Alnemn, E. S., and Wang, X. 1997. Cytochrome c and dATP-dependent formation of Apaf-1/caspase-9 complex initiates an apoptotic protease cascade. Cell 91: 479-489.

Lindner, G., Botchkarev, V.A., Botchkareva, N.V., Ling, G., van der Veen, C., and Paus, R. 1997. Analysis of apoptosis during hair follicle regression. The American Jounal of Pathology 151: 1601-1617.

Luanpitpong, S., Talbott, S. J., Rojanasakul, Y., Nimmannit, U., Pongrakhananon, V., Wang, L., and Chanvorachote, P. 2010. Regulation of lung cancer cell migration and invasion by reactive oxygen species and caveolin-1. The Journal of Biological Chemistry 285: 38832-38840.

Lutz, G. 1994. Effects of cyclosporin A on hair. Skin Pharmacology 7: 101-104.

Martin, S. S., and Vuori, K. 2004. Regulation of Bcl-2 proteins during anoikis and amorphosis. Biochimica et Biophysica Acta 1692: 145-157.

McGravey, E. L., Baum, L. D., Pinkerton, R. C., and Rogers L. M. Psychological sequelae and alopecia among women with cancer. Cancer Practise 9: 283-289.

Messenger, A. G., and Rundegren, J. 2004. Minoxidil: mechanisms of action on hair growth. British Journal of Dermatology 150: 186-194.

Mignotte, B., and Vayssiere, J. L. 1998. Mitochondria and apoptosis. European Journal of Biochemistry 252: 1-15.

Minotti, G., Menna, P., Salvatorelli, E., Cairo, G., and Gianni, L. 2004. Anthracyclines: molecular advances and pharmacologic developments in antitumor activity and cardiotoxicity. Pharmacological Reviews 56: 185-229.

Muller, M., Wilder, S., Bannasch, D., Israeli, D., Lehlbach, K., Li-Weber, M., Friedman, S. L., Galle, P. R., Stremmel, W., Oren, M., and Krammer, P. H. 1998. p53 activates the CD95 (Apo-1/Fas) gene in response to DNA damage by anticancer drugs. The Journal of Experimental Medicine 188: 2033-2045.

Muller-Rover, S., Rossiter, H., Lindner, G., Peters, E.M.J., Kupper, T.S., and Paus, R. 1999. Hair follicle apoptosis and Bcl-2. Journal of Investigative Dermatology Symposium Proceedings 4: 272-277.

Munstedt, K., Manthey, N., Sachsse, S., and Vahrson, H. 1997. Changes in self-concept and body image during alopecia induced cancer chemotherapy. Support Care Cancer 5: 139-143.

Nakashima-Kamimura, N., Nishimaki, K., Mori, T., Asoh, S., and Ohta, S. 2008. Prevention of hemotherapy-induced alopecia by anti-death FNK protein. Life Sciences 82: 218-225.

Ohnemus, U., Uenalan, M., Inzunza, J., Gustafsson, J.A., and Paus, R. 2006. The hair follicle as an estrogen target and source. Endocrine Reviews 27: 677-706.

O'Leary, A. 1990. Stress, emotion, and human immune function. Psychological Bulletin 108: 363-382.

Pabla, N., and Dong, Z. 2008. Cisplatin nephrotoxicity: mechanisms and renoprotective strategies. Kidney International 73: 994-1007.

Park, M. S., Leon, M. D., and Devarajan, P. 2002. Cisplatin induces apoptosis in LLC-PK1 cells via activation of mitochondrial pathways. Journal of the American Society of Nephrology13: 858-865.

Paus, R., Stenn, K. S., and Link, R. E. 1989. The induction of anagen hair growth in telogen mouse skin by cyclosporine A administration. Laboratory Investigation 60: 365-369.

Peters, E. M., Foitzik, K., Paus, R., Ray, S., and Holick, M. F. 2001. A new strategy for modulating chemotherapy-induced alopecia, using PTH/PTHrP receptor agonist and antagonist. Journal of Investigative Dermatology 117: 171-178.

Porter, A. G., and Janicke, R. U. 1999. Emerging roles of caspase-3 in apoptosis. Cell Death and Differentiation 6: 99-104.

Pozo-Kaderman, C., Kaderman, R. A., and Toonkel, R. 1999. The psychological aspects of breast cancer. Nursing Practitioner Forum 10: 165-174.

Raisova, M., Hossini, A. M., Eberle, J., Riebeling, C., Wieder, T., Sturm, I., Daniel, P. T., Orfanos, C. E., and Geilen, C. C. 2001. The Bax/Bcl-2 ratio determines the susceptibility of human melanoma cells to CD95/Fas-mediated apoptosis. Journal of Investigative Dermatology 117: 333-340.

Randall, V.A., Sundberg, J.P., and Philpott, M.P. 2003. Animal and in vitro models for the study of hair follicles. Journal of Investigative Dermatology Symposium Proceedings 8: 39-45.

Rogers, G.E., and Hynd, P.I. 2001. Animal models and culture methods in the study of hair growth. Clinics in Dermatology 19: 105-119.

Ruvolo, P. P., Deng, X., and May, W. S. 2001. Phosphorylation of Bcl-2 and regulation of apoptosis. Leukemia 15: 515-522.

Ruwanpura, S. M., McLachlan, R. I., and Meachem, S. J. 2010. Hormonal regulation of male germ cell development. Journal of Endocrinology 205: 117-131.

Rybak, L.P., Whitworth, C.A., Mukherjea, D., and Ramkumar, V. 2007. Mechanisms of cisplatin-induced ototoxicity and prevention. Hearing Reseacrch 226: 157-167.

Sakita, S., Ohtani, O., and Morohashi, M. 1995. Dynamic changes in the microvascular architecture of rat hair follicles during the hair cycle. Medical Electron Microscopy 28: 187-192.

Salakou, S., Kardamakis, D., Tsamandas, A. C., Zolota, V., Apostolakis, E., Tzelepi, V., Papathanasopoulos, P., Bonikos, D. S., Papapetropoulps, T., Petsas, T., and Dougenesis, D. 2007. Increased Bax/Bcl-2 ratio up-regulates caspase-3 and increases apoptosis in the thymus of patients with myasthenia gravis. In Vivo 21: 123-132.

Sawaya, M. E. 2001. Regulation of the human hair cycle. Current Problem in Dermatology 13: 206-210.

Schilli, M.B., Paus, R., and Menrad, A. 1998. Reduction of intrafollicular apoptosis in chemotherapy-induced alopecia by topical-calcitriol analogs. The Journal of Investigative Dermatology 111: 598-604.

Setsukinai, K., Urano, Y., Kakinuma, K., Majima, H. J., and Nagano, T. 2003. Development of novel fluorescence probes than can reliably detect reactive oxygen species and distinguish specific species. The Journal of Biological Chemistry 278: 3170-3175.

Sharov, A.A., Li, G-Z., Palkina, T.N., Sharova, T.Y., Gilchrest, B.A., and Botchkareva, V.A. 2003. Fas and c-kit are involved in the control of hair follicle melanocyte apoptosis and migration in chemotherapy-induced hair loss. The Journal of Investigative Dermatology 120: 27-35.

Sharov, A. A., Siebanhaar, F., Sharova, T. Y., Botchkareva, N. V., Gilchrest, B. A., and Botchkarev, V. A. 2004. Fas signalling is involved in the control of hair follicle response to chemotherapy. Cancer Research 64: 6266-6270.

Simon, H. U., Haj-Yehia, A., and Levi-Schaffer, F. 2000. Role of reactive oxygen species (ROS) in apoptosis induction. Apoptosis 5: 415-418.

Spallorossa, P., Garibaldi, S., Altieri, P., Fabbi, P., Manca, V., Nasti, S., Rossettin, P., Ghigliotti, G., Ballestrero, A., Patrone, F., Barsotti, A., and Brunelli, C. 2004. Carvedilol prevents doxorubicin-induced free radical release and apoptosis in cardiomyocytes in vitro. Journal of Molecular and Cellular Cardiology 37: 837-846.

Spiegel, D., and Giese-Davis, J. 2003. Depression and cancer: mechanisms and disease progression. Biological Psychiatry 54: 269-282.

Sredeni, B., Xu, R. H., Albeck, M., Gafter, U., Gal, R., Shani, A., Tichler, T., Shapira, J., Bruderman, I., Catanae, R., Kaufman, B., Whisnant, J. K., Mettinger, K. L., and Kalechman, Y. 1996. The protective role of immunomodulator AS101 against chemotherapy-induced alopecia studies on human and animal models. International Journal of Cancer 65: 97-103.

Stenn, K.S., and Paus, R. 2001. Control of hair follicle cycling. Physiological Reviews 81: 449-494.

Su, B., and Karin, M. 1996. Mitogen-activated protein kinase cascades and regulation of gene expression. Current Opinion in Immunology 8: 402-411

Taylor, M., Ashcroft, A. T., and Messenger, A G. 1993. Cyclosporin A prolongs human hair growth *in vitro*. Journal of Investigative Dermatology 100: 365-369.

Torri, V., Harper, P.G., Colombo, N., Sandercock, J., and Parmar, M.K.B. 2000. Paclitaxel and cisplatin in ovarian cancer. Journal of Clinical Oncology 18: 2349-2351.

Trueb, R.M. 2002. Molecular mechanisms of androgenetic alopecia. Experimental Gerontology 37: 981-990.

Trueb, R.M. 2009. Chemotherapy-induced alopecia. Seminars in Cutaneous Medicine and Surgery 28: 11-14.

Tsang, W.P., Chau, S.P.Y., Kong, S.K., Fung, K.P., and Kwok, T.T. 2003. Reactive oxygen species mediate doxorubicin induced p53-independent apoptosis. Life Sciences 73: 2047-2058.

Tsuda, T., Ohmori, Y., Muramatsu, H., Hosaka, Y., Takigushi, K., Saitoh, F., Kato, K., Nakayama, K., Nakamura, N., Nagata, S., and Mochizuki, H. 2001. Inhibitory effect of M50054, a novel inhibitor of apoptosis, on anti-Fas-antibody-induced hepatitis and chemotherapy-induced alopecia. European Journal of Pharmacology 433: 43337-43345.

Tsujimoto, Y. 1998. Role of Bcl-2 family proteins in apoptosis: apoptosomes or mitochondria. Genes to Cell 3: 697-707.

Valko, M., Rhodes, C.J., Moncol, J., Izakovic, M., and Mazur, M. 2006. Free radicals, metals and antioxidants in oxidative stress-induced cancer. Chemico-Biological Interaction 160: 1-40.

Vousden, K.H., and Lane, D.P. 2007. p53 in heath and disease. Nature Reviews Molecular Cell Biology 8: 275-283.

Wang, S., Kanorev, E.A., Kotamraju, S., Joseph, J., Kalivendi, S., and Kalyanaraman, B. 2004. Doxorubicin induces apoptosis in normal and tumor cells via distinctly different mechanisms. The Journal of Biological Chemistry 279: 25535-25543.

Wang, J., Lu, Z., and Au, J.L.S. 2006. Protection against chemotherapy-induced alopecia. Pharmaceutical Research 23: 2505-2514.

Wang, L., Chanvorachote, P., Toledo, D., Stehlik, C., Mercer, R.R., Castranova, V., and Rojanasakul, Y. 2008. Peroxide is a key mediator of Bcl-2 down-regulation and apoptosis induction by cisplatin in human lung cancer cells. Molecular Pharmacology 73: 119-127.

Wilkes, G. M. Potential toxicities and nursing management. In: M. Barton Burke, G. M. Wilkes, and K. Inguersen (eds.), Cancer Chemotherapy: a Nursing Process Approach, pp. 130-135. Boston: Jones & Bartlet, 1996.

Yu, B., Zhao, X., Lee, L. J., and Lee, R. J. 2009. Targeted delivery systems for oligonucleotide therapeutics. The AAPS Journal 11: 195-203.

Zamble, D.B., Jacks, T., and Lippard, S.J. 1998. p53-dependent and –independent responses to cisplatin in mouse testicular teratocarcinoma cells. Proceedings of the National Academy of Sciences of the United States of America 95: 6163-6168.

Zhang, H., Joseph, J., Feix, J., Hogg, N., and Kalyanaraman, B. 2001. Nitration and oxidation of a hydrophobic tyrosine probe by peroxynitrite in membranes: comparison with nitration and oxidation of tyrosine by peroxynitrite in aqueous solution. Biochemistry 40: 7675-7686.

APPENDICES

APPENDIX A

PROTECTIVE EFFECT OF EMBLICA EXTRACT

Phyllanthus emblica Linn. or emblica fruits have been shown to contain a number of biologically active anti-oxidants, such as vitamin C and polyphenols (Khopde et al., 2001). Since ROS plays a key role on cisplatin-induced apoptosis of hair follicular cells, emblica extract might, somehow, show a protective effect on apoptosis by cisplatin.

21. Extraction and sample preparation

Fresh emblica fruits were cut into small pieces. The materials (1 kg) were macerated and agitated in distilled water (5 l) and then filtered. The filtrate was converted to powder form by spray drying. Yield of the extract was approximately 35%. The extract contained 308-320 mg/g of total phenolics calculated as Gallic Acid Equivalent using Folin-Ciocalteu's reaction. Various samples of emblica extract were prepared by dissolving the dry emblica extract powder in deionized water to the indicated concentration (10-500 μg/ml).

22. Effect of emblica extract on cisplatin-induced toxicity

The cytoprotective effect of emblica extract on cisplatin-induced toxicity of HFDPC cells was first evaluated. Cells were treated with cisplatin (100 μM) in the presence or absence of various concentrations of emblica extract (100-500 μg/l) for 24 hours, and their viability was determined by MTT assay. Figure 59 shows that emblica extract dose-dependently increased the viability of HFDPC cells.

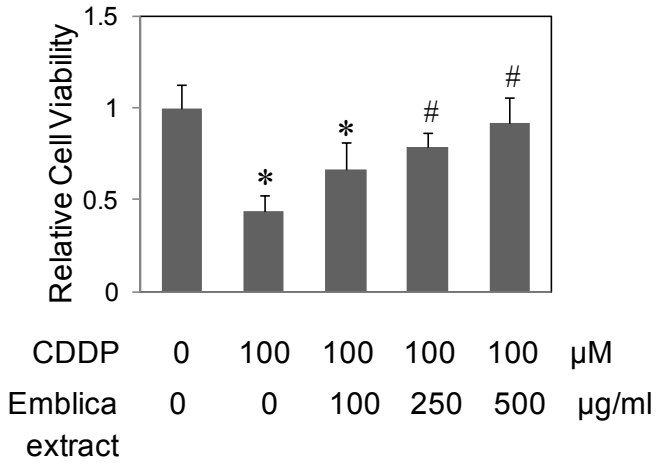

Figure 59. Effect of emblica extract on cisplatin-induced toxicity. HFDPC cells were co-treated with cisplatin (100 μM) and emblica extract (0-500 μg/ml) for 24 h. Cell toxicity was determined by MTT assay. Plots are mean ± S.D. (n = 3). *, $p < 0.05$ versus non-treated control. #, $p < 0.05$ versus cisplatin-treated control.

23. Effect of emblica extract on cisplatin-induced apoptosis

Having demonstrated that apoptosis is the mechanism of cisplatin-induced cytotoxicity, HFDPC cells were similarly treated with cisplatin and various concentration of emblica extract, and apoptosis was determined by Hoechst 33342 assay. Apoptotic cells exhibited condensed and/or fragmented nuclei with bright nuclear fluorescence. Emblica extract was able to inhibit cisplatin-induced apoptosis, with the complete inhibition at the concentration of 250-500 μg/ml (Fig. 60A). Figure 60B shows representative micrographs of the cells treated with cisplatin in the absence or presence of emblica extract.

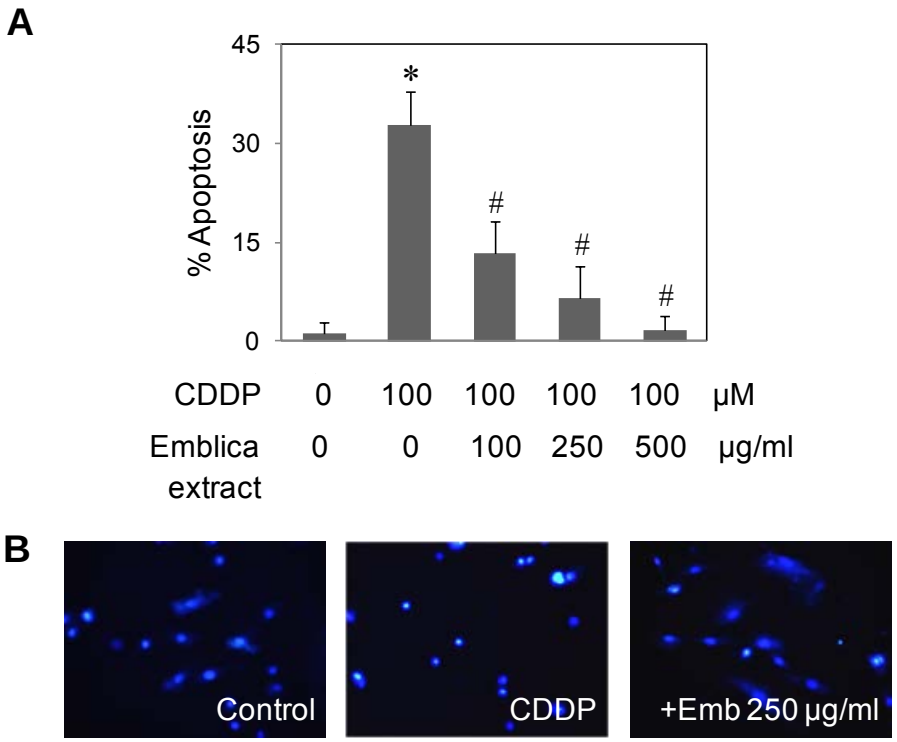

Figure 60. Effect of emblica extract on cisplatin-induced apoptosis. **A** HFDPC cells were co-treated with cisplatin (100 μM) and emblica extract (0-500 μg/ml) for 24 h. Apoptosis was determined by Hoechst 33342 assay. **B** fluorescence micrographs of the treated cells stained with Hoechst dye. Plots are mean ± S.D. (n = 3). *, $p < 0.05$ versus non-treated control. #, $p < 0.05$ versus cisplatin-treated control.

24. Effect of emblica extract on cisplatin-induced ROS generation

In provide the evidence for protective mechanism of emblica extract through inhibition of ROS generation, HFDPC cells were co-treated with cisplatin (100 μM) and emblica extract (0-250 μg/ml) for 2 h, and cellular ROS levels were determined by fluorescence microscopy using H_2DCF-DA as a fluorescence probe. Figure 61 shows that emblica extract was able to scavenge ROS induced by cisplatin in a dose-dependent manner. Altogether, these results reveal the protective effect of emblica extract on cisplatin-induced apoptosis through ROS-dependent mechanism.

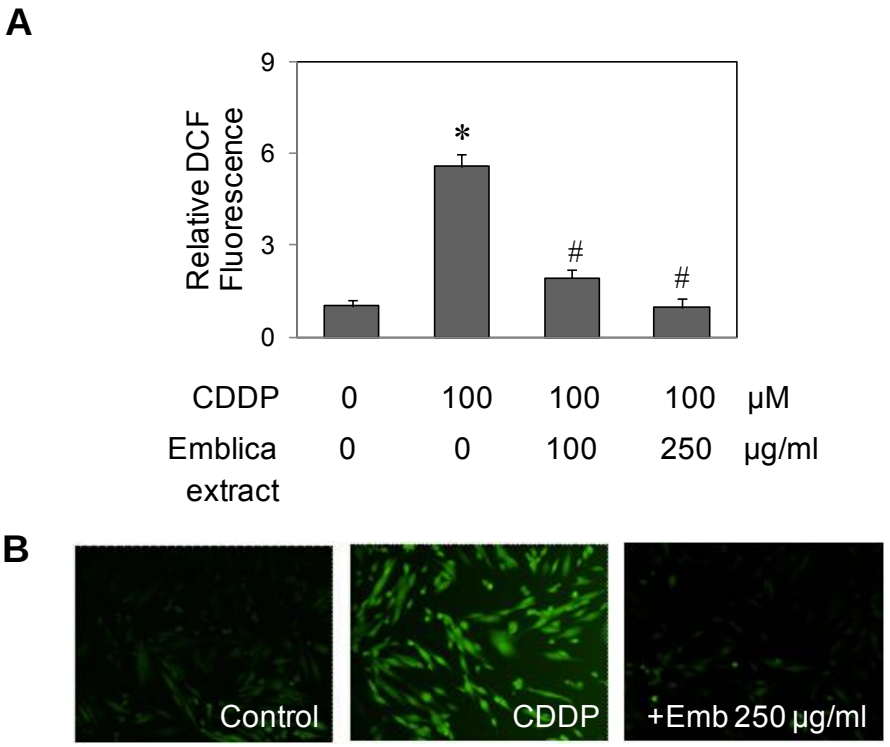

Figure 61. Effect of emblica extract on cisplatin-induced ROS generation. HFDPC cells were co-treated with cisplatin (100 μM) and emblica extract (0-250 μg/ml) for 2 h, after which they were analyzed for ROS generation by fluorescence microscopy using H_2DCF-DA as a fluorescence probe. **A** representative fluorescence micrographs of DCF measurements in the treated cells. **B** analysis of fluorescence micrographs. Plots are mean ± S.D. (n = 3). *, $p < 0.05$ versus non-treated control. #, $p < 0.05$ versus cisplatin-treated control.

APPENDIX B

SUPPLEMENTARY MATERIAL

Cisplatin

1. Time course measurements of caspase-3 activation

To further support the role of ROS in cellular signaling, supplementary time course measurements on caspase-3 enzymatic activity induced by cisplatin were provided. While the ROS response peaks at 2 h (Fig. 11), caspase-3 activation was observed after 6 h (Fig. 62), suggesting that ROS signaling is upstream of caspase-3 activation and apoptosis.

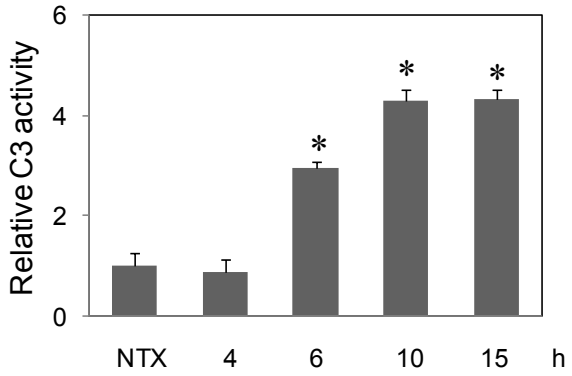

Figure 62. Time course measurements of caspase-3 activation by cisplatin. HaCaT cells were treated with cisplatin (25 μM) for various times (0-15 h), and caspase-3 enzymatic activity was analyzed using the fluorometric substrate FAM-DEVD-fmk. Plots are mean ± S.D. (n = 3). *, $p < 0.05$ versus non-treated control.

2. Cisplatin induces caspase-9 activation

Cisplatin was previously shown to induce apoptosis through the mitochondrial pathway. To confirm that cisplatin induces apoptosis through this pathway in the tested cells, activation of caspase-9, an apical caspase of the mitochondrial death pathway, was determined by Western blotting. Figure 63 shows that cisplatin induced caspase-9 activation in a dose-dependent manner, as indicated by the dose-dependent increase of cleaved caspase-9.

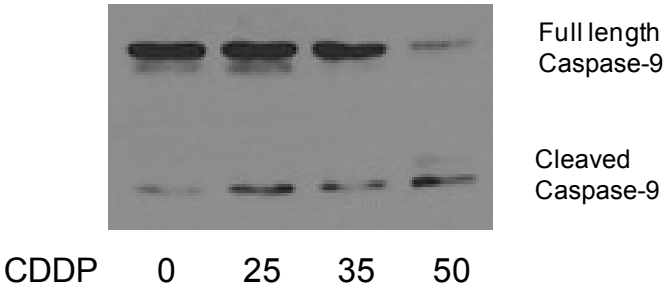

Figure 63. Cisplatin induces caspase-9 acivation. HaCaT cells were treated with cisplatin various concentration of cisplatin (25-50 μM) for 24 h and caspase-9 activation was determined b Western blotting using caspase-9 antibody.

3. Time course measurements of the effect of ROS scavengers on ROS generation

Time course measurements of the effect of ROS scavengers on ROS generation were also shown (Fig. 64). At all time points, the hydroxyl radical scavenger sodium formate (NaFM) was able to inhibit the ROS induction by cisplatin, whereas catalase and MnTBAP had no significant effect.

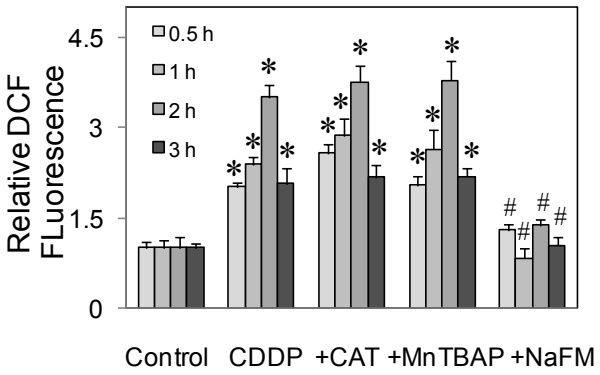

Figure 64. Time course measurements of the effects of ROS scavengers on ROS generation. HaCaT cells were pretreated for 30 min with catalase (CAT) (7,500 U/ml), MnTBAP (50 μM), or sodium formate (NaFM) (2.5 mM) followed by cisplatin treatment (25 μM). ROS generation was determined at various times (0.5-3 h) by fluorescence plate reader using H_2DCF-DA as a probe. Plots are mean ± S.D. (n = 3). *, $p < 0.05$ versus non-treated control. #, $p < 0.05$ versus cisplatin-treated control.

4. Fluorescence micrographs of the effect of ROS scavengers on ROS generation

To provide supplementary qualitative data on cellular ROS generation induced by cisplatin and the role of hydroxyl radical, fluorescence micrographs of cisplatin-treated cells in the presence or absence of hydroxyl radical scavenger sodium formate were shown. Cisplatin dose-dependent induced ROS generation, the effect of which inhibited by the addition of sodium formate in both HFDPC (Fig. 65) and HaCaT (Fig. 66) cells.

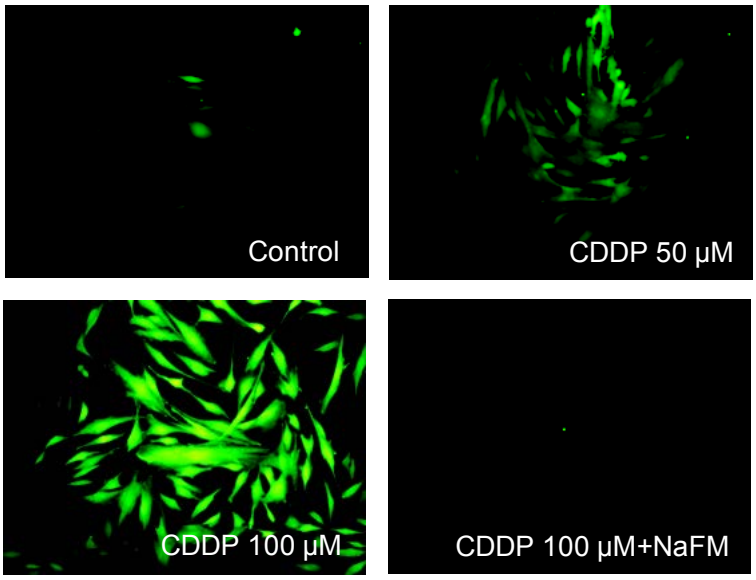

Figure 65. Cisplatin induced ROS generation in HFDPC cells. Cells were treated with various concentration of cisplatin (0-100 μM) in the presence or absence of sodium formate (NaFM) (2.5 mM) for 2 h. Cellular ROS level were determined under fluorescence microscope using H_2DCF-DA as a specific ROS probe.

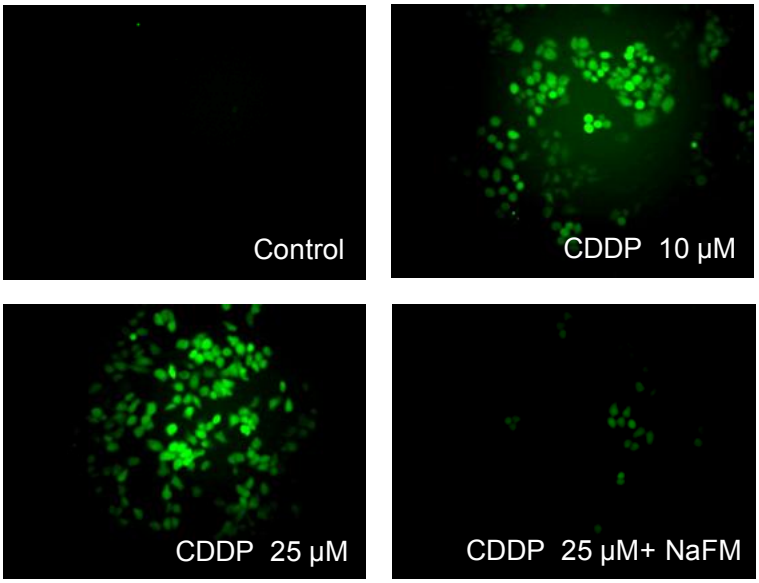

Figure 66. Cisplatin induced ROS generation in HaCaT cells. Cells were treated with various concentration of cisplatin (0-25 μM) in the presence or absence of sodium

formate (NaFM) (2.5 mM) for 2 h. Cellular ROS level were determined under fluorescence microscope using H_2DCF-DA as a specific ROS probe.

Doxorubicin

1. Time course measurements of the superoxide generation by doxorubicin

Time course measurement for superoxide generation by doxorubicin were analyzed using DHE as a specific fluorescent probe and found the maximum response time of 2 h (Fig. 67).

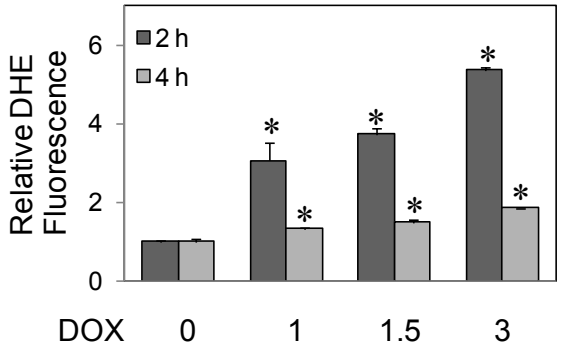

Figure 67. Time course measurements of superoxide generation by doxorubicin. HaCaT cells were treated with doxorubicin (0-3 μM) for various times (2-4 h), after which they were analyzed for ROS generation by fluorescence plate reader using DHE as a specific probe**.** Plots are mean ± S.D. (n = 3). *, $p < 0.05$ versus non-treated control.

2. Time course measurement of the effect of ROS scavengers on superoxide generation

Time course measurements of the effect of ROS scavengers on ROS generation were also shown (Fig. 68). At all time points, the superoxide scavenger MnTBAP was able to inhibit the superoxide induction by doxorubicin, whereas catalase and DMTU had no significant effect.

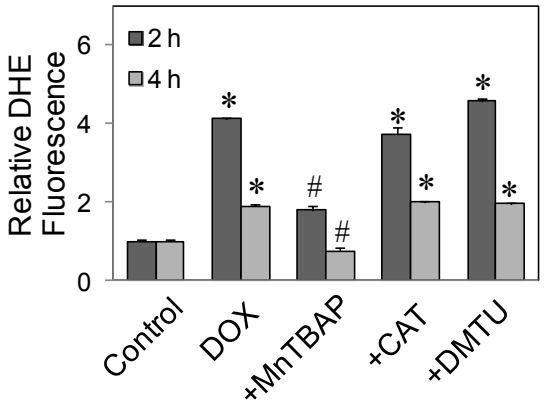

Figure 68. Time course measurements of the effects of ROS scavengers on superoxide generation. HaCaT cells were pretreated for 30 min with MnTBAP (50 μM), catalase (CAT) (7,500 U/ml), or DMTU (5 mM) followed by doxorubicin treatment (1.5 μM). Superoxide generation was determined at various times (2-4 h) by fluorescence plate reader using DHE as a probe. Plots are mean ± S.D. (n = 3). *, $p < 0.05$ versus non-treated control. #, $p < 0.05$ versus doxorubicin-treated control.

3. Fluorescence micrographs of the effect of ROS scavengers on ROS generation

To provide supplementary qualitative data on ROS generation induced by doxorubicin and the role of superoxide anion, fluorescence micrographs of doxorubicin-treated cells in the presence or absence of superoxide scavenger DMTU

were shown. Doxorubicin dose-dependent induced ROS generation, the effect of which inhibited by the addition of MnTBAP in both HFDPC (Fig. 69) and HaCaT (Fig. 70) cells.

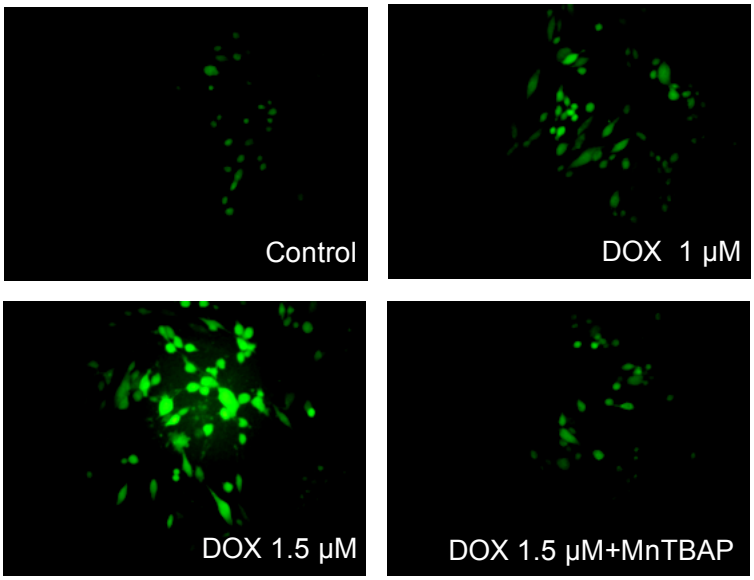

Figure 69. Doxorubicin induced ROS generation in HFDPC cells. Cells were treated with various concentration of doxorubicin (0-1.5 μM) in the presence or absence of MnTBAP (50 μM) for 2 h. Cellular ROS level were determined under fluorescence microscope using H_2DCF-DA as a specific ROS probe.

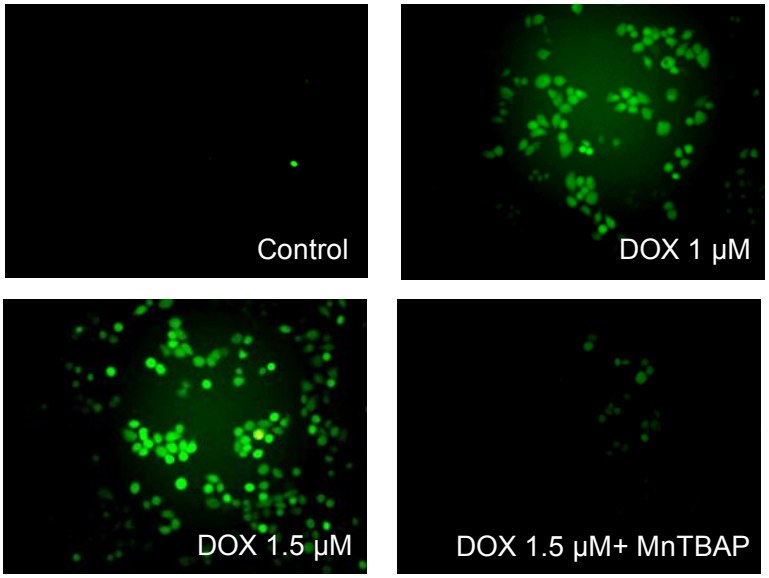

Figure 70. Doxorubicin induced ROS generation in HaCaT cells. Cells were treated with various concentration of doxorubicin (0-1.5 μM) in the presence or absence of MnTBAP (50 μM) for 2 h. Cellular ROS level were determined under fluorescence microscope using H_2DCF-DA as a specific ROS probe.

APPENDIX C

TABLE OF EXPERIMENTAL RESULTS

Table 1. Percentage of apoptotic cells induced by cisplatin at 24 h.

Cisplatin (μM)	% Apoptosis HFDPC	**Cisplatin (μM)**	% Apoptosis HaCaT
0	0.69 ± 0.43	0	0.89 ± 0.90
50	12.62 ± 3.51*	10	9.51 ± 3.21*
100	24.20 ± 3.46*	25	24.82 ± 3.35*
250	38.71 ± 5.84*	50	44.39 ± 6.35*
100 + zVAD	6.25 ± 2.11#	25 + zVAD	2.89 ± 1.75#

Each value represents mean ± S.D. of four independent experiments. *, $p < 0.05$ versus non-treated control. #, $p < 0.05$ versus cisplatin-treated control.

Table 2. Percentage of apoptotic cells induced by cisplatin in the presence or absence of antioxidants at 24 h.

Treatments	% Apoptosis HFDPC	**Treatments**	% Apoptosis HaCaT
None	0.69 ± 0.43	None	0.89 ± 0.90
CDDP 100 μM	24.20 ± 3.46*	CDDP 100 μM	24.82 ± 3.35*
+ NAC	3.22 ± 1.38#	+ NAC	7.43 ± 1.14#
+ GSH	1.22 ± 2.17#	+ GSH	5.58 ± 2.58#

Each value represents mean ± S.D. of four independent experiments. *, $p < 0.05$ versus non-treated control. #, $p < 0.05$ versus cisplatin-treated control.

Table 3. Percentage of apoptotic cells induced by cisplatin in the presence or absence of various specific ROS scavengers at 24 h.

Treatments	% Apoptosis HFDPC	**Treatments**	% Apoptosis HaCaT
None	0.80 ± 0.33	None	1.10 ± 0.49
CDDP 100 μM	26.23 ± 2.86*	CDDP 100 μM	23.17 ± 5.18*
+ Catalase	20.03 ± 5.44*	+ Catalase	20.24 ± 4.98*
+ MnTBAP	19.46 ± 4.60*	+ MnTBAP	26.6 ± 4.39*
+ NaFM	5.50 ± 3.40#	+ NaFM	8.84 ± 1.41#

Each value represents mean ± S.D. of four independent experiments. *, $p < 0.05$ versus non-treated control. #, $p < 0.05$ versus cisplatin-treated control.

Table 4. Percentage of apoptotic cells induced by cisplatin at 24 h in comparison between HFDPC and HaCaT cells.

Cisplatin (μM)	% Apoptosis HFDPC	% Apoptosis HaCaT
0	0.49 ± 0.33	1.10 ± 1.14
25	2.32 ± 0.15	26.46 ± 4.41**
100	26.23 ± 4.17*	86.64 ± 11.88**

Each value represents mean ± S.D. of four independent experiments. *, $p < 0.05$ versus non-treated HFDPC cells. #, $p < 0.05$ versus cisplatin-treated HFDPC cells.

Table 5. Percentage of apoptotic cells induced by cisplatin at 24 h in comparison between pcDNA3 and Bcl-2 overexpressed HaCaT cells.

Cisplatin (μM)	% Apoptosis	% Apoptosis
	HaCaT	HaCaT/Bcl-2
0	1.42 ± 1.57	3.33 ± 0.48
25	24.19 ± 5.64*	5.85 ± 2.01#
35	42.36 ± 2.53*	14.23 ± 2.36#
50	60.67 ± 11.59*	43.43 ± 4.20#

Each value represents mean ± S.D. of three independent experiments. *, $p < 0.05$ versus non-treated vector-transfected HaCaT cells. #, $p < 0.05$ versus cisplatin-treated vector-transfected HaCaT cells.

Table 6. Percentage of apoptotic cells induced by doxorubicin at 24 h.

Doxorubicin (μM)	% Apoptosis	% Apoptosis
	HFDPC	HaCaT
0	3.37 ± 1.31	2.61 ± 1.86
1	13.55 ± 2.70*	16.68 ± 3.33*
1.5	21.11 ± 3.77*	25.25 ± 5.66*
3	30.90 ± 2.38*	38.28 ± 8.67*
1.5 + zVAD	7.91 ± 2.27#	9.17 ± 4.23#

Each value represents mean ± S.D. of three independent experiments. *, $p < 0.05$ versus non-treated control. #, $p < 0.05$ versus doxorubicin-treated control.

Table 7. Percentage of apoptotic cells induced by doxorubicin in the presence or absence of various ROS scavengers at 24 h.

Treatments	% Apoptosis	% Apoptosis
	HFDPC	HaCaT
None	3.37 ± 1.31	1.26 ± 1.86
DOX 1.5 μM	21.33 ± 3.77*	23.74 ± 0.31*
+ MnTBAP	0.71 ± 1.89#	3.33 ± 1.65#
+ Catalase	21.49 ± 4.01*	19.31 ± 2.94*
+ DMTU	17.27 ± 2.27*	25.25 ± 2.66*

Each value represents mean ± S.D. of three independent experiments. *, $p < 0.05$ versus non-treated control. #, $p < 0.05$ versus doxorubicin-treated control.

Table 8. Percentage of apoptotic cells induced by doxorubicin at 24 h in comparison between pcDNA3 and MnSOD overexpressed HaCaT cells.

Doxorubicin (μM)	% Apoptosis	% Apoptosis
	HaCaT	HaCaT/MnSOD
0	5.68 ± 1.28	2.51 ± 0.27
1	10.29 ± 3.42*	3.40 ± 2.00#
1.5	18.90 ± 4.33*	4.77 ± 1.75#
3	41.05 ± 5.22*	28.57 ±4.15#

Each value represents mean ± S.D. of three independent experiments. *, $p < 0.05$ versus non-treated vector-transfected HaCaT cells. #, $p < 0.05$ versus doxorubicin-treated vector-transfected HaCaT cells.

Table 9. Percentage of apoptotic cells induced by cisplatin in the presence or absence of emblica extract in HFDPC cells at 24 h.

Treatments	% Apoptosis
	HFDPC
None	1.22 ± 1.72
CDDP 100 μM	32.68 ± 5.35*
+ emblica 100 μg/ml	13.33 ± 4.75#
+ emblica 250 μg/ml	6.47 ± 4.99#
+ emblica 500 μg/ml	1.56 ± 2.21#

Each value represents mean ± S.D. of four independent experiments. *, $p < 0.05$ versus non-treated control. #, $p < 0.05$ versus cisplatin-treated control.

VITA

Sudjit Luanpitpong was born in Bangkok, Thailand. After completing her study at Saint Joseph Covent School, Bangkok, in 2001, she entered Faculty of Pharmaceutical Sciences, Chulalongkorn University. She received the degree of Bachelor of Science in Pharmacy (B.Sc. in Pharm) with honors from Chulalongkorn University in February 2007. The following June she entered the International Graduate Program in Pharmaceutical Technology, Faculty of Pharmaceutical Sciences, Chulalongkorn University and is a candidate for the Degree of Doctor of Philosophy. She received her Ph.D. grant from The Royal Golden Jubilee Ph.D. Program. During the degree seeking, she worked as a Research Assistant in Dr. Nimmannit's laboratory, Chulalongkorn University, focusing on nano-delivery system, and as a Research Scholar in Dr. Rojanasakul's laboratory, Health Sciences Center, West Virginia University, focusing on carcinogenesis and nanotoxicity.